Investigation of Miniaturized Microstrip Antenna Efficiency Enhancement

by

Robin Raju

A Thesis submitted to the Faculty of Graduate Studies of

The University of Manitoba

in partial fulfilment of the requirements of the degree of

MASTER OF SCIENCE

Department of Electrical and Computer Engineering

University of Manitoba

MB, Canada

Abstract

Radiation Efficiency improvement of miniaturized microstrip antenna is studied in this thesis. It is shown that, the loss reduction in miniaturized Microstrip Antenna can be achieved through two possible ways. The first is by modifying the materials used for building the antenna, and the second method is by increasing the radiation conductance of the antenna. Material modification at nano/micro scale by replacing conductors with Metallo-Dielectric one dimensional medium for applications in loss reduction is investigated first. It is shown by the Transfer Matrix Method and using simulations that, for a one dimensional medium replacing very thin conductors (less than skin depth) by laminated multilayered conductors reduce losses. However, the improvement does not exceed the case of single conductor which is a few times thicker than skin depth. Secondly, the efficiency improvement of a small H-Shaped patch antenna by using closely coupled stacked parasitic resonators is studied. It is shown that significant improvement in efficiency can be achieved with minimal changes in the foot print, radiation pattern and cross polarization levels of the antenna. The effect of the overall thickness and superstrate dielectric constant on the efficiency improvement is studied parametrically. It is shown that by using 5 radiating resonators and appropriate choice of inter-conductor dielectric constant, for a small increase in thickness of 0.127mm (5mil), the radiation efficiency can be increased from 2.34% to 6.3%. This efficiency improvement can be made very significant from 2.4% to 33%, by increasing the height to 1.27mm (50mil). These translate to a gain improvement of 4dB and 13dB, respectively. This technique is also demonstrated experimentally in H-Shaped antennas with two different levels of miniaturizations.

Acknowledgment

Firstly, I would like to thank my academic advisor, Dr. Lotfollah Shafai, for all of his support, encouragement and time during my MSc studies.

I would like to express my appreciation to my MSc committee for their efforts in the evaluation and improvement of this work.

I would also like to thank Mr. Brad Tabachnick and Mr. Cory Smit for their help in fabrication and measurements. Special thanks are due to Ms. Amy Dario and Ms. Shelly Girardin for their administrative assistance and support.

I extend my gratitude to the Government of Manitoba, Natural Sciences and Engineering Research Council of Canada and the University of Manitoba Research Grant Program for the financial support.

Finally, I would like to thank all my family, friends and colleagues for their unwavering support and love.

Contents

List of Tables

List of Figures

List of Symbols and Acronyms

Symbol	Description	Symbol	Description
(r, θ,φ)	Spherical Co-ordinate System	P_t	Total Power
(x, y, z)	Rectangular Co-ordinate System	Q	Quality Factor
AMC	Artificial Magnetic Conductors	R/Γ	reflection coefficient
BW	Bandwidth	R_s	Surface Resistance
CPW	Coplanar Waveguide	SL	Slot Length
CRLH	Composite right-/left-handed	S_w	Slot Width
D	Directivity	T	Transmission coefficient
DNG	Double Negative	tan(δ)	Loss Tangent
EBG	Electromagnetic Band-Gap	TEM	Transverse Electromagnetic
E_z	z- Component of electric field	TMM	Transfer Matrix Method
E_θ	θ-Component of Electric	UWB	Ultra Wideband
E_ϕ	ϕ-Component of Electric	v	Phase Velocity
f	Frequency in Hz	V0	Input voltage
f_h	Higher Resonant Frequency	W	Width of Patch Antenna
f_l	Lower Resonant Frequency	W_e /W_{eff}	Effective Width
f_r	Resonant Frequency	W_T	Total Stored Energy
FSS	Frequency Selective Surfaces	X_s	Surface Reactance
G	Gain	Z0	Characteristics Impedance
G_c	Conductance due to conductor loss	Z_s	Surface Impedance
G_d	Conductance due to dielectric loss	α	Attenuation Constant
G_L	Total Loss Conductance	α	W/L
G_{rad}/G_R	Radiation conductance	β	Phase Constant
G_{sw}	Conductance due to surface waves	γ	Propagation Constant
G_T	Total Conductance	δ	Skin Depth
h	Substrate Height	ϵ	Permittivity
H_s	Normal Component Of Magnetic Field	ϵ_0	Permittivity of Free space
J	Current Density	ϵ_r	Dielectric Constant
k	Free Space Wave Number	ϵ_{reff}	Effective Dielectric Constant
L	Length of Patch Antenna	η	Intrinsic Impedance
L_e/L_{eff}	Effective Length	η	Radiation Efficiency
P_{acc}	Accepted Power	η_{rad}	Radiation Efficiency
P_c	Power lost in conductor	λ/ λ_0	Free Space Wavelength
P_d	Power lost in dielectric	μ	Permeability
PEC	Perfect Electric Conductor	μ_0	Permeability of Free space
PMC	Perfect Magnetic Conductor	μ_r	Relative Permeability
P_{rad}/P_r	Radiated Power	σ	Conductivity
P_{sw}	Power lost through surface waves	ω	Angular Frequency

Chapter 1

Introduction to Small Antennas

As predicted by Moore's law, the size of both digital and analog electronic systems has been reducing ever since they were developed. Each year new generations of electronic devices which are smaller, faster and more efficient replace the older ones. Antennas and RF front ends, which form the integral part of wireless systems, have also not been exempted from this demand for miniaturization. However, the challenges in making these devices smaller have never been better emphasized, than by Harold Wheeler - one of the pioneers in the field of Antenna Miniaturization, as:

"*It was the IRE(IEEE) that embraced the new field of wireless and radio, which became the fertile field for electronics and later computer age. But the antennas and propagation will always retain their identity, being immune to Miniaturization or Digitization*."

-Harold Wheeler

Nevertheless, the advancements in the field of material sciences and fabrication technologies have led to the development of novel materials in Natural, Meta and Active states. This in turn has paved the way for researchers in Antenna Miniaturization to engage actively in adding new dimensions to the field. In the next section, a brief survey of Antenna miniaturization techniques is provided, which is followed by the design considerations to be taken into account for effective antenna miniaturization.

1.1 ANTENNA MINIATURIZATION TECHNIQUES

A number of techniques have been in use for antenna miniaturization. In the following section a brief discussion of some of these techniques is provided.

i. Antenna miniaturization by High Contrast Material Loading

Material loading is one of the most popular techniques used for antenna miniaturization. The basic idea behind miniaturization here is that, the velocity of wave reduces with an increase in the refractive index of the material. In other words, if one could design antennas using a high refractive index medium, then its size may be reduced by a factor of $1/\sqrt{\epsilon_r \mu_r}$ (where ϵ_r and μ_r are the relative permittivity and permeability of the medium). Clearly, a high dielectric constant, high relative permeability or both may be used to achieve miniaturization. In [1] it has been shown that, a good impedance match is obtained when the material used for the antenna has $\epsilon_r = \mu_r$. However, it is seen that naturally occurring magnetic materials exhibit high loss at high frequencies [2], thus limiting their applications in antennas. Furthermore, it is observed that in order to achieve high μ_r the frequency of operation should be at the natural resonant frequency of the material [3]. Around this frequency range however, the material loss also peaks, thereby, limiting the extent to which the antenna may be magnetically loaded. In [2], the effect of material losses on the performance of material loaded spiral antenna was presented. It was shown that the gain dropped by about 3dB due to an increase in loss tangent from 0 to 0.01. Despite this, several antennas incorporating magneto-dielectric substrates have been presented in [4], [5], [6], [7]. Much attention has been directed towards high dielectric constant materials like ceramic owing to their low loss characteristics, in spite of the fact that such antennas exhibit

low impedance bandwidth, low radiation efficiency and difficulty in impedance matching. Loading the substrate, as well as, superstrates have been effectively in use in planar structures like microstrip patch antennas, printed dipoles and spiral antennas [8], [9]. Recently, polymer-ceramic composites which provide a dielectric constant ranging from 2 to 30 have gained much popularity in antenna engineering [10].

ii. Antenna miniaturization by shaping

Miniaturization by shaping is one of the most extensively used techniques for designing small antennas. Shaping includes various geometric modifications of the antenna such as bending, meandering, folding, slot loading, fractal folding etc. Bending and folding is usually applied to antennas which are 3-dimensional and shaped similar to a monopole. The Printed Inverted-F (PIFA) is one such antenna widely used in handheld wireless devices [11] as shown in Figure 1.1a. Folding is also widely used for miniaturization of Ultra Wideband (UWB) monopole antennas [12]. These techniques reduce the size of the antenna in the desired direction at the expense of an increase in size in another direction or increase in volume of the antenna [10].

Adding slots is another popular technique used widely in planar antennas such as microstrip patch antennas. The addition of slots in most cases increases the resonant length of the antenna, thereby reducing the resonant frequency of operation [13], [14]. This is illustrated for the case of a rectangular patch antenna in Figure 1.1b. In rectangular patch antenna the currents flow from one edge to the other. Addition of slots however changes the direction and requiring the current to take a longer path. Thus, the resonant frequency of the patch is reduced.

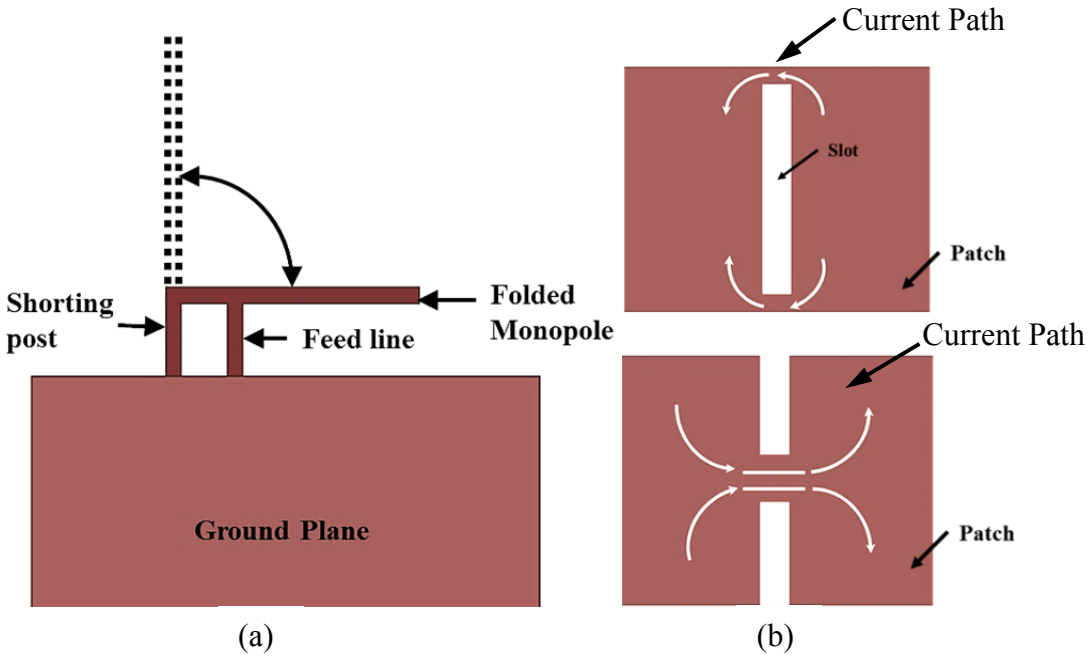

Figure 1.1 (a) Printed Inverted-F antenna. (b) Microstrip Patches with slot illustrating the current path.

iii. Antenna miniaturization by lumped element loading

In applications where shaping may not be favourable, effects similar to the addition of slots and meandering may be obtained by including equivalent lumped elements, generally capacitors and inductors. In [15] a Coplanar Waveguide (CPW) folded slot antenna with capacitive loading using chip capacitors was reported. A 22% size reduction was achieved using this technique at the expense of a 2.7 dB reduction in the measured gain and 11% in 10 dB return loss bandwidth of the antenna. Another similar example for capacitive loading can was reported in [16]. There, the authors have studied the effect of miniaturization of loop antenna with multiple periodically arranged shunt capacitances. The results indicated a seven fold size reduction of the original antenna, with a 7dB reduction in the gain. In [17] Lumped inductors for miniaturizing loop antenna, have also been demonstrated.

iv. Antenna miniaturization by using artificially engineered materials

In recent years artificial materials have gained a lot of interest in the field of antenna miniaturization. These materials, made up of periodic sub-wavelength elements, generate unique material properties utilizing element resonances. Examples of such materials are Electromagnetic Band-Gap (EBG) materials [18], Double Negative (DNG) materials, Artificial Magnetic Conductors (AMC), Frequency Selective Surfaces (FSS), etc. EBG materials and ground planes are found to be of particular interest in antenna design. It has been shown in [19] that EBG can be used to reduce the distance between the radiating element and its ground effectively. These materials also find applications in surface wave reduction of patch antennas [20]. As shown in [21], Composite right-/left-handed (CRLH) transmission-line antennas are other candidates for antenna miniaturization in both leaky wave and resonant antenna structures. However a loss of energy is one of the fundamental limitations associated with meta-materials. It has been shown in [22] that any effort to reduce the loss in meta-material, reduces the artificial property (negative refractive index) associated with it. This follows from the fundamental principles of causality obtained from the dispersion relations of the material.

1.2 CONSIDERATIONS WITH SMALL ANTENNAS

All conventional, passive electrically small antennas show limitations in their performance characteristics; namely gain, impedance bandwidth and radiation efficiency with the achievable electrical size. Considerable work has been carried out by researchers in the estimation of fundamental limitations on some of the important characteristics such as, Quality Factor (Q), Frequency Bandwidth (BW) and the Directive Gain (D) of passive

electrically small antennas [23] . This has led to the determination of the lower bound on the Quality factor Q_L to be given by:

$$Q_L = \frac{3}{2}\eta\left[\frac{1}{(ka)^3} + \frac{1}{ka}\right] \tag{1.1}$$

Here, η is the radiation efficiency of the antenna $k = 2\pi/\lambda$ is its resonant wave number and a the radius of the smallest sphere enclosing the antenna. This lower bound on the Q of the antenna gives the maximum achievable bandwidth related to the commonly used expression for the half power voltage standing wave ratio (VSWR) bandwidth $BW = 2/Q_L$ [24]. It can be noted from (1.1) that one can achieve a higher BW, trading for higher loss in the antenna. This however is considered to be highly undesirable for most applications. Recently in [25] & [26], Gustafsson et. al. studied the relation between the effective volume occupied by an antenna enclosed in the smallest possible sphere and its maximum D/Q ratio based on scattering and absorption theory, which for a nonmagnetic, linear and reciprocal antenna is given by:

$$\left[\frac{D = G/\eta}{Q}\right]_{max} = \frac{k^3}{2\pi}\gamma \tag{1.2}$$

where, γ is a constant purely dependent on the volume and geometry of the antenna under consideration. With $\gamma/4\pi a^3$ having a maximum value of 1 for an antenna occupying the entire sphere, and for other geometries like circular disc and cylindrical element it takes the values 0.42 and 0.0056 respectively [25]. It is evident here that an antenna that utilizes its volume effectively has better D/Q ratio.

1.3 MOTIVATION AND PURPOSE OF THE CURRENT WORK

Expressions (1.1) and (1.2) also indicate that the antenna radiation efficiency is an important parameter in terms of its operating characteristics. Radiation efficiency of an antenna is defined as the ratio of the total power radiated by the antenna to the total power accepted by the antenna at its input terminals ($\eta_{rad} = \frac{P_{rad}}{P_{acc}} = \frac{G}{D}$). By using spherical mode expansion it has been shown in [27] that though theoretically a large directivity may be achieved in both the near and far fields with a proper combination of modes, the radiation efficiency plays an important role in defining the maximum realizable gain from small antennas and super gain antennas. It is also illustrated in [27] that lossless small antennas are characterized by large value of Q (stored energy). For dissipative cases involving non ideal materials (conductors and dielectrics) small antennas are characterized by high power dissipation and in both ideal and non-ideal cases the near-field is characterized by extremely large field intensities. This may be attributed to the increase in the energy density of the structure with reduction in its overall volume [23].

In other words, when an antenna is miniaturized, antenna design engineers face the dilemma of reduced radiation efficiency (or increased power loss) in the antenna, although the material properties accounting for the loss in the structure (conductivity and loss tangent) have not changed. The purpose of the current thesis is to study this reduction in the radiation efficiency for the case of small Microstrip Antennas and thereby develop possible techniques to improve the radiation characteristics of the antenna.

1.4 ORGANISATION OF THIS THESIS

This thesis is organized into six chapters. Chapter 1 serves as an introduction to challenges in antenna miniaturization with emphasis on antenna radiation efficiency. In chapter 2 the loss mechanism associated with miniaturizing a simple rectangular patch antenna is studied. It is shown that the loss in microstrip antenna may be reduced by improving the radiation conductance of the antenna or by replacing antenna materials with lower loss materials. In Chapter 3 the feasibility of micro/nano scale modification of conductors to achieve lower loss is investigated. The radiation conductance improvement technique of miniaturized H-Shaped patch antenna with multiple radiating parasitic elements is studied in chapters 4 and 5. The thesis is concluded in chapter 6, where a summary of the current work and the studies to be carried out in the future work are addressed.

1.5 CONCLUSIONS

This chapter presented an overview of antenna miniaturization techniques and the important challenges in the design of miniaturized antennas. It was seen that the efficiency reduction, by reducing the antenna size, is one of the key factors that limits the performance of small antennas. In the following chapters the radiation efficiency of microstrip patch antenna is discussed and techniques to improve the radiation efficiency are demonstrated.

Chapter 2

Effect of Miniaturization on the Efficiency of Microstrip Patch Antennas

2.1 INTRODUCTION

Several methods to miniaturize microstrip antennas were discussed in chapter 1, owing to their simplicity two of the most widely used techniques are dielectric loading and slot loading. In both cases the miniaturization was achieved through an increase of effective resonant dimension of the antenna. In this chapter the effect of miniaturization of a simple patch antenna, using an increased substrate dielectric constant is studied using well established literature. Following this, the concept is extended further for the case of miniaturization by slot loading of a square patch antenna using numerical simulations.

The power accepted by a microstrip antenna is mainly accounted for in four forms- the radiated power (P_r), the power lost due to the imperfections in the conductor (P_c), dielectric loss (P_d), and also the power loss in the form of surface wave (P_{sw}). Let the antenna be characterized by a simple cavity model. Then, each of P_r, P_c, P_d and P_{sw} are directly related to their respective slot conductances G_R, G_c, G_d and G_{sw} through which the input power leaks out of the cavity. Since, the antennas considered in the following discussions, are thin and of low dielectric constant, the surface waves may be neglected. The expressions for the powers P_r, P_c, and P_d are given by the following equations [8], [11].

$$P_r = \frac{1}{2\eta_0}\int_0^{2\pi}\int_0^{\pi/2}\left(|E_\theta|^2+\left|E_\phi\right|^2\right)r^2 sin(\theta)\, d\theta\, d\varphi \tag{2.1}$$

$$P_d = \frac{\omega\epsilon_0\epsilon_r tan(\delta)}{2}\iiint |E_z|^2\, dV = \omega tan(\delta) W_T \tag{2.2}$$

$$P_c = R_s \iint |H_s|^2\, ds \approx \frac{\omega W_T}{h\sqrt{\pi f \mu_0 \sigma}} \tag{2.3}$$

where E_θ and E_ϕ are the electric far field components in spherical coordinates and can be found from cavity model analysis, surface current distribution method or other full wave analysis methods [8], W_T is the total stored energy of the antenna at the resonant frequency f_r and is given by:

$$W_T = \frac{\epsilon_0\epsilon_r}{2}\iiint |E_z|^2 dV \tag{2.4}$$

where σ, ϵ_r and $\tan(\delta)$ are the conductivity of the conductor, permittivity and loss tangent of the substrate of height h respectively. The known loss-free cavity fields are used to evaluate the losses in the cavity by perturbation technique (in the cavity model). The dielectric losses are found by integrating the electric field (E_z) over the volume of the cavity and the conductor losses are found by integrating the normal component of magnetic fields (H_s) on the conductor surface, from these powers the conductances G_R, G_c and G_d are obtained from a given input voltage V_0 at the radiating slot, using the relation $P = ½\ G\ V_0^2$.

2.2 LOSSES IN RECTANGULAR MICROSTRIP PATCH ANTENNA

As an example let us now extend the discussion to a rectangular microstrip antenna of size $L \times W$ ($\alpha = W/L$), height h, on a substrate of dielectric constant ϵ_r and operating in

fundamental TM_{01} mode *for L>W>h*). The radiation conductance of the patch antenna is obtained by integrating the total radiated power, which can be obtained either from the cavity model, as described in [28] or, by using the Green's function approach given in [29]. However, The Green's function approach gives a better representation of the radiated fields in terms of the substrate effect, which the cavity model does not take into account. The radiation conductance thus obtained is given by [29]:

$$G_r = \frac{2}{Z_0^2}\frac{60\epsilon_{re}}{\pi}\int_0^{2\pi}\int_0^{\frac{\pi}{2}} \frac{cos^2\left(\frac{\pi\, sin\theta\, cos\phi}{2\sqrt{\epsilon_{re}}}\right)}{(sin^2\theta\, cos^2\phi - \epsilon_{re})^2}\, sinc^2\left(\frac{k_0\, W\, sin\theta\, sin\phi}{2}\right) sin\theta$$

$$\cdot\left[\frac{cos^2\theta sin^2\phi}{(\epsilon_r - sin^2\theta)\, cot^2\left(k_0 h\sqrt{\epsilon_r - sin^2\theta}\right) + cos^2\theta}\right. \tag{2.5}$$

$$\left. + \frac{(\epsilon_r - sin^2\theta)cos^2\theta\, cos^2\phi}{(\epsilon_r - sin^2\theta) + {\epsilon_r}^2 cos^2\theta cot^2\left(k_0 h\sqrt{\epsilon_r - sin^2\theta}\right)}\right] d\theta d\phi$$

where Z_0 is the characteristics impedance of the line of which the microstrip antenna is a part of (Appendix I).

The conductances associated with the copper and dielectric losses in the antenna are obtained from the fields under the patch using the cavity modal, and are given by [28], [8]:

$$G_c = \frac{\alpha\pi^2(\pi f_r \mu_0)^{-3/2}}{8h^2\sqrt{\sigma}} \tag{2.6}$$

$$G_d = \frac{\alpha\, \pi\, tan(\delta)}{8\mu_0 h\, f_r} \tag{2.7}$$

It can be seen from (2.6) and (2.7) that, the conductive losses depend on the conductivity of the medium and the dielectric losses depend directly on the loss tangent of the substrate. In addition to the material properties, other factors influencing losses are the stored energy, resonant frequency and the height of the substrate. The conductor and the dielectric losses become smaller as the resonant frequency and the thickness increase for a fixed mode structure. Also, the higher the stored energy the higher is the loss. Figure 2.1 shows the variation of the total conductance $G_T = G_R + G_c + G_d$, loss conductance $G_L = G_c + G_d$ and the radiation conductance (G_R), for a square patch on an infinite ground plane, with respect to the normalized physical length of the antenna, for different substrate heights. Here, the electrical length (or L_{eff}) of the antenna is varied by varying the dielectric constant of the substrate and the physical size is kept constant. It is clear here that, when the physical length of the antenna approaches the resonant free space half electrical length, G_t approaches G_R and G_L becomes less significant. Thus indicating power is lost through the structure dominantly in the form of radiation. On the other hand, as the antenna becomes smaller G_L increases considerably and G_R becomes smaller, so in this case G_T approaches G_L. Thus, the power is lost from the structure dominantly in the material imperfections. Figure 2.2 shows the equivalent fraction of the power lost through the conductive losses (P_d), dielectric losses (P_d) and the power radiated (P_r) by the antenna. It is clear here that when the antenna becomes smaller, conductive losses dominate both the dielectric loss and radiation. Thus, indicating the major cause of loss being the finite conductivity of the antenna. In order to investigate the extension of these discussions to other types of miniaturization techniques, in the following section a rectangular patch antenna with slots is investigated.

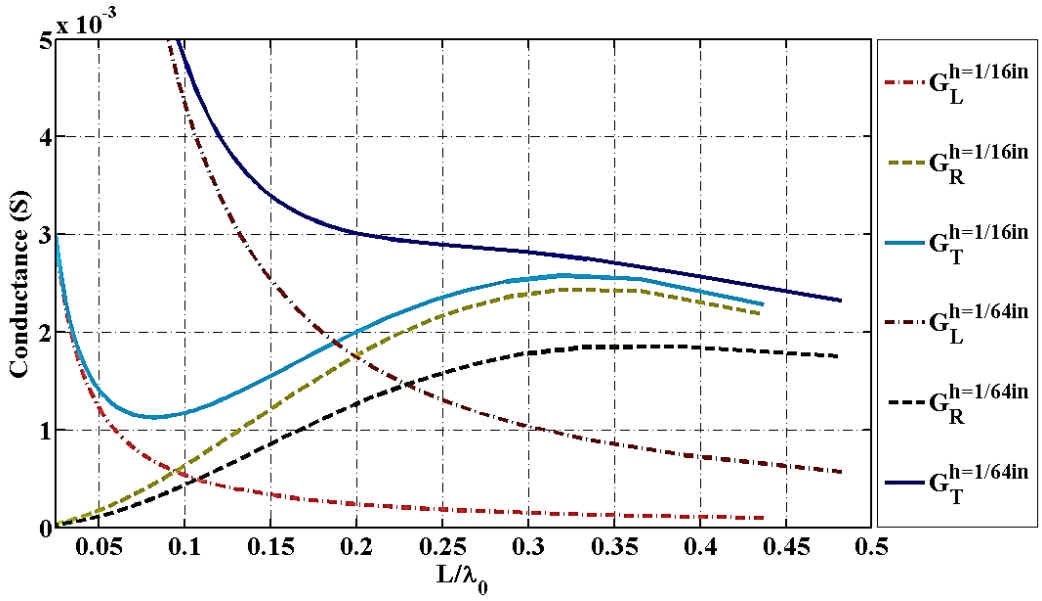

Figure 2.1 Variation of total conductance $G_T = G_R + G_c + G_d$, loss conductance $G_L = G_c + G_d$ and the radiation conductance (G_R) with normalized physical length for substrate heights h=1/64 and =1/16 inches. $\sigma = 5.8 \times 10^7$, tan(δ)=0.0018, L=W=0.015m on infinite ground plane

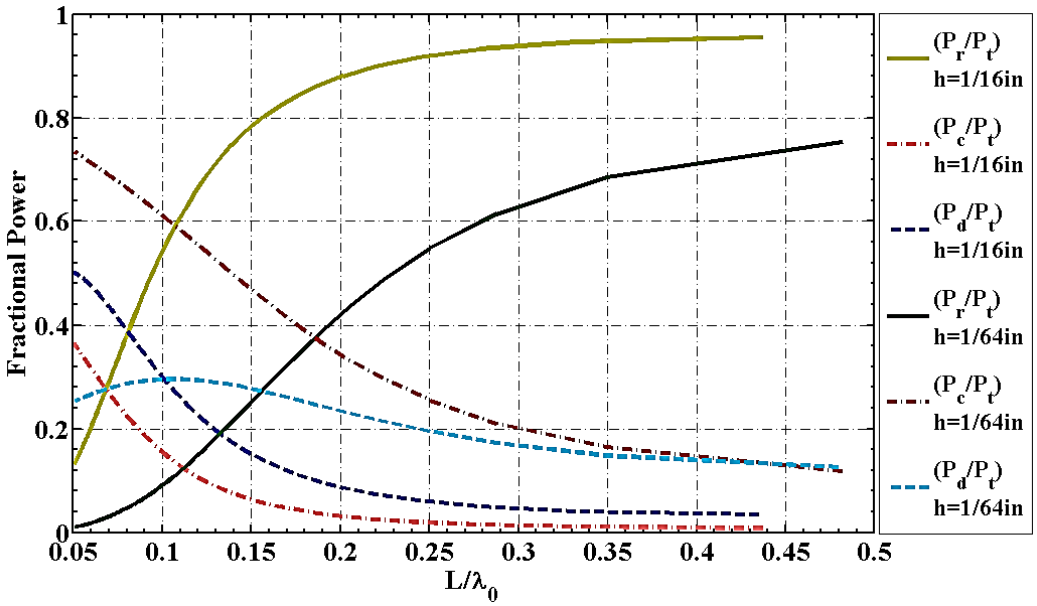

Figure 2.2 Variation of Radiated Power (P_r), Conductive loss (P_c) and Dielectric Loss (P_d) with antenna size for a square patch antenna of heights h=1/64 and =1/16 inches. $\sigma = 5.8 \times 10^7$, tan(δ)=0.0018, L=W=0.015m. On infinite ground plane, here P_t is the total accepted power

It can further be seen from (2.6) and (2.7) that for the given mode, the loss conductances G_c and G_d are inversely proportional to the frequency. If the frequency, substrate, conductors and the aspect ratio ($\alpha = W/L$) of the patch are not changed, the loss conductance (G_L=G_c+G_d) does not change even if the antenna is miniaturized. This indicates that the loss in such case accounts from reduction in the radiation conductance reduction, which causes a higher fraction of the power accepted by the antenna to be dissipated through the loss conductance though they might be small.

2.3 LOSSES IN MINIATURIZED H-SHAPED PATCH ANTENNA

One of the popular methods of miniaturization of rectangular patch antenna is by the addition of slots and notches. Various shapes may be obtained by positioning the slots/notches at different locations on the patch antenna, U-shaped, C shaped, H shaped and square annular ring being the popular ones. The H-shaped patch antenna is made by adding two notches at non-radiating edges of the rectangular patch antenna (Figure 2.3). The total slot conductance for the case of a regular rectangular patch antenna can be easily obtained from its input impedance by using the known sinusoidal current distribution [8]. However, with the addition of slots the current distribution on the patch antenna and the fields inside the cavity perturbs, making it difficult to analytically determine the input impedance. Hence, in the current work numerical simulations are used to obtain the variation of total conductance at the radiating edge of the H-shaped patch using the commercially available Finite Element Method Solver – HFSS. For the initial design of the H-shaped patch, depending on the length and width of the notches the approximate resonant effective length

and width of the antenna may be calculated by taking account of changes in the current distribution on the patch for small values of S_L [13]:

$$L_e = L + S_L$$

$$W_e = \frac{W(L - S_w) + (W - S_L)S_w}{L}$$

For $S_L > 0.8 \times W/2$ the effective length is modified and is given by [13]:

$$L_e = L + 2S_L$$

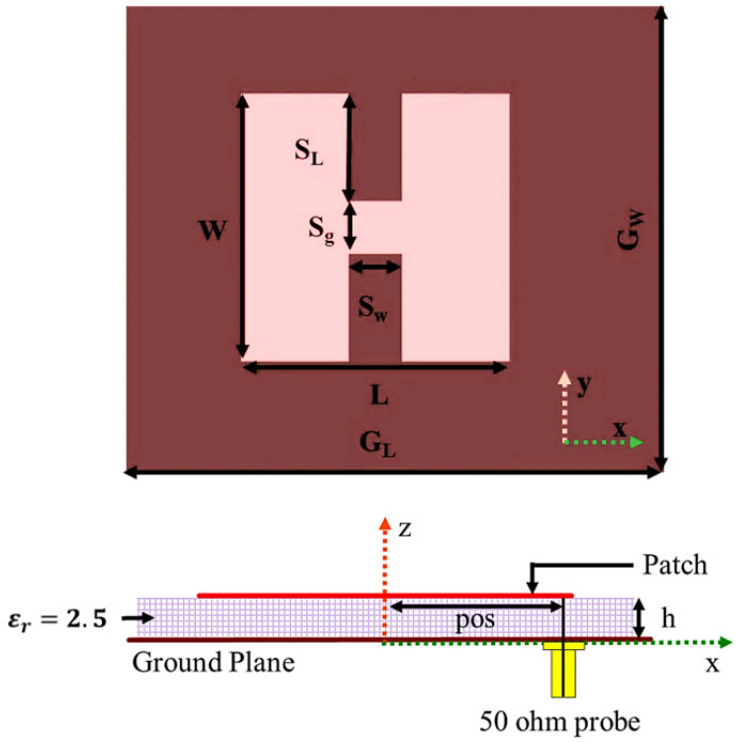

Figure 2.3 Geometry of H-Shaped Patch Antenna L= W = 20mm, S_w= 4mm, Substrate height h=0.031in, ε_r=2.5, loss tangent tan(δ) = 0.0018, ground plane size = 50mm×50mm, probe position the pos = 9.5mm

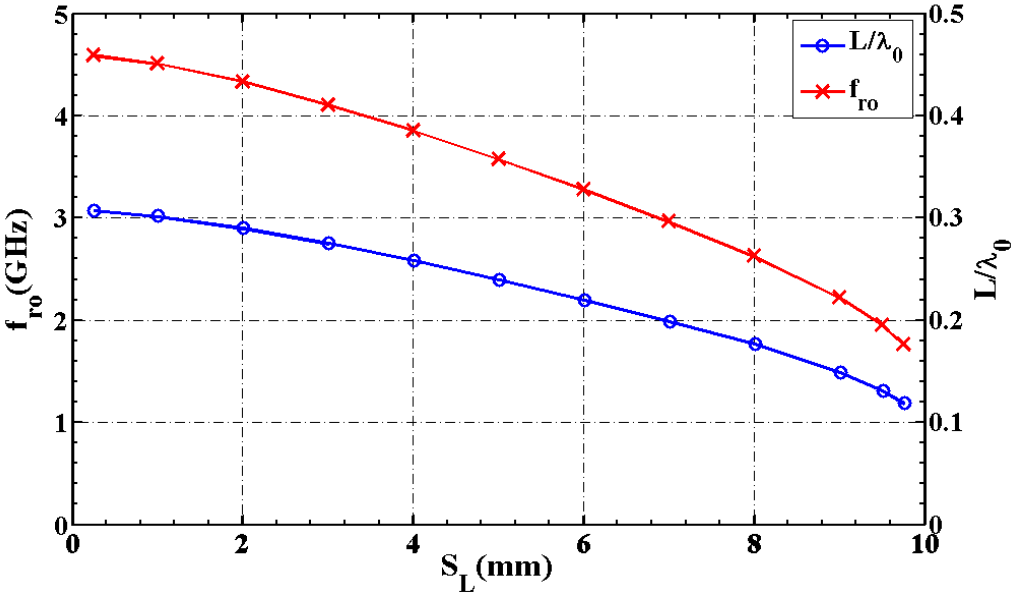

Figure 2.4 Resonant frequency and Resonant Length of the Antenna shown in Figure 2.3 for different values of Slot Length S_L

Using these values of L_e and W_e and the well-known equations for the resonant frequency of Rectangular patch antenna (Appendix I) [8], [11], the approximate resonant frequencies for different values S_L and S_w can be obtained for the H-Shaped patch antenna. Figure 2.3 shows the geometry of the H- Shaped Patch antenna under consideration**.** Figure 2.4 shows the variation of resonant frequency and size of the H-Shaped patch antenna with the increase in the slot length, while all other parameters of the antenna being kept constant.

Simulations corresponding to a range of electrical sizes where the material losses do not start to dominate were carried out. The feed is placed at the edge of the patch to obtain the approximate values of total conductance G_T. This is shown in Figure 2.5. The simulations include the factors like the effect of slot conductance from the non-radiating edges of the patch, presence of the probe with a finite diameter, contribution of higher order modes with probe position and reflections from the finite sized ground plane, which were neglected in the

analytical cavity model, described in the previous section for the simple rectangular patch antenna. But it should however, be noted that the separation of G_t into the individual conductance, due to radiation G_r, conductor loss G_c and dielectric loss G_d from the simulated data is a fairly difficult task and is not attempted here. In Figure 2.6 , Figure 2.7 and Figure 2.8 the reduction in gain and efficiency of the H-shaped patch antenna with the reduction in resonant length of the antenna are shown. These results show a similar trend seen for the case of miniaturization of patch antenna using a substrate with high dielectric constant. Thus, it is inferred that the major loss in Gain or efficiency with miniaturization comes from the reduction in the Radiation Conductance G_r of the antenna and the increase in the energy density within the small volume, causing a higher fraction of the power being dissipated in the volume of the dielectric G_d and the conducting walls G_c.

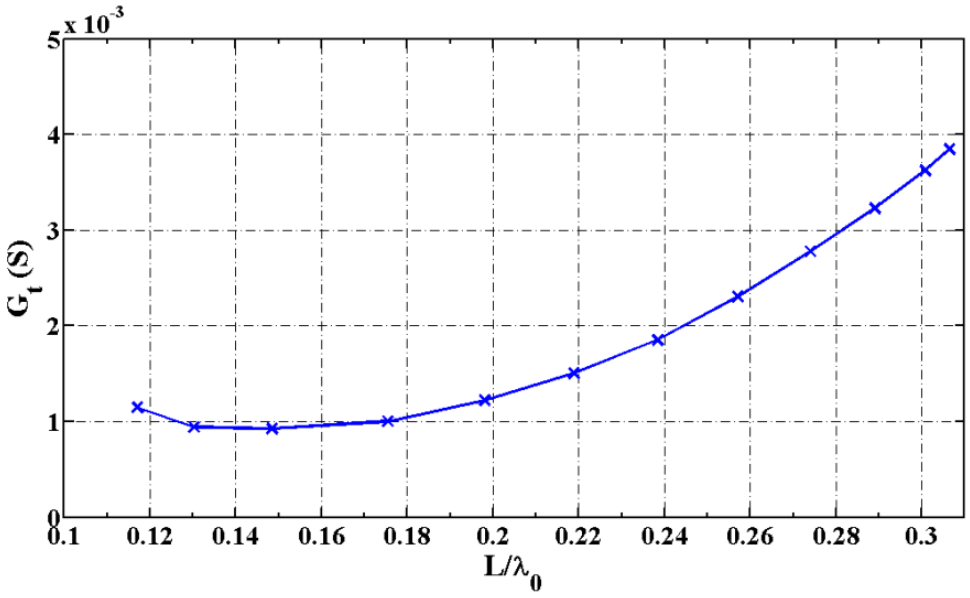

Figure 2.5 HFSS results showing total conductance G_t for the H-Shaped Patch Antenna shown in Figure 2.3 for different values of resonant lengths

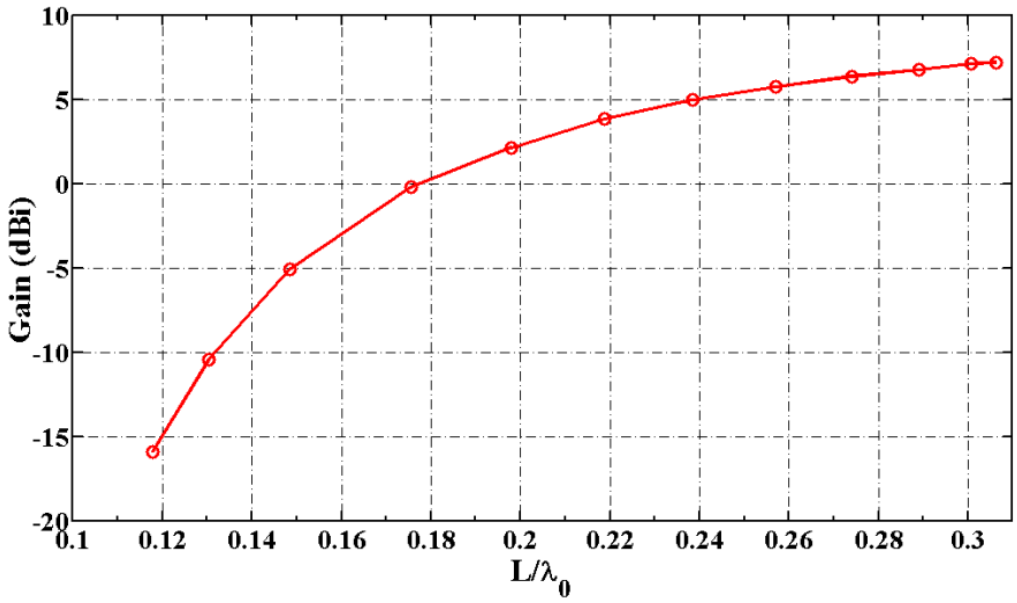

Figure 2.6 HFSS results showing the Peak Gain of the H-Shaped Patch Antenna shown in Figure 2.3 different values of resonant lengths

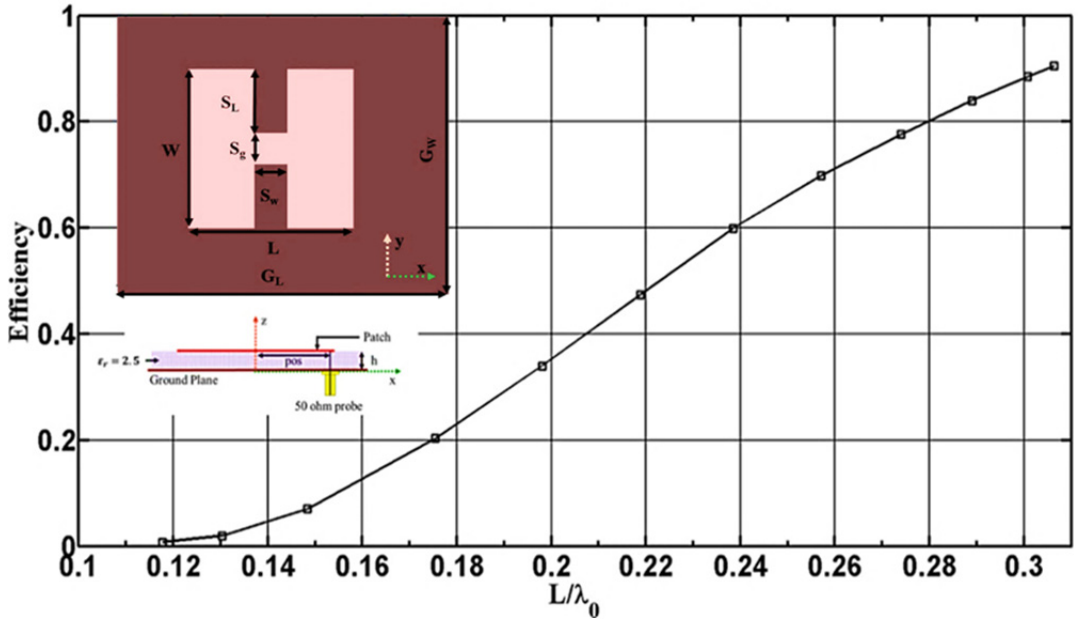

Figure 2.7 HFSS results showing the radiation efficiency of the H-Shaped Patch Antenna shown in Figure 2.3 for different values of resonant lengths

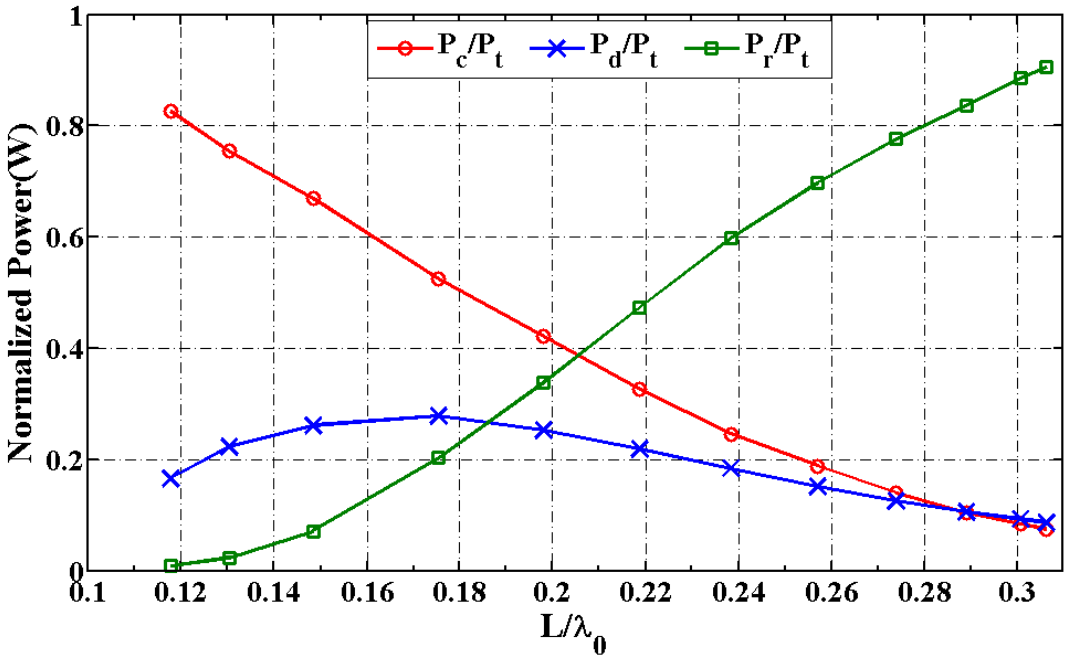

Figure 2.8 HFSS results of the variation in fractional power distribution into P_r, P_c, and P_d for the H-Shaped Patch Antenna shown in Figure 2.3 with antenna size, where P_t is the total input power

From the definition of Gain ($G = \eta_{rad} D$, where G is the Gain, η_{rad} is the radiation efficiency and D the directivity) of an antenna, any loss in efficiency would account for a drop in the gain and any increase in the efficiency would account for an increase in the gain of the antenna as long as the radiation patterns remain the same. It should however be kept in mind here that, the gain is also dependant on the ground plane size (G_L/λ_0), at the operating frequency [30], [31]. In the current case since the ground plane size is constant, with miniaturization the size of the ground plane with respect to the operating frequency becomes smaller, thus causing higher levels of back lobes (Figure 2.9**)**. Nevertheless, for the cases with sufficiently large ground plane size the radiation patterns remained the same, thus for these cases the efficiency drop could be directly deduced from the drop in the gain of the antenna.

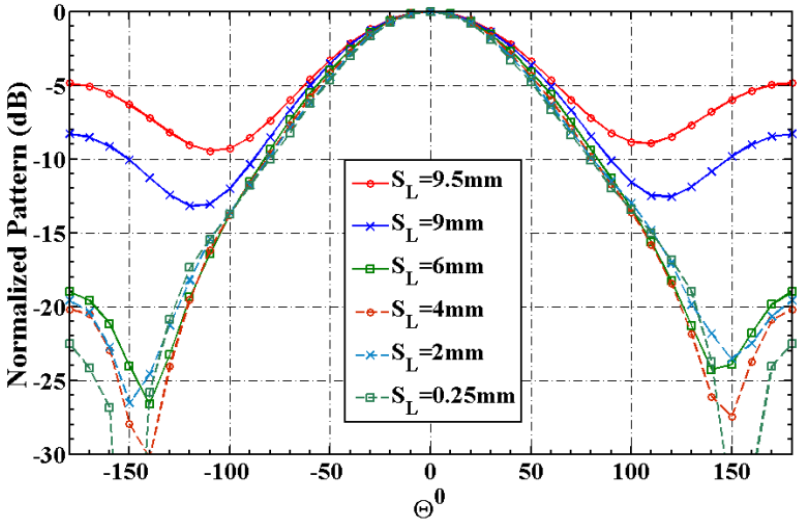

Figure 2.9 Normalised E-Plane Pattern of the H-Shaped Patch Antenna shown in Figure 2.3 for different resonant lengths

To improve the efficiency of the antenna, the two obvious ways are to either increase the fraction of power radiated, or decrease power loss associated with the antenna. In other words, the radiation conductance (G_R) of the antenna has to be increased and the loss conductance ($G_L=G_c+G_d$) has to be decreased. It is apparent here that to decrease G_L, the antenna, material losses has to be reduced or the height of the Antenna has to be increased. However, increasing the height causes a larger fraction of the power to be coupled into the surface waves which in turn causes spurious radiation and unwanted interferences with the antenna radiation patterns [29].

On the other hand, to increase the radiation conductance of the antenna the shape or geometry of the antenna has to be modified. The radiation conductance of a rectangular microstrip patch antenna does not change much when W/λ_0 is considerably large. For smaller values of W/λ_0, G_R is found to increase with increase in h and W [8]. Having W>L also gives increased radiation conductance, bandwidth and efficiency, but a proper excitation has to be chosen to avoid undesirable modes ($1<W/L<2$ is usually recommended) [8].This

however increases the foot-print of the antenna considerably. Nevertheless, for the type of antenna and different levels of miniaturization, G_r is found to converge as the antenna becomes smaller (L< radian length ($\lambda_0/2\pi$)), similar to the behaviour of electrically small dipole antennas, where the radiation resistance reduces with the size reduction [32].

2.4 CONCLUSIONS

In this chapter the effect of miniaturization of microstrip antenna on its efficiency was studied. It was shown that the power loss in an antenna made of low loss materials comes dominantly from the reduction of the radiation conductance of the antenna. This effect was studied in the two different techniques of miniaturization, namely – using the high dielectric constant and slot loading. Further, a discussion on the efficiency improvement by reducing the loss conductance of the antenna and increasing the radiation conductance, was presented. The first may be achieved through changes in the material, and the later by geometrical modifications.

Chapter 3

Study of 1-D Metallo-Dielectric Layered Medium for Loss Reduction

From the discussions seen in the previous chapters, it is clear that the loss in small antennas is an important problem. It was shown in chapter 2 that the loss accounted for the finite conductivity of conductors, dominates as the antenna becomes smaller and operates at larger wavelengths. It was also clear that the loss in patch antennas can be reduced fundamentally by either reducing the loss conductance or by increasing the radiation conductance. The loss conductance of the antenna mainly depends on the material properties and the radiation conductance inherently depends on the antenna shape or geometry. In this chapter, study on artificial material modification at micro/nano scale, to reduce the loss at microwave frequencies in naturally occurring conducting media is carried out.

3.1 Loss in Conductors

It is well known that when an electromagnetic wave propagates in a medium with high conductivity its amplitude decays exponentially. At high frequencies, this causes the fields to be confined almost entirely to a very thin sheet (thickness-δ) on the surface of the conductor, causing a higher resistive loss in the structure than expected from its operation at low frequency/d-c characteristics [33] [34]. This is illustrated in the following discussion.

For a plane wave having a frequency ω rad/sec propagating in a linear, isotropic and homogenous conducting medium of permittivity ϵ F/m, permeability μ H/m and conductivity σ S/m, the propagation constant is given by

$$\gamma = \alpha + j\beta = \sqrt{(j\omega\mu)(\sigma + j\omega\epsilon)} \qquad m^{-1} \qquad (3.1)$$

which may be rearranged as

$$\gamma = \sqrt{(j\omega\mu\sigma)\left(1 + j\frac{\omega\epsilon}{\sigma}\right)} \qquad m^{-1} \qquad (3.2)$$

For good conductors the conductivity is high and $\frac{\omega\epsilon}{\sigma} \ll 1$, therefore

$$\gamma \approx \sqrt{j\omega\mu\sigma} \qquad m^{-1} \qquad (3.3)$$

Thus, the attenuation constant (α) and phase constant (β) are,

$$\alpha \approx \beta \approx \sqrt{\frac{\omega\mu\sigma}{2}} \qquad (3.4)$$

The phase velocity (v) and the intrinsic impedance (η) in the conductor may be then obtained as

$$v = \frac{\omega}{\beta} = \sqrt{\frac{2\omega}{\mu\sigma}} \qquad ms^{-1} \qquad (3.5)$$

$$\eta = \sqrt{\frac{j\omega\mu}{\sigma + j\omega\epsilon}} \approx \sqrt{\frac{j\omega\mu}{\sigma}} \approx \sqrt{\frac{\omega\mu}{\sigma}}\angle 45° \qquad \Omega \qquad (3.6)$$

From these equations (3.1-3.6) it is seen that for good conductors, the attenuation and phase constants (α & β) are high. That is, the wave attenuates rapidly as it propagates through the

conductor and it also undergoes rapid phase shifts per unit length. The velocity of the wave and intrinsic impedance are small.

The penetration depth or the skin depth (δ) of a conductor is defined as that depth in which a wave propagating in the medium has been attenuated to 1/e (or ~37%) of its original value and is given by (3.7). It can be seen here that, the skin depth gets reduced as the frequency of operation goes high

$$\delta = \frac{1}{\alpha} \approx \sqrt{\frac{2}{\omega\mu\sigma}} \qquad m \qquad (3.7)$$

The surface Impedance (Z_s) is often used to model the loss in conductors, coming from the confinement of most of the field across the skin depth at the surface of the conductor. For a thick good conductor ($t_c >> \delta$) the surface impedance is related to the material properties as

$$Z_s = \sqrt{\frac{j\omega\mu}{\sigma}} \qquad \Omega \qquad (3.8)$$

The surface resistance and the reactance is deduced from (3.8) as

$$R_s = X_s = \sqrt{\frac{\omega\mu}{2\sigma}} = \frac{1}{\sigma\delta} \qquad \Omega \qquad (3.9)$$

The surface resistance of a flat conductor at any frequency is equal to the d-c resistance of a thickness δ of the same conductor. Thus, the power loss per unit area of a plane conductor is $J^2 R_s$, where J is the current density in the conductor.

3.2 LAMINATED CONDUCTORS FOR REDUCTION OF SKIN EFFECT LOSSES

From the discussion in the previous section it is apparent that in order to reduce the loss or improve the efficiency of a conducting medium at high frequencies, the surface resistance of the material has to be reduced. From equation (3.9) it is seen that the conspicuous way to achieve this without changing the conductivity of the medium is by increasing the depth of penetration of the electromagnetic wave. Several attempts have previously been made by researchers to achieve this. In [35], it was shown by the author that if a thick conductor is replaced by conductors of many insulated laminae or filaments of the same material, with transverse dimension smaller than that of skin depth and arranged parallel to the flow of current, then at the frequency of operation the waves will penetrate more into the conducting medium. It was shown that the skin depth of the effective medium is increased at the desired frequency. For the case of coaxial line with center conductor replaced with laminated filaments of conducting segments, it was seen that the new transmission line had a higher initial attenuation, but remained constant at higher frequencies. At high enough frequencies the attenuation of the laminated line rises at a rate directly proportional to frequency, and then eventually approaches the attenuation of the thick single conductor line [35]. This technique were used to demonstrate efficiency improvement in travelling wave structures like coaxial cable and parallel plate waveguides used to carry large power at lower end of radio frequencies.

With the advancement in fabrication techniques at micro/nano scales, similar techniques to achieve unique characteristics, otherwise unusual, have been developed at optical scales in metals. It was shown in [36] that the transmissive properties of metals can be altered by using alternate layers of metals and dielectrics. It was demonstrated that the

concept of skin depth loses its meaning in the case of a periodic structure, in the presence of closely spaced boundaries. That is, spatial discontinuities of the index of refraction, alters the physical properties like effective group velocity near the band edge, reflection coefficient, transmission coefficient and absorption coefficient of the structure. By using periodic arrangements of metal-dielectric interfaces of thicknesses of the order of skin depth, it was shown by the authors [36] that frequency selective transmission (~65%) of visible light may be achieved using metals which are otherwise used only for reflective applications.

Recently similar techniques have been applied to microwave components like filters [37], resonators [38] and antennas [39], for their improvement in quality factor by ohmic loss reduction. In [38] a circular disc microstrip resonator was constructed using laminated conductors of sub-micron thickness. It was shown that by optimizing the thickness of the laminations the electromagnetic waves penetrated deeper at the resonant condition. It was also shown that with the increase in the number of laminated conductors the surface resistance of the material decreased, and thus improving the Q factor of the resonator. In the following section, the possibility of extension of these techniques to miniaturized antennas for efficiency improvement is studied using plane wave incidence. Firstly the plane wave problem is solved using the Transfer Matrix Method, the results of which are then verified using HFSS simulations.

3.3 Plane Wave Incident on a 1-D Layered Medium using Transfer Matrix Method (TMM)

Antennas are largely employed for the reception of information in the form of plane waves. Hence, to evaluate the application of laminated conductors to antennas, consider normal

incidence of a plane wave from free space on alternate layers of conducting and dielectric media along the z-axis, as shown in Figure 3.1. The layers extend to infinity in both x and y directions. Previously in [39] & [40] this problem was investigated by using the incident and reflected wave equations in each media and solving for its amplitude coefficients by applying boundary conditions at each dielectric-conductor interface. This method however, when used for highly conductive thin layers encounters difficulties with matrix inversions. In the current work the same is solved using the Wave Matrix Method [41].

Let each layer in Figure 3.1 assumed to be -homogenous and isotropic, its intrinsic properties can be represented by μ_0, ϵ_0, σ_0, μ_1; ϵ_1, σ_1, μ_2, ϵ_2, σ_2; μ_3, ϵ_3, σ_3 . . . μ_i, ϵ_i, σ_i . . . μ_n, ϵ_n, σ_n. Here, μ, ϵ and σ have their usual meanings, and then the reflection coefficient of a wave incident from medium 'i-1' is given by

$$R_i = \frac{Y_{i-1} - Y_i}{Y_{i-1} + Y_i} \tag{3.10}$$

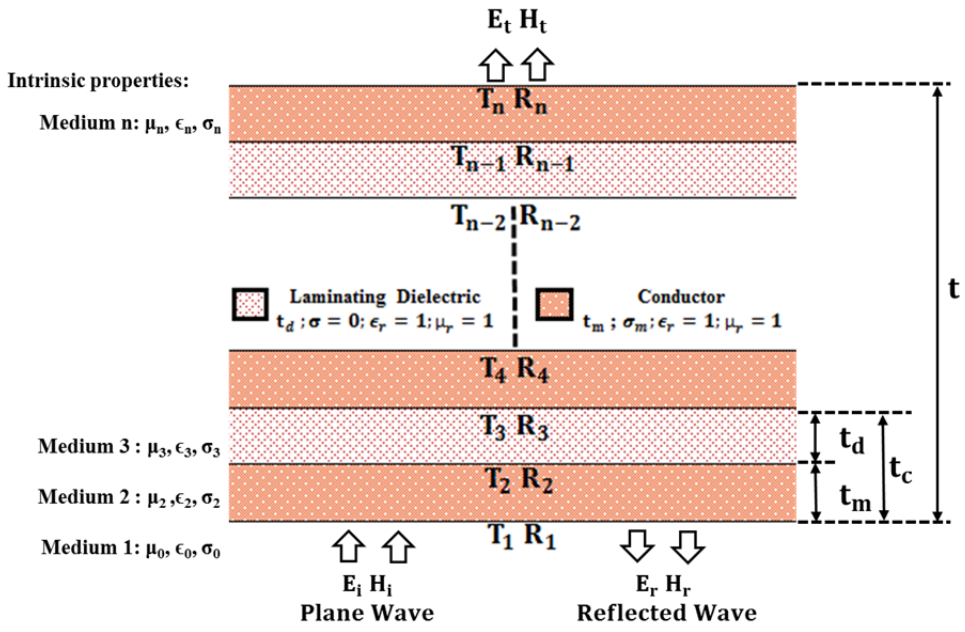

Figure 3.1 Structure of 1D Metallo-Dielectric Medium

Similarly the transmission coefficient of a wave incident from medium 'i-1' to medium 'i' is given by:

$$T_i = 1 + R_i \tag{3.13}$$

where Y_i is the wave admittance of the medium 'i', directly related to its intrinsic properties by

$$Y_i = \sqrt{\frac{\sigma_i + j\omega\epsilon_i}{j\omega\mu_i}} \tag{3.14}$$

For time harmonic waves propagating in the forward and backward directions along the z-axis in medium 'i' the wave functions can be denoted by:

$$A_i e^{j\gamma_i z} \;\&\; B_i e^{-j\gamma_i z} \tag{3.15}$$

, where γ_i is the propagation constant of the medium 'i' and is given by:

$$\gamma_i = \sqrt{(j\omega\mu_i)(\sigma_i + j\omega\epsilon_i)} \tag{3.16}$$

If each medium is of thickness 't_i' then the amplitude of the output wave in medium (n+1) is related to the amplitude of the input wave by the wave propagation matrix:

$$\begin{bmatrix} A_1 \\ B_1 \end{bmatrix} = \prod_{i=1}^{n} \frac{1}{T_i} \begin{bmatrix} e^{j\gamma_i t_i} & R_i e^{-j\gamma_i t_i} \\ R_i e^{j\gamma_i t_i} & e^{-j\gamma_i t_i} \end{bmatrix} \begin{bmatrix} A_{n+1} \\ B_{n+1} \end{bmatrix} \tag{3.17}$$

$$\begin{bmatrix} A_1 \\ B_1 \end{bmatrix} = \begin{bmatrix} C_{11} & C_{12} \\ C_{21} & C_{22} \end{bmatrix} \begin{bmatrix} A_{n+1} \\ B_{n+1} \end{bmatrix} \tag{3.18}$$

Let the amplitude of the input wave A_1 = 1 V/m, and assume that the last medium is infinite in extent therefore there is no reflected wave or B_{n+1}=0, we have the relations:

$$A_{n+1} = A_1 / C_{11} \tag{3.19}$$

$$B_1 = C_{21} A_{n+1} \tag{3.20}$$

Now that the transmitted and reflected field amplitudes are known, the total power lost in the medium can be calculated by using the expression:

$$\text{Power Loss} = \frac{1}{2\eta} - \frac{|A_{n+1}|^2}{2\eta} - \frac{|B_1|^2}{2\eta} \tag{3.11}$$

where $\eta = 1/Y_0 = 1/Y_{n+1}$ is the free space wave impedance.

For performing numerical calculations here, each laminated conductor layer $t_c=t_d+t_m$ comprises of a conducting layer with an infinitesimal thickness (t_m) and the laminating dielectric layer having a thickness (t_d) around the skin depth. The permittivity and the permeability of the media are taken to be $\epsilon = \epsilon_0 = 8.854 \times 10^{-12} \frac{\text{F}}{\text{m}}$ and $\mu = \mu_0 = 4\pi \times 10^{-7}$ H/m for the given frequency range of 1GHz to 10 GHz.

For an incident power of 1.3mW, the power lost for two different variations of laminated conductors, namely with progressively increasing overall thickness (Figure 3.2), and with constant overall thickness, (Figure 3.3), were obtained for different number of conducting layers. Figure 3.4 shows the loss in a single conductor with different thicknesses. To aid in easy simulation and verification of results using HFSS software, in all the cases the conductivity of the metallic layer was chosen to be $\sigma_m = 10^5$ S/m. The results were obtained numerically using MATLAB (Appendix II).

The region between the two conducting layers, in all the cases, was taken to be loss free. It is seen that changing the dielectric constant between the conducting layers had no effect on the power loss and the same plot as that of Figure 3.2 and Figure 3.3 were obtained. To avoid redundancy, these results are not shown explicitly.

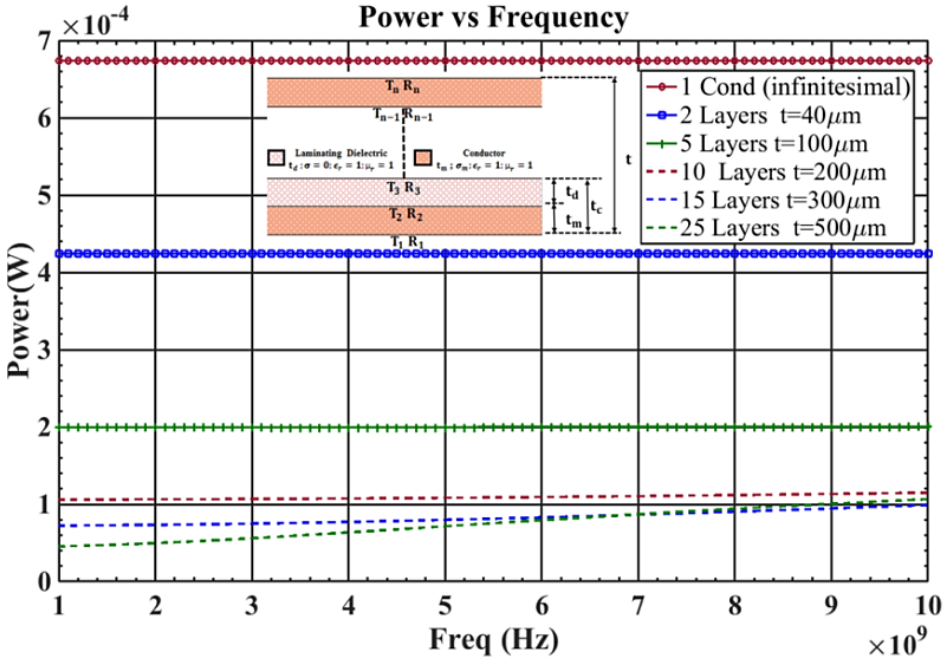

Figure 3.2 TMM Results: Loss in multiple laminated conducting layers instead of a single conducting layer. Total thickness (t) increasing progressively with number of layers, $t_d = 20 \times 10^{-6}$µm, $t_m = 0.125 \times 10^{-6}$µm, $\sigma_m = 10^5$ S/m Skin depth is 50.3µm at 1 GHz.

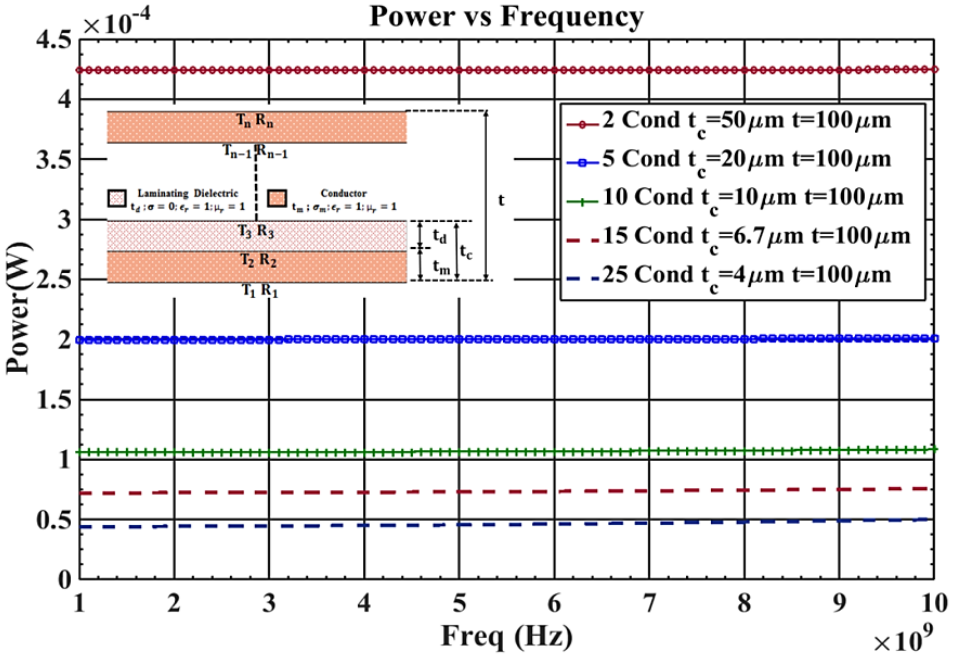

Figure 3.3 TMM Results: Loss in multiple laminated conducting layers instead of a single conducting layer. Total thickness (t) is constant, $t_c = t_m + t_d$, $t_m = 0.125 \times 10^{-6}$µm, $\sigma_m = 10^5$ S/m Skin depth is 50.3µm at 1 GHz.

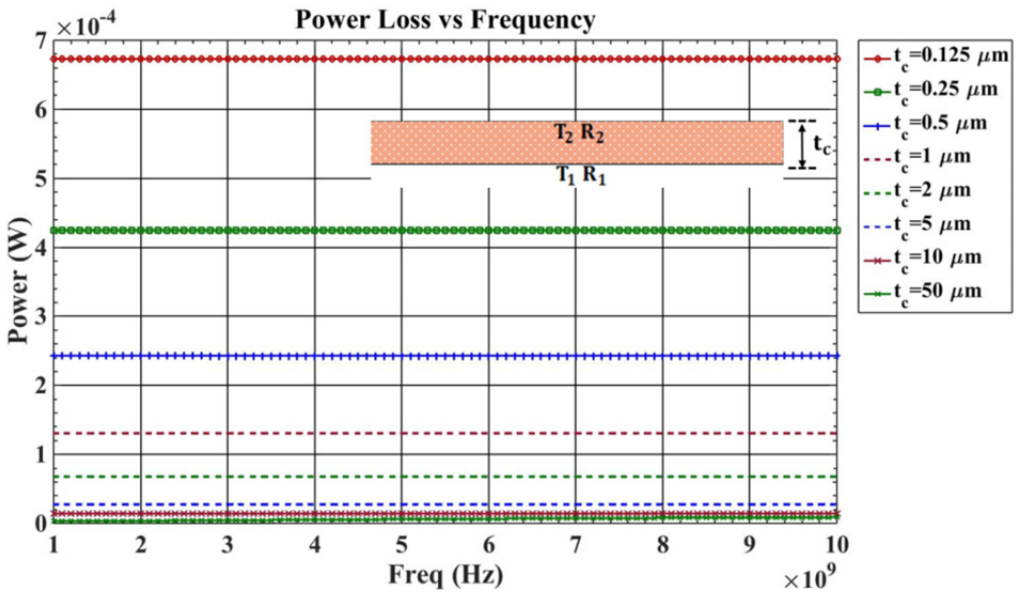

Figure 3.4 TMM Results: Loss in single conductor with different thicknesses $t_m = t_c$, $\sigma_m = 10^5$ S/m Skin depth is 50.3μm at 1 GHz.

3.4 PLANE WAVE INCIDENT ON 1-D LAYERED MEDIUM USING HFSS

The results obtained using the TMM method is verified using the Finite Element Solver HFSS. In order to model plane wave incidence on the 1-D layered media, infinite in two dimensions, the parallel plate waveguide technique is used. In this technique a parallel plate waveguide is obtained by establishing appropriate boundary conditions and 2-port TEM wave assignments as show in Figure 3.5 and Figure 3.6. The power lost inside the medium under the test is easily obtained from the two port S-parameters. The results thus obtained are given in Figure 3.7 to Figure 3.9. Similar to the TMM analysis, for an incident power of 1.3mW, the power lost for two different variations of laminated conductors, namely with progressively increasing overall thickness (Figure 3.7), and with constant overall thickness (Figure 3.8), were obtained for different number of conducting layers. Figure 3.9 shows the loss in a single conductor with different thicknesses.

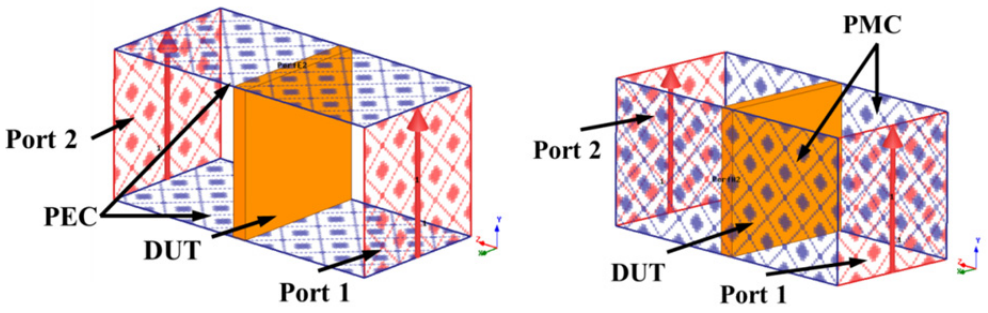

Figure 3.5 Illustration of parallel plate waveguide simulation in HFSS showing perfect electric PEC boundary, perfect magnetic PM boundary, ports and solid conductor.

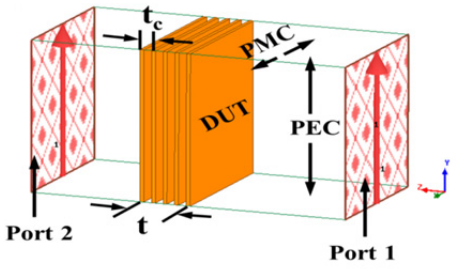

Figure 3.6 Illustration of parallel plate waveguide simulation in HFSS showing perfect electric PEC boundary, perfect magnetic PM boundary, ports and laminated conductor.

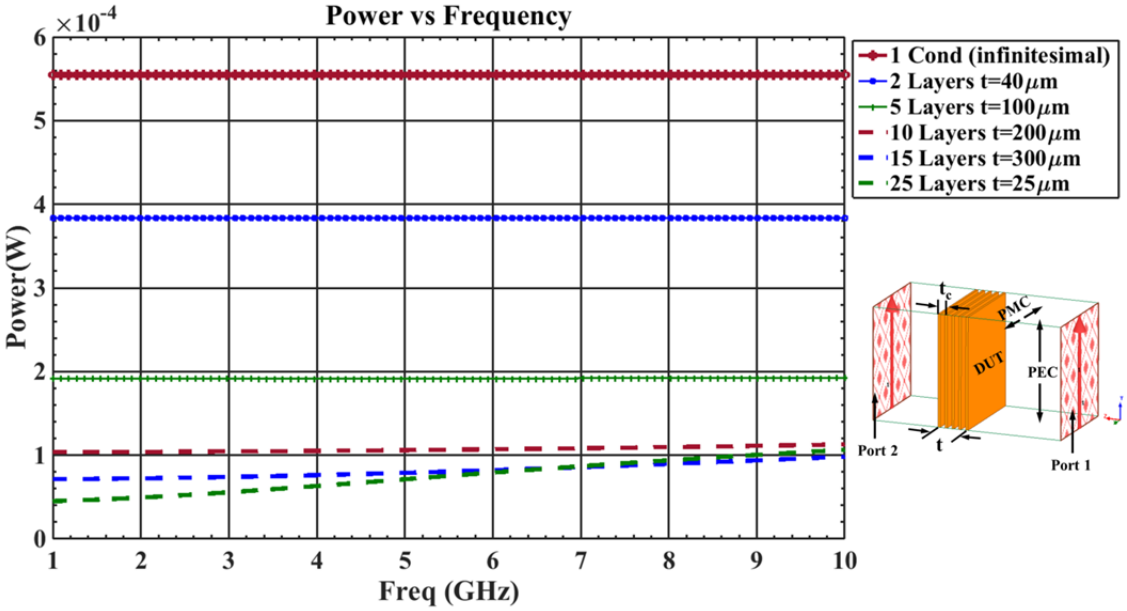

Figure 3.7 HFSS Results: Loss in multiple laminated conducting layers instead of a single conducting layer. Total thickness (t) increasing progressively with number of layers, $t_d = 20 \times 10^{-6}$µm, $t_m = 0.125 \times 10^{-6}$µm, $\sigma_m = 10^5$ S/m Skin depth is 50.3µm at 1 GHz.

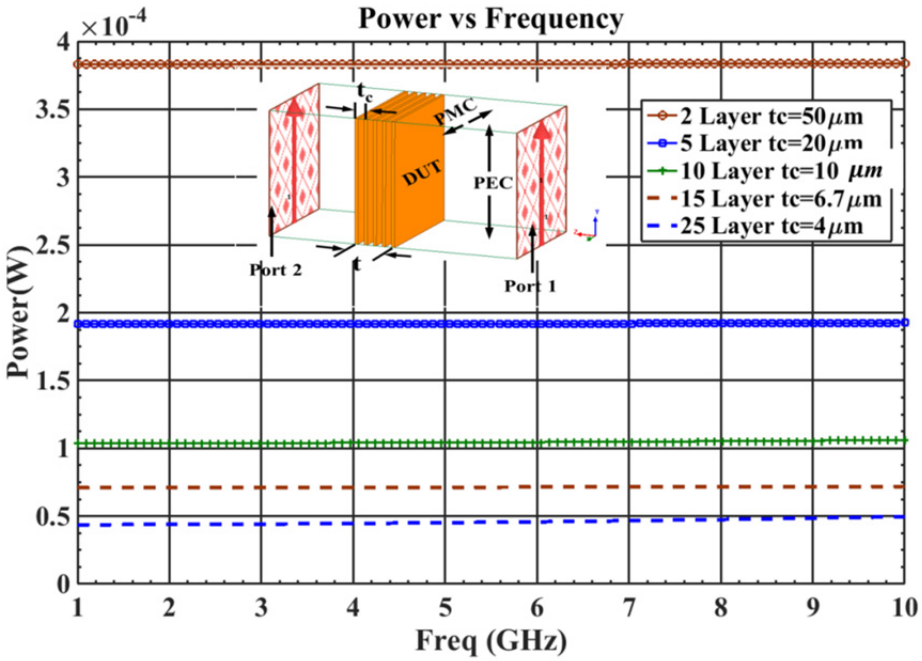

Figure 3.8 HFSS Results: Loss in multiple laminated conducting layers instead of a single conducting layer. Total thickness (t) is constant; $t_c = t_m + t_d$, $t_m = 0.125 \times 10^{-6}$μm, $\sigma_m = 10^5$ S/m Skin depth is 50.3μm at 1 GHz

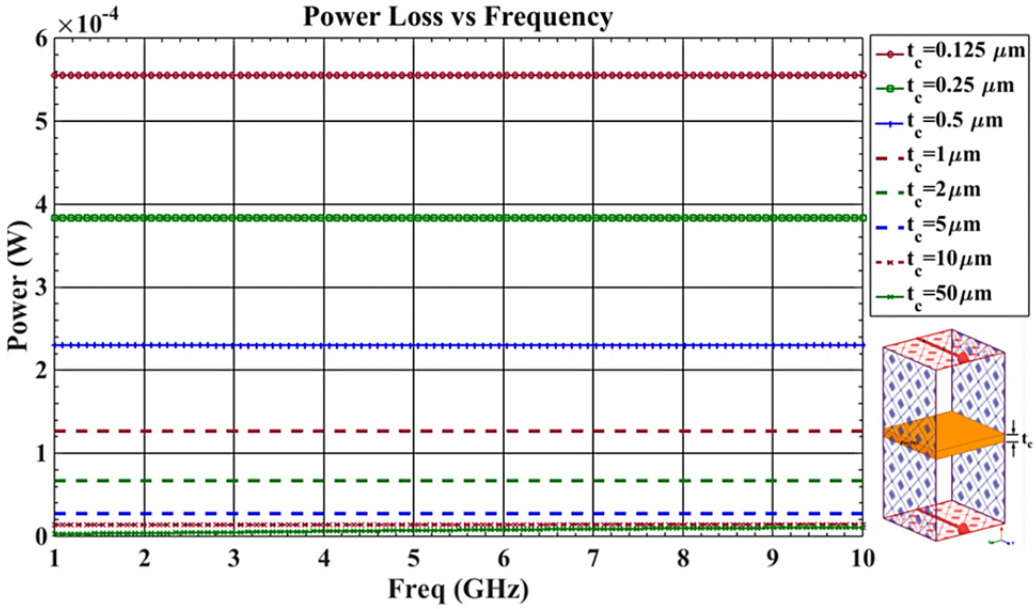

Figure 3.9 HFSS Results: Loss in single conductor with different thicknesses $t = t_m = t_c$, $\sigma_m = 10^5$ S/m Skin depth is 50.3μm at 1 GHz

Table 3-I
Comparison of HFSS and TMM methods for the case of increasing overall thickness t of the Multilayered medium with $\sigma_m = 10^5$ S/m Skin depth is 50.3μm at 1 GHz

No. of Layers	t(μm)	Power Loss (mW)	
		TMM	HFSS
1	0.125	0.78	0.58
2	40	0.42	0.38
5	100	0.20	0.20
10	200	0.10	0.10
15	300	0.08	0.08
25	500	0.04	0.04

Table 3-II
Comparison of HFSS and TMM methods for the case of constant overall thickness t of the Multilayered medium with $\sigma_m = 10^5$ S/m Skin depth is 50.3μm at 1 GHz

No. of Layers	t_c(μm)	Power Loss (mW)	
		TMM	HFSS
1	0.125	0.78	0.58
2	50	0.43	0.39
5	20	0.2	0.2
10	10	0.1	0.1
15	6.7	0.053	0.053
25	4	0.05	0.05

Table 3-III
Comparison of HFSS and TMM methods for single conductor case $\sigma_m = 10^5$ S/m Skin depth is 50.3μm at 1 GHz

$t_m=t_c=t$ (μm)	Power Loss (mW)	
	TMM	HFSS
0.125	0.78	0.58
1	0.12	0.12
2	0.8	0.8
5	0.04	0.04
10	0.01	0.01
50	0.01	0.01

Tables 3-I to 3-III show a comparison of HFSS and TMM solutions for the three cases considered in the above discussion. Both TMM and HFSS results show close agreement, especially for the case of thick media. However when the thicknesses are small, there are deviations. These deviations in the simulated results may be attributed to the finite number of

meshes that HFSS utilizes for the calculation of fields inside the conducting medium [42]. Though increasing the number of meshes by user defined options might decrease the error, this would require a large amount of meshes inside the conductor, which in turn would require large computational time and memory, hence this was carried out here.

3.5 DISCUSSION OF RESULTS

In the two cases of multiple laminated conductors of infinite extent considered here, both TMM and HFSS results show that significant loss reduction occurs even when a few number of laminated conductor layers (2 or 5) are used. Although with 15 layers or more, the loss reduction can be observed, however, after 25 layers, the loss reduction is not significant, but still the power loss is less than that of the single layer of infinitesimal thickness (t_m=0.125μm). It should however be noted that, in either cases the loss reduction achieved does not exceed the case of a single conductor of thickness equal to or greater than the skin depth as indicated by the results in Figure 3.4 (TMM) and Figure 3.9 (HFSS). This technique may be generally suited for applications involving thin conductors with high loss like Transparent Conductor Oxides as demonstrated in [43]. These results were found to be in close agreement with that of the results previously obtained in [39]. However, the conclusion drawn here is in contrary to [39]. Unlike here, in [39] comparisons between the power lost through a single thick conductor ($t_m \geq \delta$) and the layered medium of the given infinitesimal thickness (t_m =0.125um) were not provided. This has led the authors in [39] into false conclusions. The conductors used in the experimental verification of [39] & [40] are conventional ones, that is, the thicknesses of each of the conductors, used to build the antennas are much greater than their skin depth ($t_m >> \delta$).

3.6 CONCLUSION

In this chapter it was shown that using thin one dimensional Metallo-Dielectric structures the loss in a thin layer of metal may be reduced, but a single conductor of thickness equal to or greater than the skin depth was found to be more efficient than the laminated conducting media. This technique may be generally suited for applications involving thin conductors with high loss like Transparent Conductor Oxides. However, these results are limited to the structure of infinite extent in two dimensions. Conventional antennas utilize conductors with thicknesses fivefold larger than skin depth and are finite in extent. Further studies are required to predict the behavior of laminated conductors of finite size with each lamination thickness being less than its skin depth.

Chapter 4

Effect of Stacking on the Radiation Efficiency of Miniaturized H-Shaped Patch Antenna

4.1 INTRODUCTION

Several techniques have been in use to improve the gain/directivity of patch antennas. In [44] it was shown that the dielectric superstrate may be used for this purpose. Fabry–Perot Resonant Cavities have also been used to increase the directivity of patch antennas using both dielectric [45] and novel meta-material screens [46], [47]. It has also been shown that by using stacked parasitic directors, the directivity can be improved [48]. Stacked patch antennas have also been important candidates for wideband and multi-band designs [49]. It was seen in previous chapters that one of the ways to improve the radiation efficiency of a patch antenna is to increase the radiation conductance of the patch by geometrical modifications. Several ways to achieve this are known in the literature. In [50] it has been shown that having a stacked configuration increases the efficiency of the antenna. In [51] it was demonstrated that when more than one radiating elements are present for a dipole antenna the total radiation resistance of the antenna can be increased. Similarly in [11] it was determined that having multiple turns on a loop antenna would improve its radiation resistance. In this chapter the effect of stacking closely spaced parasitic resonant patches on the efficiency of miniaturized antenna is studied. A number of studies have previously been carried out on conventional stacked patch antennas [49] [52]. It is well known that when two antennas are stacked both the resonant frequencies and the resonant impedances change.

Some of the key observations in the behaviour of the resonant frequency characteristics of the stacked rectangular patch antenna with two resonators are [53]:

1. Let f_A and f_B $(where, f_A < f_B)$ be the resonant frequencies of two uncoupled patch antennas of sizes $A_x \times A_y$ and $B_x \times B_y$ (where, A > B), when the resonators are coupled by stacking, two new resonances f_l & f_h are generated which have no direct, simple relation to the frequencies f_A &f_B. However, by employing the equivalent circuit model for the stacked configuration, they may be related through their equivalent circuit parameters as shown in [54].
2. One of these newly generated resonant frequencies f_l, is lower than f_A & f_B and the other resonant frequency (f_h) is higher than f_A & f_B. The separation between f_l & f_h strongly depend on the coupling between the two resonators. Any change to the dimensions of individual antenna elements (A & B) affects both these frequencies.
3. When the separation between the two patches is very small the impedance characteristics at one of the resonant frequencies (f_l) approaches the uncoupled case of f_A. The second resonant frequency (f_h) still exists but it has to be excited separately, due to its small input impedance. Similarly when the distance between the two patches is large, there is only one resonance(f_h), However, the other resonance (f_l) disappears due to low coupling of the reactive energy.
4. Another particularly interesting effect of stacked configuration pertaining to the current work, is the peak of the input impedance of the antenna system at resonance. It can be seen from Figure 4.1 that the input resistance decreases at both upper and lower resonant frequencies for an appropriate separation between patches.

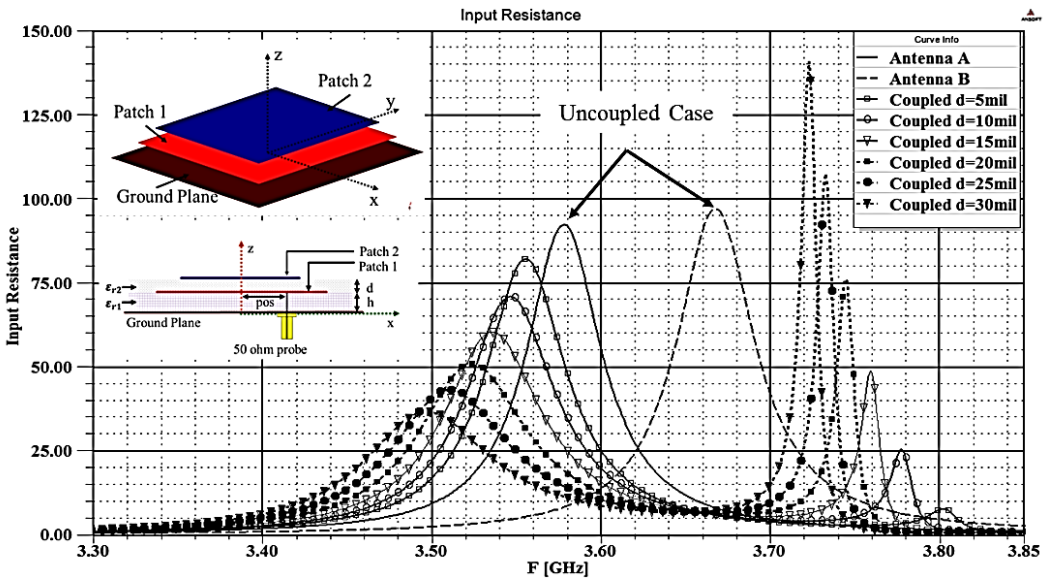

Figure 4.1 Input Resistance (ohm) of stacked patch antenna of sizes $Pach\ 1: A_x \times A_y = 40mm \times 35mm, Patch\ 2: B_x \times B_y = 39mm \times 34mm$ with different distance (d) between the two Antennas substrate height h=0.031in, ε_{r1}=1, ε_{r2}=1 and loss tangent tan(δ)=0, Infinite ground plane size probe position pos=7.5mm from the center.

If we consider the loss of energy in the form of radiation is from the effective slots at the radiating edge of the antenna, as described in chapter 2, the decrease in input impedance for a constant feed location is an indication of the increase in the total conductance at the radiating edge of the patch antenna. This reduction in the input resistance at resonance may arise from two causes:

1. *Increase in the Radiated Power or efficiency improvement arising from the increase in Radiation Conductance (G_r) of the antenna.*
2. *Increase in Power Dissipation, or efficiency reduction, due to the dominant Loss Conductance ($G_L << G_R$) arising from the increased energy density in the cavity.*

Direct measurement of efficiency of the antenna would immediately give us the exact cause of this change in the input resistance of the antenna. Efficiency of an antenna may be

measured using several techniques like the radiometric method and directivity/gain method [55]. Most of these techniques require pattern measurement in the entire space around the antenna. Wheeler Cap method described in [56] [57] is a simple and yet more accurate technique used for efficiency measurement, but this technique requires additional low loss conducting enclosure for conducting the measurements. As the main interest here is to detect the relative change in efficiency, by measuring the peak gains of the antenna this can be indirectly observed. As long as the radiation pattern of the antenna does not change, the effect of stacking on the radiation efficiency of the antenna can be obtained from the variations in the levels of the Gain Pattern. However, as shown in chapter 2 that simple square/rectangular patch antennas do not suffer from high power loss when they are built using a good conductor and low to medium dielectric constant material. In order to effectively detect any change in the efficiency, the antenna under consideration has to be small and thereby have lower efficiency. Therefore, in the following discussions in order to further elucidate this idea, an H-Shaped patch antenna is chosen for further study owing to its simplicity in design, fabrication and fairly good miniaturization factor.

4.2 EFFECT OF STACKING ON MINIATURIZED H-SHAPED PATCH ANTENNA

In order to investigate the effect of stacking on the radiation performance of miniaturized antennas, two H-Shaped patch antennas operating approximately at the same frequency, but with different levels of miniaturization are taken as examples. In Antenna -1 the patch size is about ~$0.3\lambda_0$ and for Antenna 2 the patch size is about ~$0.2\lambda_0$. The difference in miniaturization is achieved by different slot lengths (S_L), all other dimensions of the antenna are kept the same.

Table 4-I shows the radiation parameters of the two antennas without any stacking. As expected the smaller antenna has a lower gain, due to a higher loss. Figure 4.2 shows the stacked geometry of the antennas under consideration with identical upper layers. The dimensions of these patches are shown in Table 4-II. In order to accurately isolate the effect of stacking on the antenna efficiency, the antennas are simulated with infinite ground plane and the substrate as well as the superstrate are chosen to be lossless with dielectric constant of ε_r=1. Thus, any loss in the antenna arises from the effect of finite conductivity of the metallization. HFSS simulations are performed for different values of the separation distance (*d*) between the top and bottom patches of the antenna, keeping all other parameters of the antenna constant.

Table 4-I
Antenna parameters for the single layer case of Antenna 1 and Antenna 2, with the geometry shown in Figure 4.2 (excluding upper layer)

Antenna	**Size(L=W)**	**S_L (mm)**	**S_w (mm)**	**S_g (mm)**	**Resonant Freq (f_r)**	**Gain**	**Gain for Lossless case**
Simple Patch 1	$0.3\lambda_0$(23mm)	9.5	3	4	3.56 GHz	5.08 dBi	8.8 dBi
Simple Patch 2	$0.2\lambda_0$(17.5mm)	8.25	3	1	3.52 GHz	1.5 dBi	8.9 dBi

Table 4-II
Patch dimensions for the stacked configuration Antenna 1 and Antenna 2 with geometry shown in Figure 4.2

Antenna	**L=W** (mm)	**S_L**(mm)	**S_w** (mm)	**S_g** (mm)	**h** (inches)
Antenna 1:					
Patch 1	23	9.5	3	4	0.031
Patch 2	23	9.5	3	4	
Antenna 2:					
Patch 1	17.5	8.25	3	1	0.031
Patch 2	17.5	8.25	3	1	

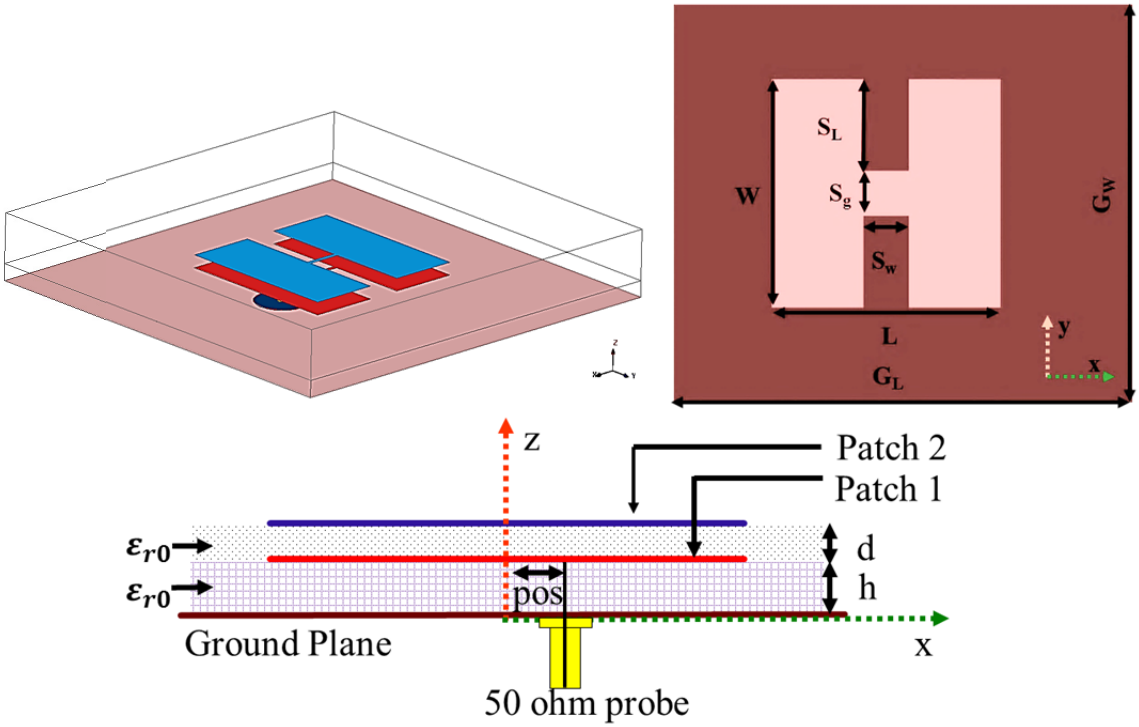

Figure 4.2 Stacked geometry of identical H-Shaped Patch Antenna pos= 1mm, dielectric constant, h=0.031in, ε_{r0}=1, loss tangent tan(δ) = 0.0 with infinite ground plane, both patch and ground are of 35µm thickness and made of copper σ=5.8 × 10^7

Figure 4.3 and Figure 4.4 show the input resistance plot for the two stacked H-Shaped antennas. One of the observations that one could make here is that, the drift of the resonant frequency for the stacked system, from the case of uncoupled single antenna configuration, becomes larger with the reduction in size. This may be attributed to the increased interaction/coupling between the top and bottom patches, with reduction in antenna size. It is known that when an antenna gets smaller the stored energy associated with it increases, as the energy is confined in a smaller physical volume, increasing the energy density, this gives rise to large surface currents and field amplitudes in the antenna and thus causing larger coupling [33].

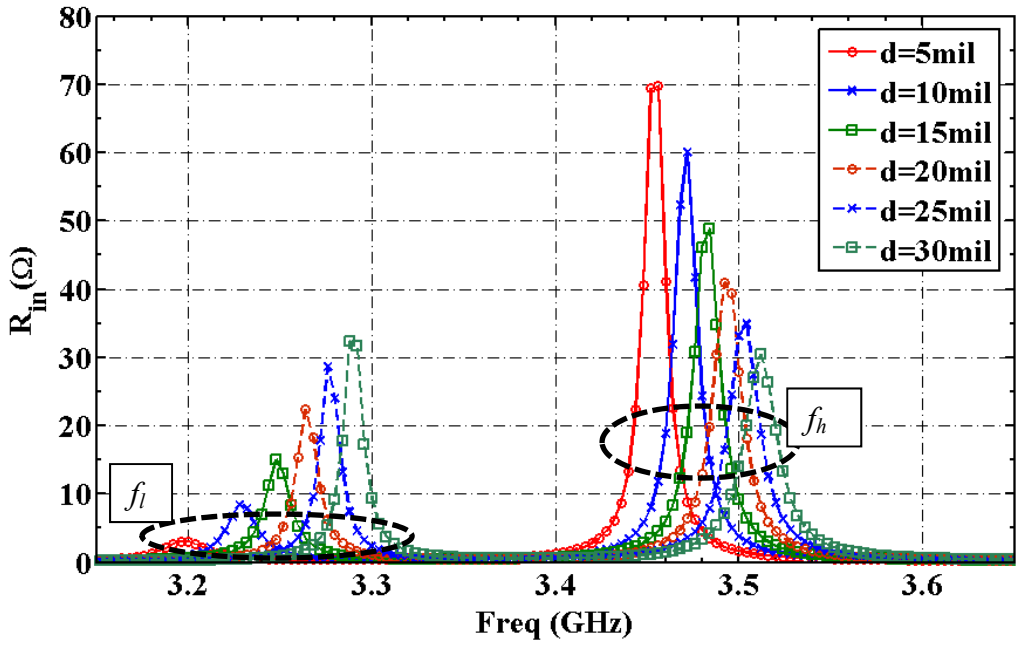

Figure 4.3 HFSS simulation showing input resistance of stacked **Antenna 1** of geometry given in Figure 4.2, for different values of separation (*d in mils*[1])

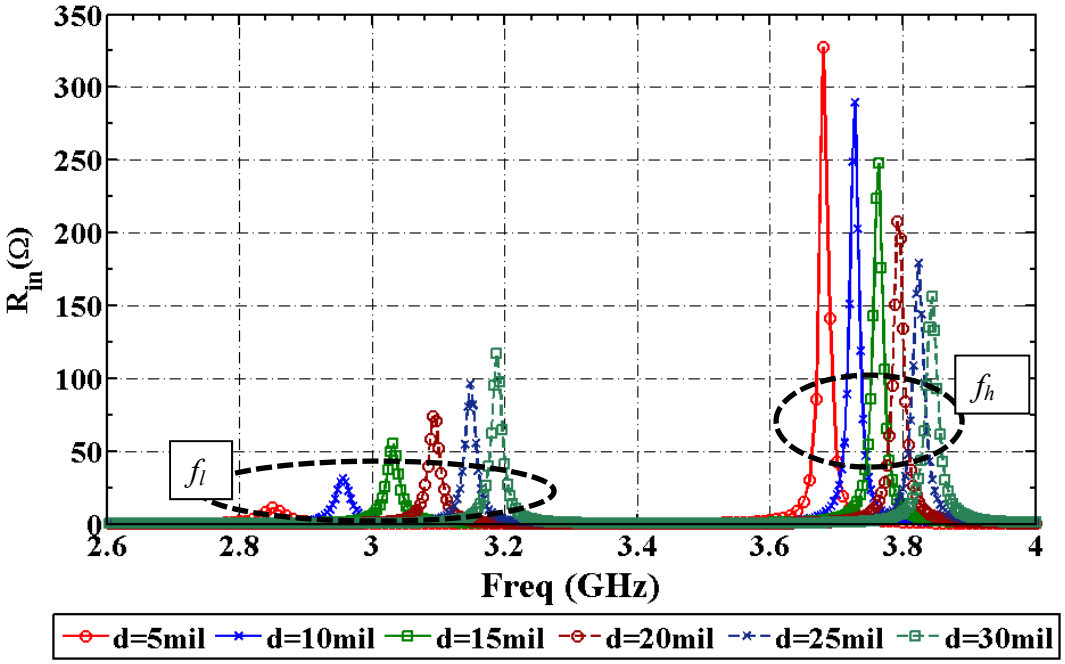

Figure 4.4 HFSS simulation showing input resistance of stacked **Antenna 2** of geometry given in Figure 4.2, for different values of separation *d*.

[1] 1mil = 0.001inches = 0.0254mm

It is also clear from these plots that, similar to the simple stacked antenna of Figure 4.1, at the resonant frequencies both antennas show reduction in the input resistance (or increase in the input conductance), The total conductance at the edge of the patch may be obtained from the input conductance, if the fields inside the patch are known [8]. With increase in the separation distance at the higher frequency f_h, the input conductance increases, whereas at lower frequency f_l the input conductance decreases with decrease in the separation between the patches. As pointed out earlier, this lowering of the input conductance may be due to increase in the radiated power and/or increase in power loss. In order to resolve this ambiguity, the radiation characteristics of the two antennas at f_h and f_l are discussed separately in the following sections. At the lower resonant frequency f_l, these results also indicate the possibility of obtaining smaller antennas with small separation between the stacked patches. In the following sections, the radiation characteristic of these stacked patches at the frequencies f_h and f_l are studied separately.

4.3 RADIATION CHARACTERISTICS AT HIGHER RESONANT FREQUENCY

Figure 4.5- Figure 4.8 show the E and H plane radiation patterns of the antennas at the higher resonant frequency (f_h). The gain pattern of the antennas for lossless (or Directivity) cases are inscribed in these plots. A summary of these results is presented in Table 4-III and Table 4-IV, where Δf is the frequency drift of the higher resonance from the case of the single layer antenna. It is apparent that for both antennas at the higher resonant frequency (f_h), by increasing the separation distance between the antenna the Gain of the antenna is improved at the same time the E-plane and H-plane radition pattern shapes remain the same. This increase in the gain indicates an improvement in the efficiency of the antenna.

As seen from here the directivity or the gain for lossless case of the antenna does not change with the change in separation between the two patches, thus implying that the increase in the total conductance, as predicted from the input impedance plots, corresponds to an increase in the Radiation Conductance (G_r) of the antenna.

Table 4-III Radition Charactersitcs of stacked Antenna 1 ($L \times W = 23\text{mm} \times 23\text{mm}$, S_L=9.5mm) of geometry given in Figure 4.2 for different values of separation *d at* f_h

d (mil)	$\boldsymbol{\Delta f = f_h - f_r}$ **(GHz)**	$\boldsymbol{\Delta f = \left(\frac{f_h - f_r}{f_r}\right) 100}$ **(%)**	**Peak Directivity (dBi)**	**Peak Gain (dBi)**	$\boldsymbol{\eta_{rad}}$ **(%[dB])**
5	0.03	0.85	8.79	6.43	58.08 [-2.36]
10	0.05	1.44	8.79	6.68	62.52 [-2.11]
15	0.06	1.72	8.79	6.94	64.66 [-1.85]
20	0.07	2	8.79	7.2	69.34 [-1.59]
25	0.08	2.29	8.79	7.42	72.95 [-1.37]
30	0.09	2.56	8.79	7.54	74.99 [-1.25]

Table 4-IV Radition Charactersitcs of stacked Antenna 2 ($L \times W = 17.5\text{mm} \times 17.5\text{mm}$, S_L=8.25mm) of geometry given in Figure 4.2 for different values of separation *d* at f_h

d (mil)	$\boldsymbol{\Delta f = f_h - f_r}$ **(GHz)**	$\boldsymbol{\Delta f = \left(\frac{f_h - f_r}{f_r}\right) 100}$ **(%)**	**Peak Directivity (dBi)**	**Peak Gain (dBi)**	$\boldsymbol{\eta_{rad}}$ **(%[dB])**
5	0.11	3.08	9.05	3.59	28.44 [-5.46]
10	0.16	4.48	9.05	4.42	34.35 [-4.64]
15	0.19	5.32	9.05	5.05	39.80 [-4.00]
20	0.22	6.16	9.05	5.6	45.18 [-3.45]
25	0.25	7.00	9.05	5.79	47.20 [-3.26]
30	0.27	7.56	9.05	6.08	50.50 [-2.96]

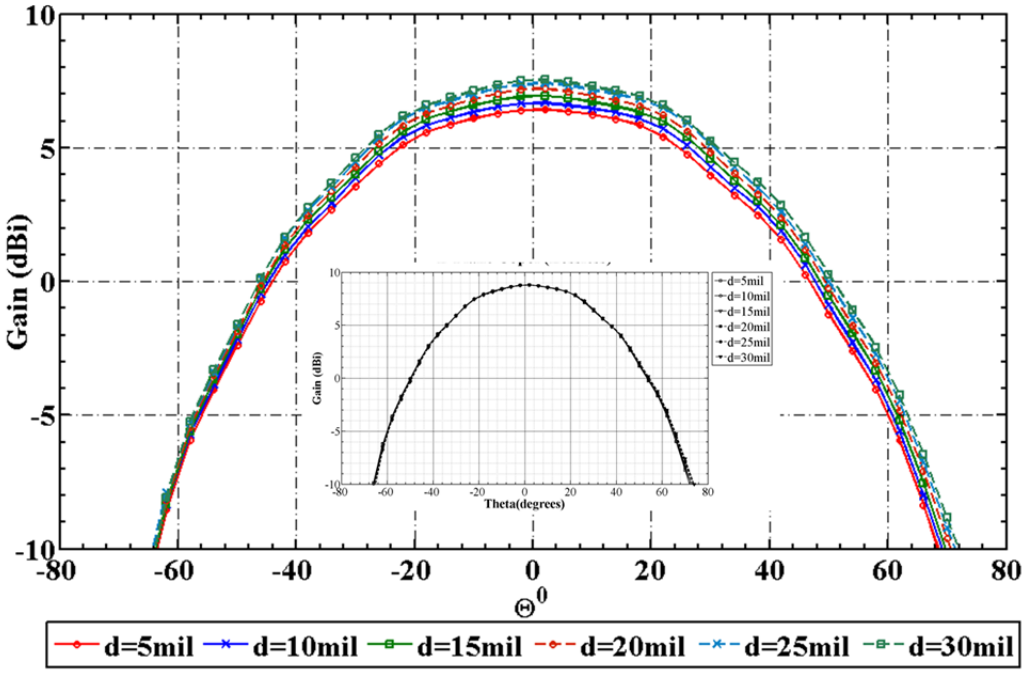

Figure 4.5 Circumscribed is the G_{phi} pattern in ϕ=90 plane of the Stacked H-Shaped **Antenna 1** as shown in Figure 4.2, for different values of separation *d* at the higher resonant frequency f_h. Inscribed is the G_{phi} pattern in ϕ=90 plane Pattern for the lossless case of the same.

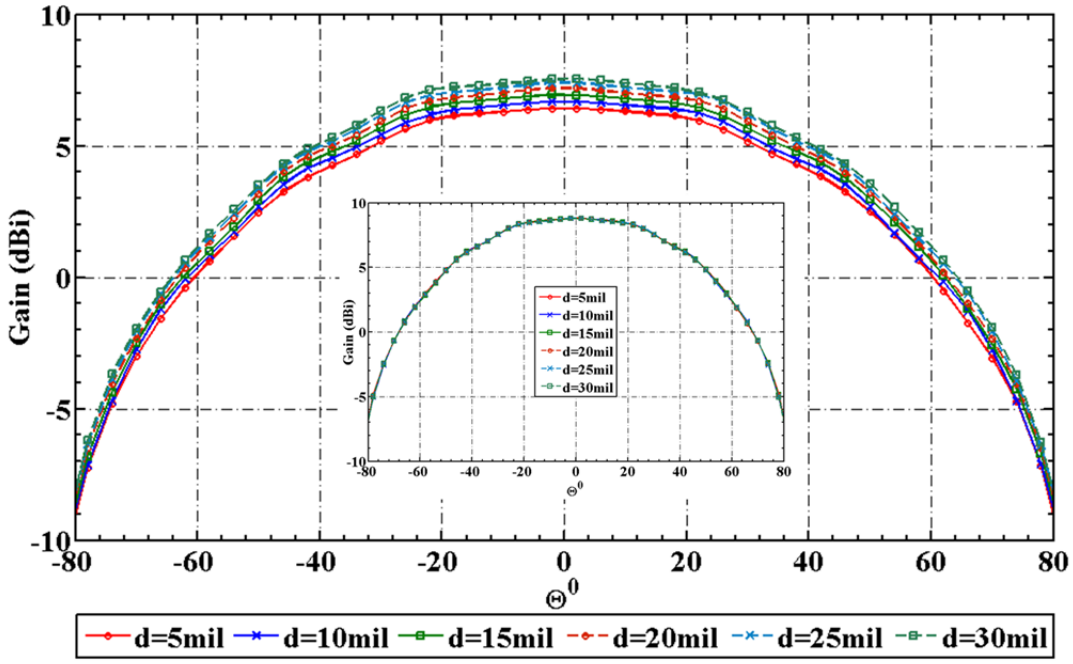

Figure 4.6 Circumscribed is the G_{theta} pattern in ϕ=0 plane of the Stacked H-Shaped **Antenna 1** as shown in Figure 4.2, for different values of separation *d* at the higher resonant frequency f_h. Inscribed is the G_{theta} pattern in ϕ=0 plane for the lossless case of the same.

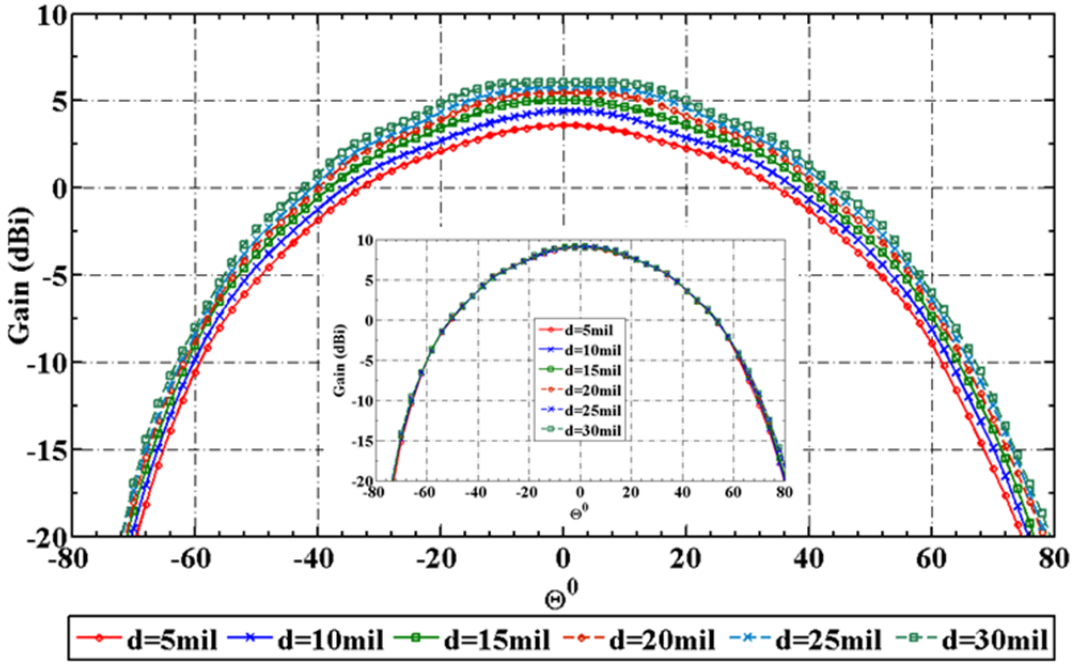

Figure 4.7 Circumscribed is the G_{phi} pattern in ϕ=90 plane of the Stacked H-Shaped **Antenna 2** as shown in Figure 4.2, for different values of separation *d* at the higher resonant frequency f_h. Inscribed is the G_{phi} pattern in ϕ=90 plane Pattern for the lossless case of the same.

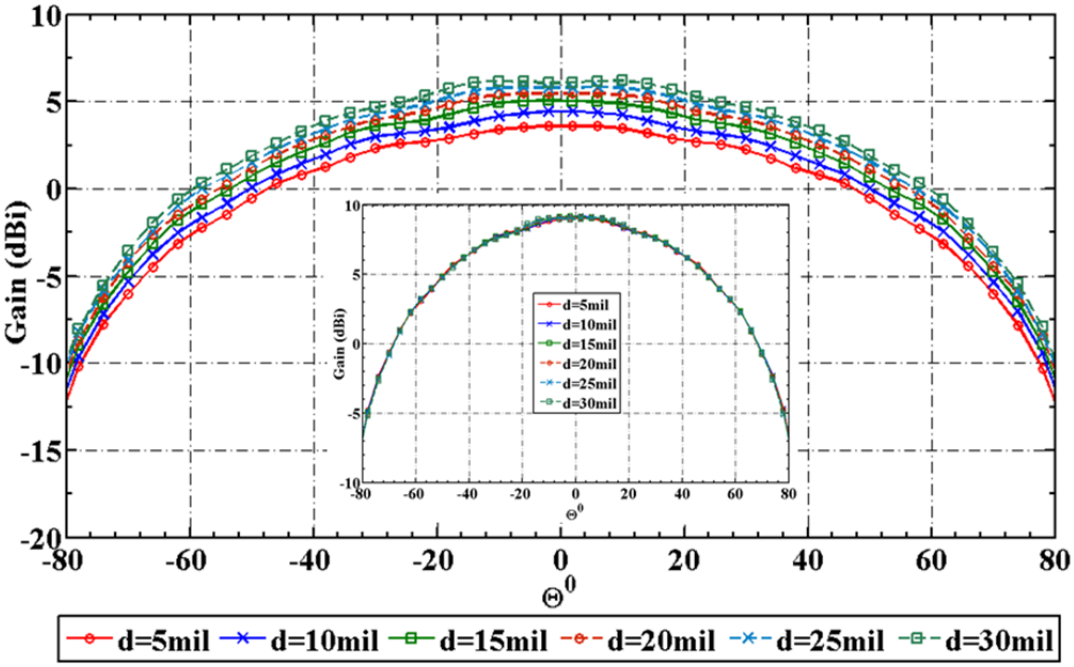

Figure 4.8 Circumscribed is the G_{theta} pattern in ϕ=0 plane of the Stacked H-Shaped **Antenna 2** as shown in Figure 4.2, for different values of separation *d* at the higher resonant frequency f_h. Inscribed is the G_{theta} pattern in ϕ=0 plane for the lossless case of the same.

It is also seen that the efficiency improvement achieved in the smaller antenna is greater (from 29% to 51%) than the larger antenna (58%to75%). With the larger values of separation *d,* the increase in efficiency however starts to saturate. The reason for increase in the radiation conductance can be hypothesised by observing the fields inside the antenna, as shown in Figure 4.9 and Figure 4.10. If the stacked antenna system is modeled as two coupled cavities Q_1 and Q_2 , similar to the analysis described in [58], at f_h it is seen that most of the fields concentrated between the lower patch and the ground plane, but yet there is a significant amount of non –resonant electromagnetic energy coupled into the upper cavity of the antenna there by improving the total volume the antenna effectively utilizes.

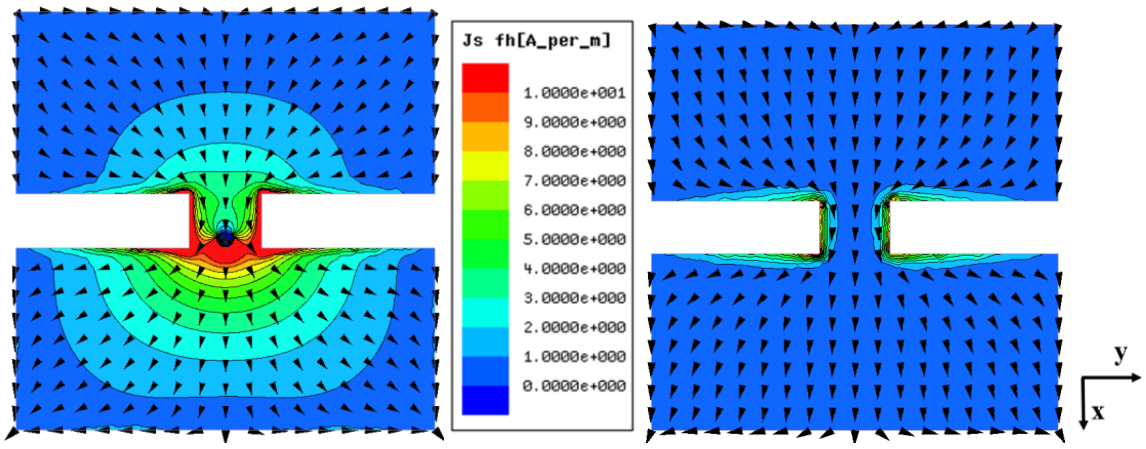

Figure 4.9 Current Distributions on the (a) Bottom Patch and (b) Top Patch of the Stacked H-Shaped **Antenna 1** of Geometry shown in geometry given in Figure 4.2 with $L \times W = 23\text{mm} \times 23\text{mm}$, S_L=9.5mm for separation *d=30mil* at the higher resonant frequency f_h

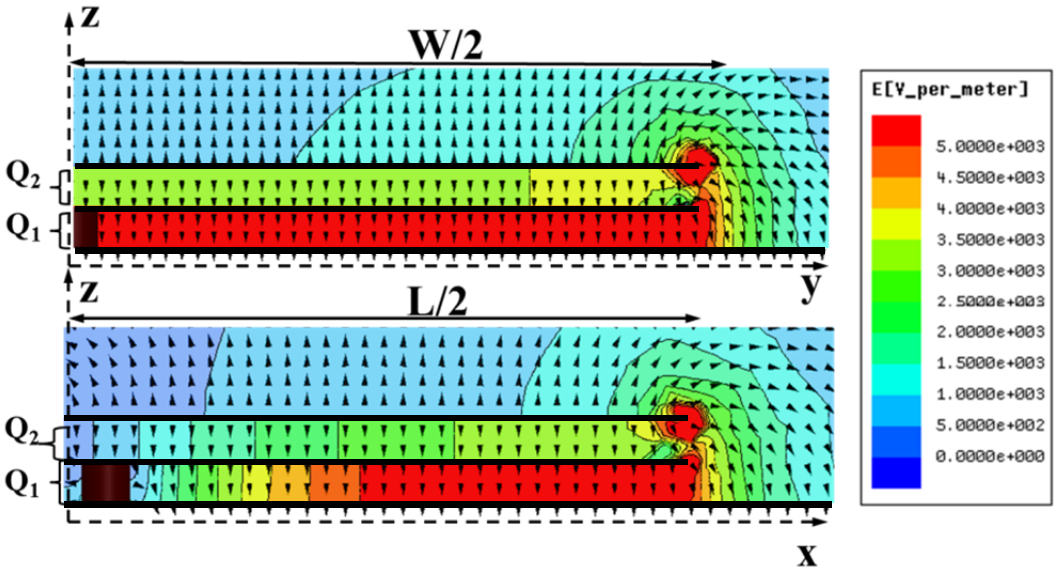

Figure 4.10 Field Distribution inside the upper and lower cavities long length and width of the Stacked H-Shaped **Antenna 1** of Geometry shown in geometry given in Figure 4.2 with $L \times \mathrm{W} = 23\mathrm{mm} \times 23\mathrm{mm}$, S_L=9.5mm for separation *d=30mil* at the higher resonant frequency f_h

Furthermore, from even and odd mode theory [59], the total field inside a coupled system can be defined as a sum of the even and odd modes. The direction of the fields in the two cavities and the currents on the two patch antenna at the frequency f_h are in the same direction. That is, this mode is dominantly even in nature. The radiation here can be considered to be caused by two radiators – Patch 1 and Patch 2. Here the currents are in the same direction and the distance between the patches is very small, thus, the phase difference between the far - fields generated by the two patches is negligible. This accounts for the antenna patterns to remain the same, and at the same time increases the radiation conductance, similar to the case of multiple dipole antennas [51], or multi turn loop antennas [60]. It should, however, also be noted that a part of efficiency improvement here also comes from the increase in the resonant size of the antenna as the frequency shifts to higher end.

4.4 RADIATION CHARACTERISTICS AT THE LOWER RESONANT FREQUENCY

Figure 4.11, Figure 4.12, Figure 4.13 and Figure 4.14 show the H plane Gain and Directivity patterns of the antennas at the lower resonant frequency (f_l). A summary of these results is presented in Table 4-V and Table 4-VI. Here, Δf is the resonant frequency drift to the lower frequency from the case of single layer antenna. Unlike the previous case at f_l the directivity of the stacked patch antenna changes (implying that the radiaiton pattern of the antenna is changing) with change in the separation distance between the two antennas but there is little change in the antenna efficiency. Thus, indicating that, though the total conductance of the antenna is increasing with decrease in the separation distance between the two patches, this increase does not come from the increase in the radiation conductance. For clarity here only the H-plane patterns of the two antennas for lossy and lossless cases are plotted.

Table 4-V Radition Charactersitcs of stacked **Antenna 1** ($L \times \mathrm{W} = 23\mathrm{mm} \times 23\mathrm{mm}$, S_L=9.5mm) of geometry given in Figure 4.2 for different values of separation *d* at the lower resonant frequency f_l

d (mil)	$\boldsymbol{\Delta f = f_r - f_l}$ **(GHz)**	$\boldsymbol{\Delta f = \left(\frac{f_r - f_l}{f_r}\right) 100}$ **(%)**	**Peak Directivity (dBi)**	**Peak Gain (dBi)**	$\boldsymbol{\eta_{rad}}$ **(%[dB])**
5	0.22	6.88	3.9	-8.6	5.6 [-12.52]
10	0.19	5.88	6.67	-8.71	2.9 [-15.38]
15	0.17	5.23	8.05	-6.88	3.2 [-14.95]
20	0.15	4.59	8.51	-5.09	4.3 [-13.67]
25	0.14	4.27	8.74	-4.051	5.3 [-12.76]
30	0.13	3.95	8.77	-3.089	6.5 [-11.87]

Table 4-VI Radition Charactersitcs of stacked **Antenna 2** ($L \times W = 17.5mm \times 17.5mm$, S_L=8.25mm) of geometry given in Figure 4.2 for different values of separation *d* at the lower resonant frequency f_l

d (mil)	$\Delta f = f_r - f_l$ **(GHz)**	$\Delta f = \left(\frac{f_r - f_l}{f_r}\right) 100$ **(%)**	**Peak Directivity (dBi)**	**Peak Gain (dBi)**	η_{rad} **(%[dB])**
5	0.71	24.82	4.77	-14.63	1.15 [-19.40]
10	0.60	20.20	5.82	-15.65	0.71 [-21.47]
15	0.53	17.43	7.06	-13.7	0.84 [-20.75]
20	0.47	15.16	7.78	-11.32	1.12 [-19.52]
25	0.42	13.33	8.59	-9.48	1.56 [-18.80]
30	0.38	11.91	8.63	-8.58	1.90 [-17.22]

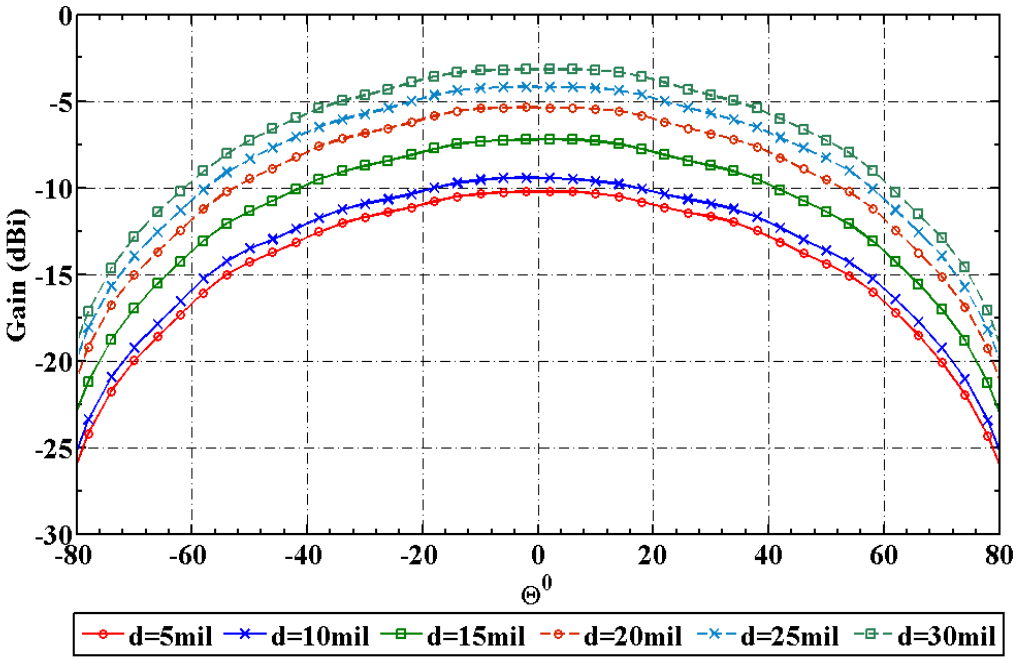

Figure 4.11 H-Plane Gain Pattern of the Stacked H-Shaped **Antenna 1** of Geometry shown in geometry given in Figure 4.2with $L \times W = 23mm \times 23mm$, S_L=9.5mm for different values of separation *d* at the lower resonant frequency f_l

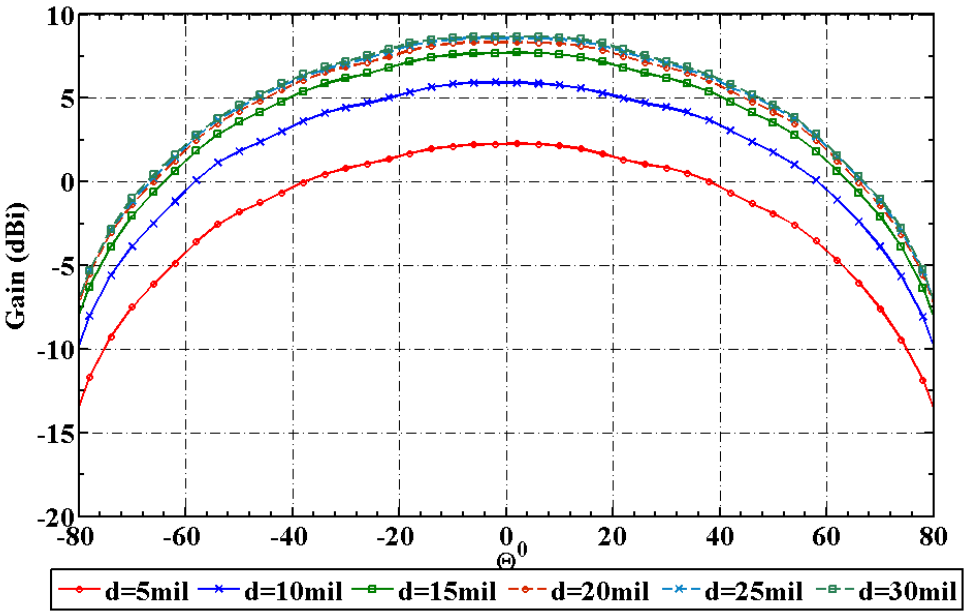

Figure 4.12 H-Plane Directivity Pattern of the Stacked H-Shaped **Antenna 1** of Geometry shown in geometry given in Figure 4.2 with $L \times W = 23\text{mm} \times 23\text{mm}$, S_L=9.5mm for different values of separation d at the lower resonant frequency f_l

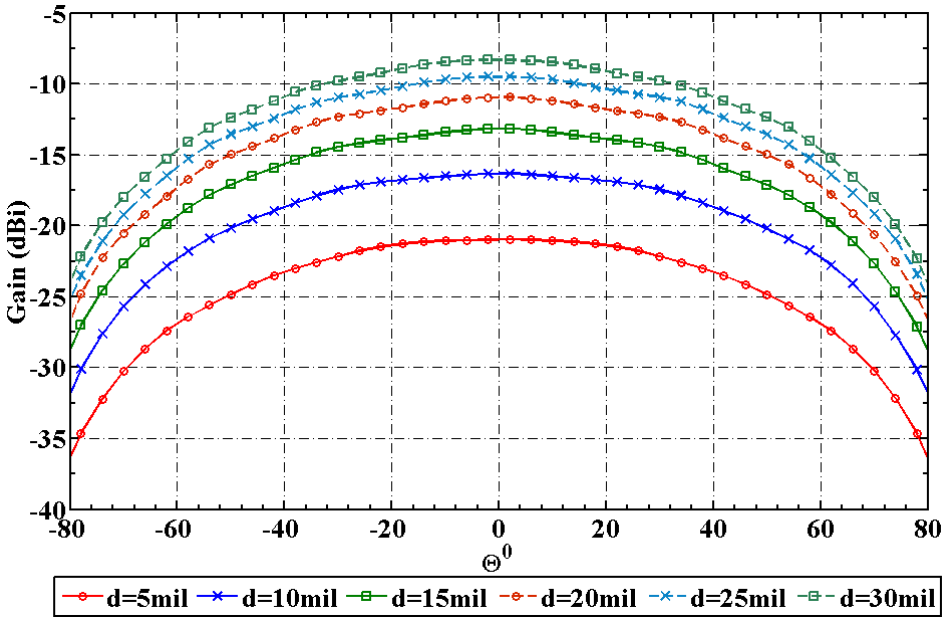

Figure 4.13 H - Plane Gain Pattern of the Stacked H-Shaped **Antenna 2** of Geometry shown in geometry given in Figure 4.2 with $L \times W = 17.5\text{mm} \times 17.5\text{mm}$, S_L=8.25mm for different values of separation d at the lower resonant frequency f_l

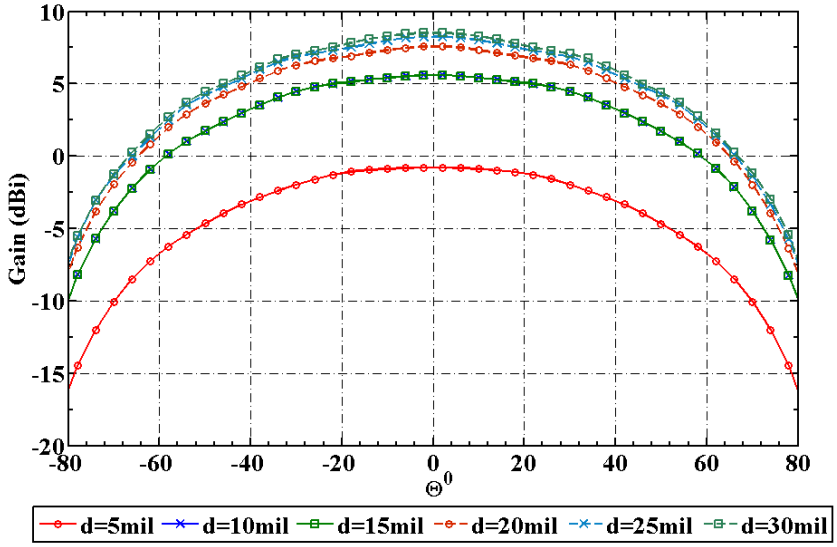

Figure 4.14 H - Plane Directivity Pattern for lossless case of the Stacked H-Shaped **Antenna 2** of Geometry shown in geometry given in Figure 4.2 with $L \times W = 17.5\text{mm} \times 17.5\text{mm}$, S_L=8.25mm for different values of separation d at the lower resonant frequency f_l

Similar to the case of higher resonant frequency f_h, by looking at the current distribution and the fields in the antenna assuming cavity model, insight into the reasons behind the change in directivity and little change in efficiency of the antenna, in spite of the increase input the total conductance of the antenna, may be obtained. Figure 4.15 shows the current distributions on the top and bottom patches at frequency f_l and Figure 4.16 shows the corresponding fields in the upper (Q_1) and lower (Q_2) cavities between the two patches and the ground. It is seen that the upper cavity has the larger part of the fields and there is significant non-resonant energy coupled into the lower cavity which plays an important role in defining the resonant lower resonant frequency f_l. The relatively low directivity and its sensitivity to the distance between the two patches may be easily related to the fields (or currents) in the two cavities. It can be seen that the currents on the top and bottom patches are in opposite direction, thus indicating that at f_l the fields are dominantly odd inside the patch antenna.

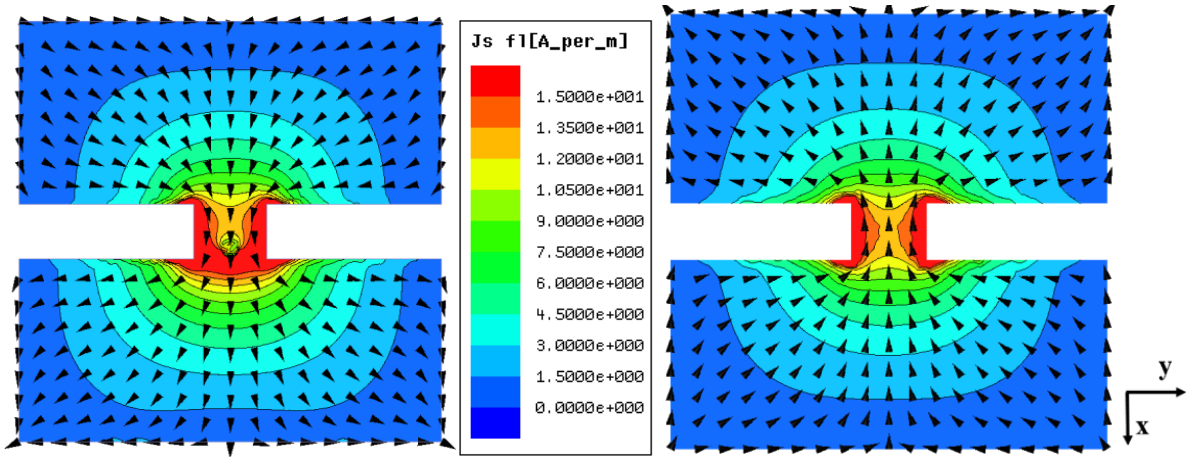

Figure 4.15 Current Distributions on the (a) Top Patch and (b) Bottom Patch of the Stacked H-Shaped **Antenna 1** of Geometry shown in geometry given in Figure 4.2 with $L \times W = 23\text{mm} \times 23\text{mm}$, S_L=9.5mm for separation *d=30mil* at the lower resonant frequency f_l

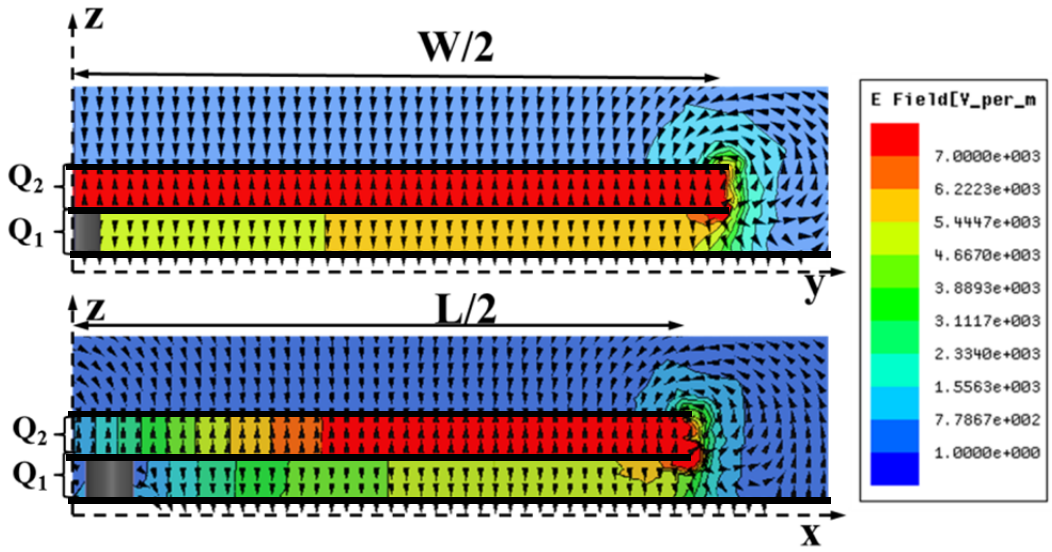

Figure 4.16 Field Distribution inside the upper and lower cavities along length and width of the Stacked H-Shaped **Antenna 1** of Geometry shown in geometry given in Figure 4.2 with $L \times W = 23\text{mm} \times 23\text{mm}$, S_L=9.5mm for separation *d=30mil* at the lower resonant frequency f_l

If the radiation is considered to be the superposition of the individual slot radiators – Patch 1 and Patch 2, in the far field region of the antenna, these fields interfere destructively, since the distance between the two patches is small ($d/\lambda_0 << 1$). In other words, the antenna

would have lower radiation conductance (G_R). When the distance between the patches is increased, the phase difference between far fields of the two radiators is no longer 180^0, thus, causing the directivity to increase. The increase in the total conductance G_t of the antenna, however, comes from the fact that at the lower frequencies the loss conductance ($G_L=G_c+G_d$) is dominant. As the frequency shifts lower with decrease in the distance between the patches, the total conductance increases due to the dominant increase in the loss conductance, when compared to the reduction in the radiation conductance (G_r). These results indicate that at these frequencies the antenna is not an efficient radiator. It should however be noted that for the case of stacked antennas with radiating elements of different sizes, the even and odd modes may not occur at the same frequencies exactly at the upper and lower resonant frequencies, respectively. This is shown in figures 4-17 to 4-20.

Table 4-VII
Patch Dimensions of Stacked Antenna with unequal radiating elements

Patch	L=W (mm)	S_L (mm)	S_W (mm)	f_h (GHz)	f_l (GHz)
Antenna 3					
Upper Patch	23	9.5	3	3.36	3.82
Lower Patch	21	8.5	3		
Antenna 4					
Upper Patch	21	8.5	3	3.14	3.36
Lower Patch	23	9.5	3		

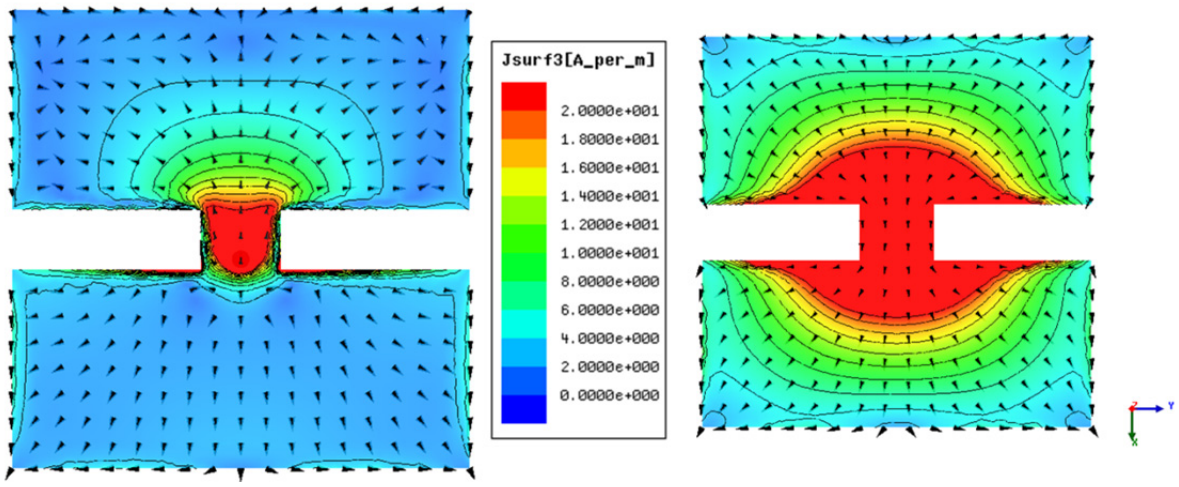

Figure 4.17 Current Distributions on the Bottom Patch (left) and Top Patch (right) of the Stacked H-Shaped **Antenna 3** of Geometry shown in geometry given in Table 4-VII at the higher resonant frequency f_h

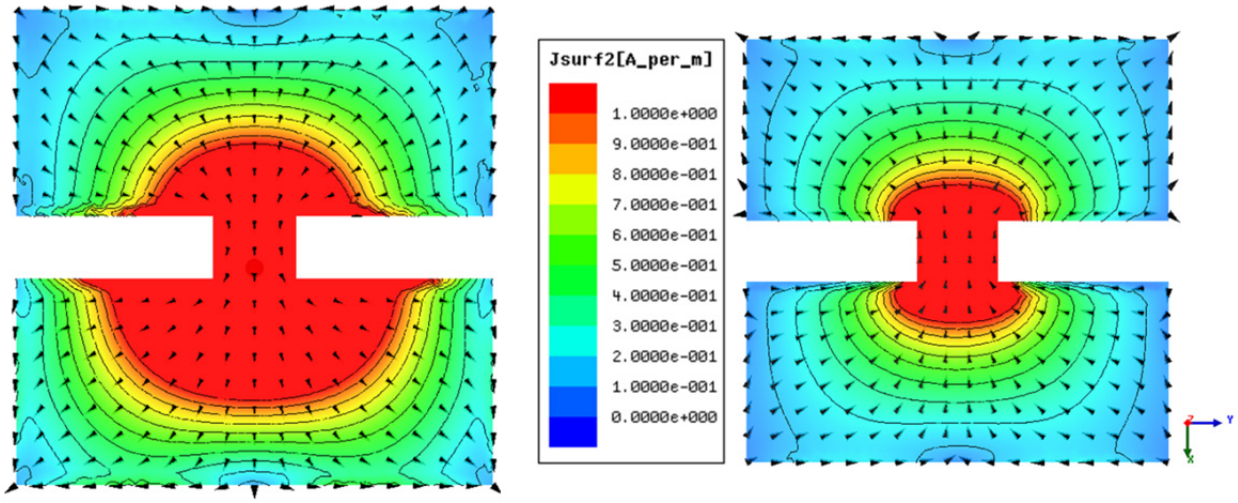

Figure 4.18 Current Distributions on the Bottom Patch (left) and Top Patch (right) of the Stacked H-Shaped **Antenna 3** of Geometry shown in geometry given in Table 4-VII at the lower resonant frequency f_l

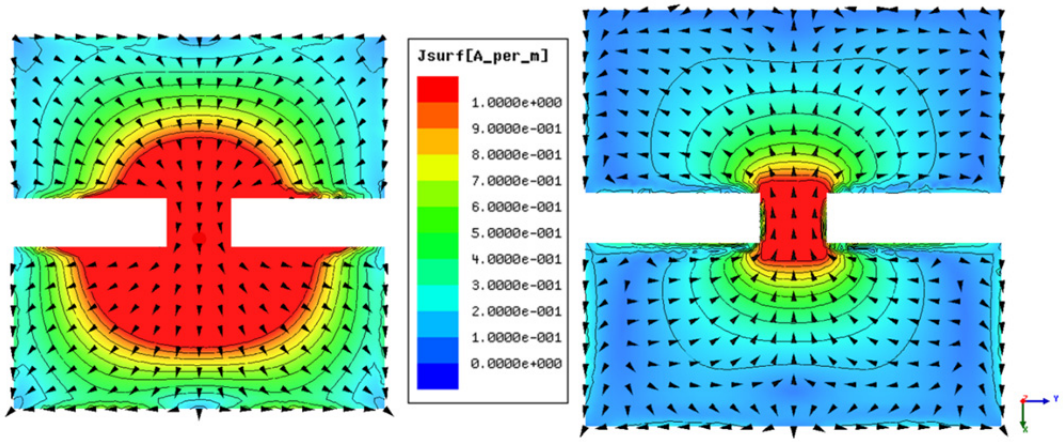

Figure 4.19 Current Distributions on the Bottom Patch (left) and Top Patch (right) of the Stacked H-Shaped **Antenna 4** of dimensions shown in geometry given in Table 4-VII at the higher resonant frequency f_h

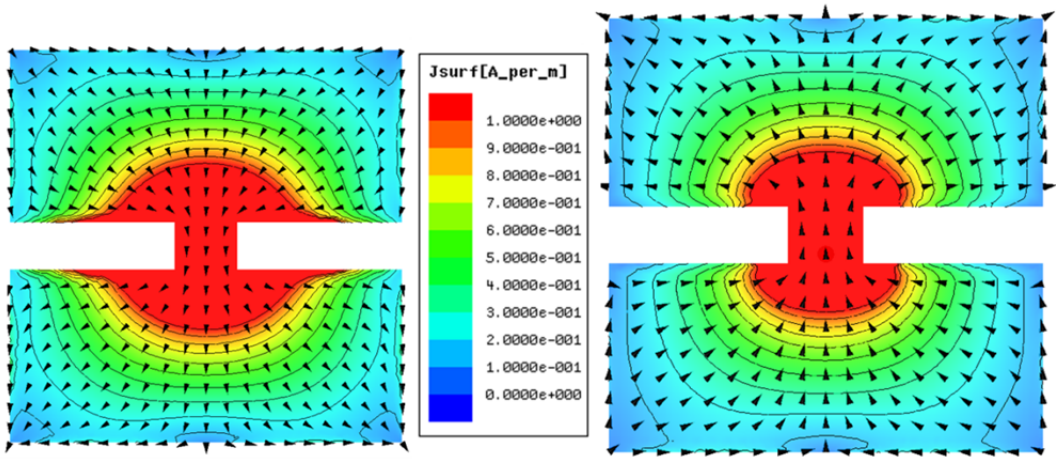

Figure 4.20 Current Distributions on the Bottom Patch (left) and Top Patch (right) of the Stacked H-Shaped **Antenna 4** of dimensions shown in geometry given in Table 4-VII at the lower resonant frequency f_l

Table 4-VII shows two antennas with different dimensions for the upper and lower patches. When the upper patch is smaller than the lower patch (Antenna 3) at f_h (Figure 4.17) the even mode dominates and at f_l (Figure 4.18) the current distribution is a combination of both even and odd modes. When the lower patch is smaller than the upper patch (Antenna 4) at both resonances the odd mode dominates (Figure 4.19 & Figure 4.20).

4.5 CONCLUSION

In this chapter the effect of stacking two identical antennas on the radiation characteristics was studied. It was shown that, at the higher resonant frequency of the antenna, the radiation conductance is improved due to increase in the in-phase currents/fields and thus increasing the efficiency of the antenna. With the increase in the distance between the two patches, this effect was seen to further dominate. On the other hand, at the lower resonant frequency the antenna exhibited poor efficiency due to the out of phase currents/fields, but with the increase in the distance between the two patches, the directivity of the antenna was seen improve and reach the case of the upper resonant frequency of the antenna. It was also seen to that it is important to have the parasitic patches to be of identical sizes to obtain even mode dominant field/current distributions, at the higher resonant frequency of the patch antenna.

Chapter 5

Effect of Multiple Resonators on Small H-Shaped Patch Antenna

5.1 INTRODUCTION

In the last chapter it was shown that having identical stacked parasitic patches improved the radiation efficiency of the antenna at the operating frequency, where the even mode of the structure dominated. Based on those discussions, in this chapter the effect of stacking multiple resonators with different superstrate dielectric materials and heights are investigated using HFSS software simulations. The results are then verified using measurement.

One of the difficulties with small antennas as seen in previous chapters is the impedance difficulty in matching. As a patch antenna becomes smaller, its input impedance becomes a high and to match microstrip antenna to high input impedance the coaxial feed location has to move be around the center, with a very high precision. There are different impedance matching techniques that may be used to circumvent this; one of the simplest ways for this is by using a gap coupled feed [8]. In the following work, a gap coupled feed line at one of the radiating edges is used to transform the high impedance to 50Ω. This is shown in Figure 5.1. The antenna can be easily impedance matched by varying the feed line parameters, namely the length and width of the line, and the gap between the patch and the line. Figure 5.2 shows the effect of varying the feed line length on the matching.

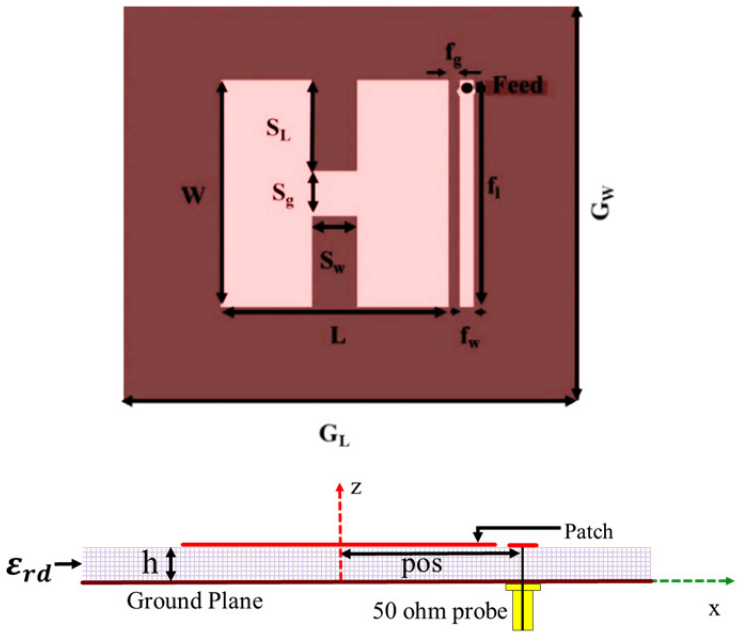

Figure 5.1 Geometry of H-Shaped Square Patch antenna with capacitive edge feed substrate height h=0.031in, $\boldsymbol{\varepsilon_r}$=2.5 and loss tangent tan(δ)=0.0018, ground plane size = 50mm × 50mm. Both patch and ground are of 35µm thickness and made of copper σ=5.8 × 10^7

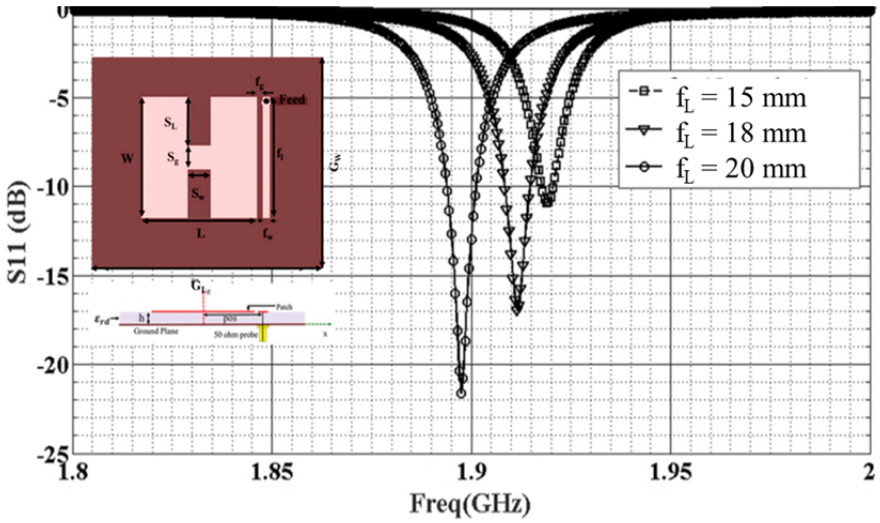

Figure 5.2 Variation of input impedance with feed line length of H-Shaped Square Patch antenna shown in Figure 5.1 with L=W=20mm, S_L=9.5mm, S_w=4mm, f_w=1mm, f_{gap}=0.5mm, substrate height h=0.031in, $\boldsymbol{\varepsilon_r}$=2.5 and loss tangent tan(δ)=0.0018, ground plane size = 50mm × 50mm. Both patch and ground are of 35µm thickness and made of copper σ=5.8 × 10^7

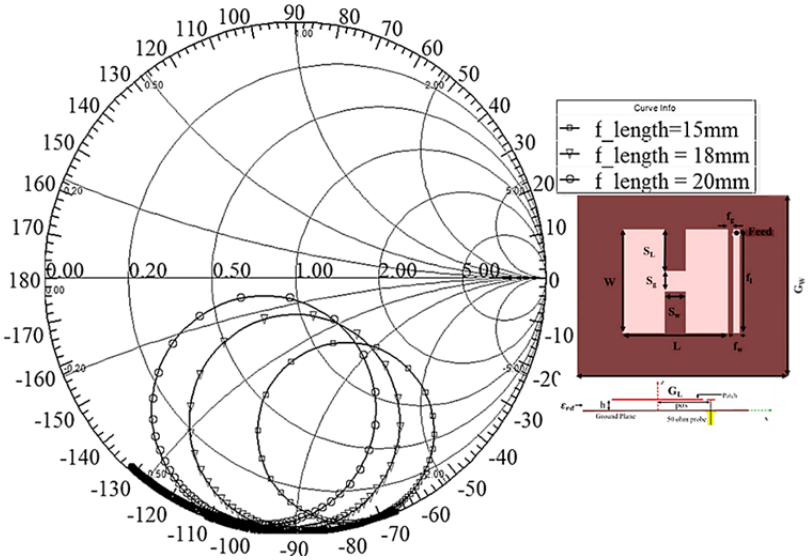

Figure 5.3 Variation of input impedance with feed line length of H-Shaped Square Patch antenna shown in Figure 5.1 with L=W=20mm, S_L=9.5mm, S_w=4mm, f_w=1mm, f_{gap}=0.5mm, substrate height h=0.031in, $\boldsymbol{\varepsilon_r}$=2.5 and loss tangent tan(δ)=0.0018, ground plane size = 50mm × 50mm. both patch and ground are of 35µm thickness and made of copper σ=5.8 × 10^7

Figure 5.4 shows the increased surface current density on the patch antenna. As expected increasing the slot length reduces the size of the antenna and causes a drop in the efficiency (Table 5-I). Here, all the structures are impedance matched (S11~-20dB) by changing the length (f_L) of the feed line and keeping the width (f_w) and gap (f_{gap}) constant.

Table 5-I
Gain and Efficiency for the H-Shaped antenna shown in Figure 5.1 for different values of slot length

Antenna	Length/width	Gain(dBi)	Radiation Efficiency (%)	S_g (mm)
(a)	0.25 λ_0	6.42	78.04	10
(b)	0.185λ_0,	1.55	30.55	5
(c)	0.154 λ_0	-2.61	12.49	2.5
(d)	0.133λ_0	-9.64	2.86	1

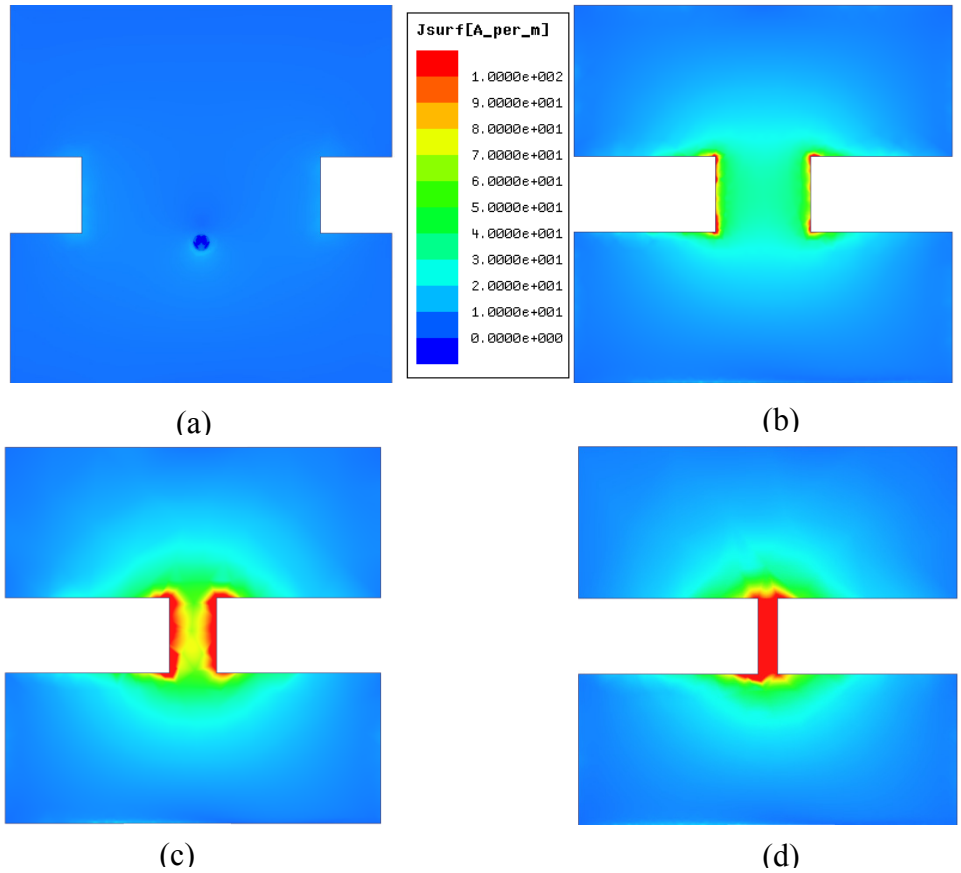

Figure 5.4 Magnitude of surface current density on the H-Shaped Square Patch antenna shown in Figure 5.1under matched condition

5.2 PARAMETRIC STUDY, RESULTS AND DISCUSSIONS

Based on the discussions given in chapter 4, in the following section a parametric study of having multiple resonator elements as superstrates with different dielectric constants and thicknesses is carried out. The geometry and the dimensions of the antenna under consideration with multiple layers are shown in Figure 5.5 and Table 5-II respectively. The parametric study for different values of the superstrate relative permittivity ε_{rs}, superstrate thicknesses t and different number of resonant patches were carried out using HFSS software. The results thus obtained are shown in figures 5.6 to 5.20.

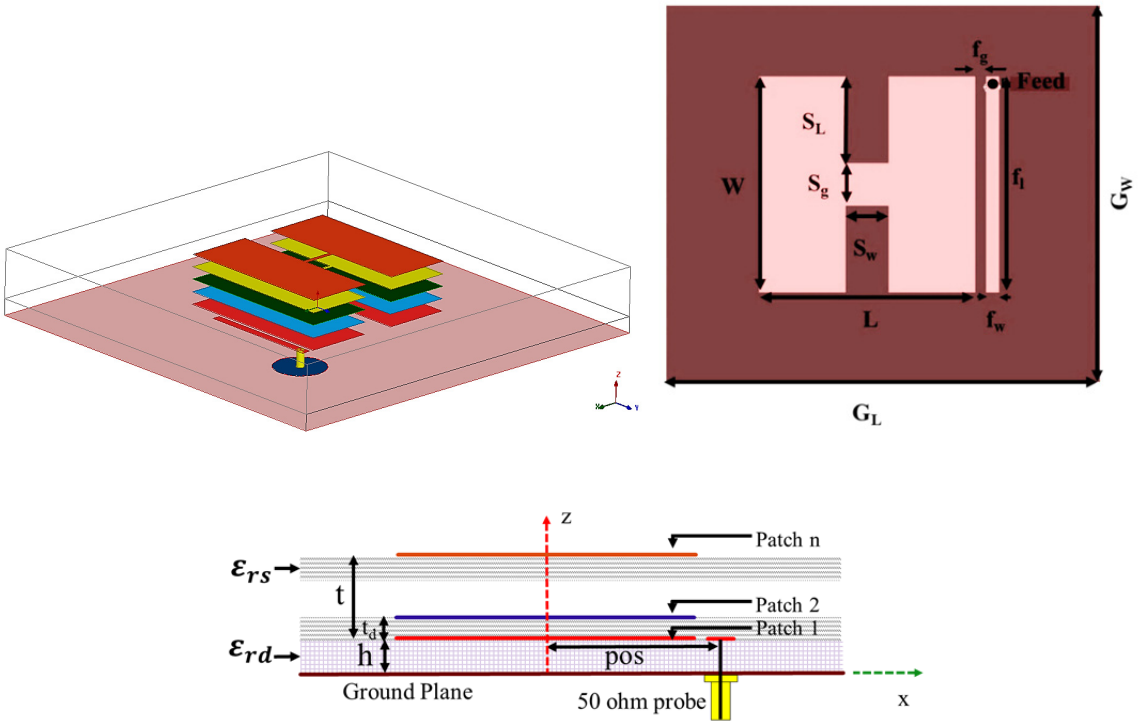

Figure 5.5 Geometry of Multilayerd H-Shaped Square Patch antenna with capacitive edge feed on a dielectric of ε_{rd} =2.5 and tanδ = 0.018 h=0.031inches.both patch and ground are of 35µm thickness and made of copper σ=5.8 × 10^7

Table 5-II
Dimensions of the patch shown in Figure 5.5

Parameter	L	W	S_w	S_L	f_l	f_w	f_g	G_L	G_W	S_g
Dimensions	*20mm*	*20mm*	*4mm*	*9.5mm*	*20mm*	*1.5mm*	*0.5mm*	*50mm*	*50mm*	*1mm*

Six cases for the antenna under consideration were studied. These are depicted in Figure 5.6. Subplots (a) and (b) in Figures 5.6, 5.7 and 5.8 show the results for the case of single patch antenna with a dielectric superstrate and multilayered substrate, respectively. Subplots (c) to (f) show the results for multiple resonators 2 to 5 respectively. The dielectric constant ε_{rs} is considered to be loss less in all the cases.

0000000

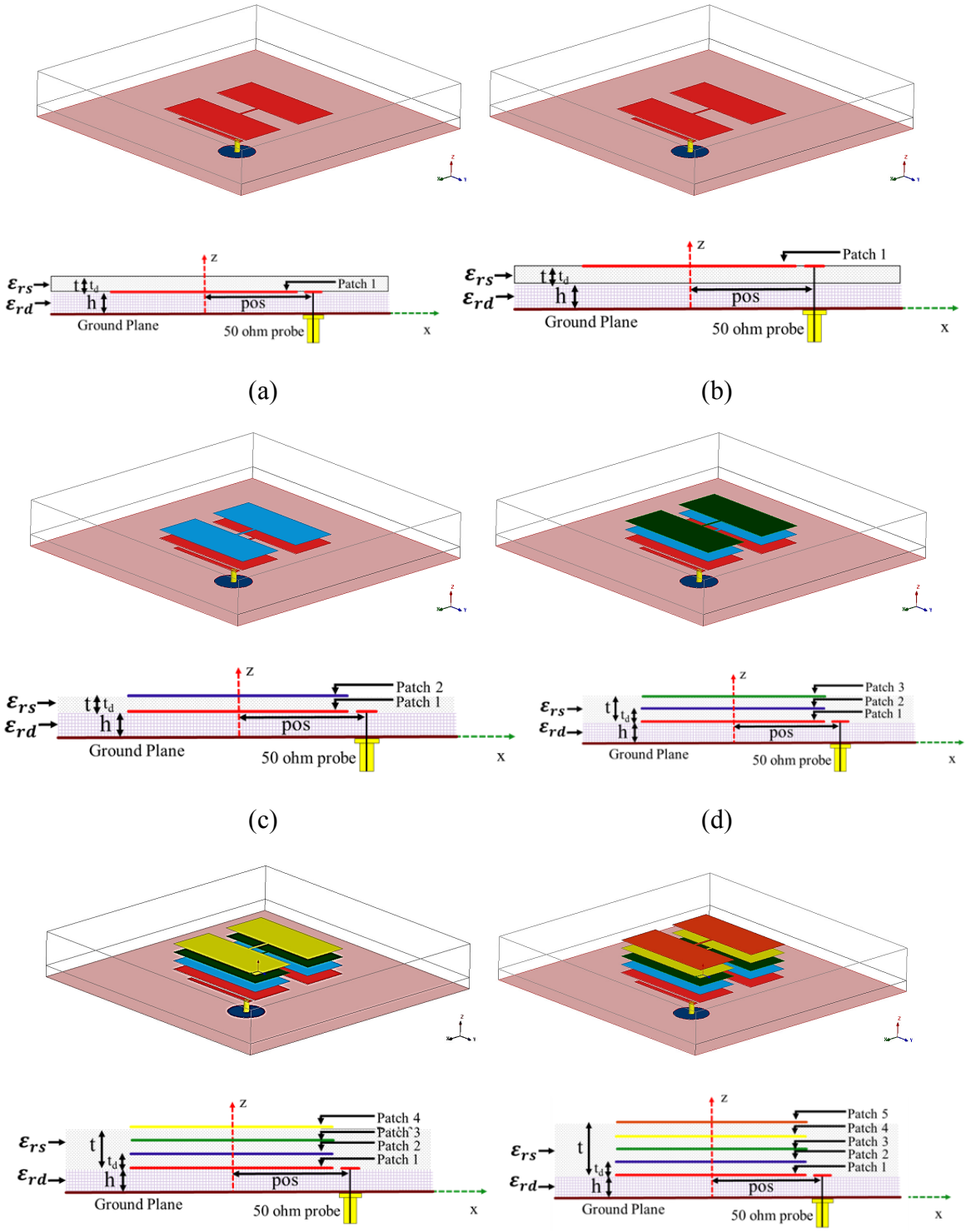

Figure 5.6 (a) Case 1: 1 resonator with superstrate (b) Case 2: 1 resonator with multilayered substrate (c) Case 3: 2 resonators (d) Case 4: 2 resonators (e) Case 5: 4 resonators (f) Case 6: 5 resonators

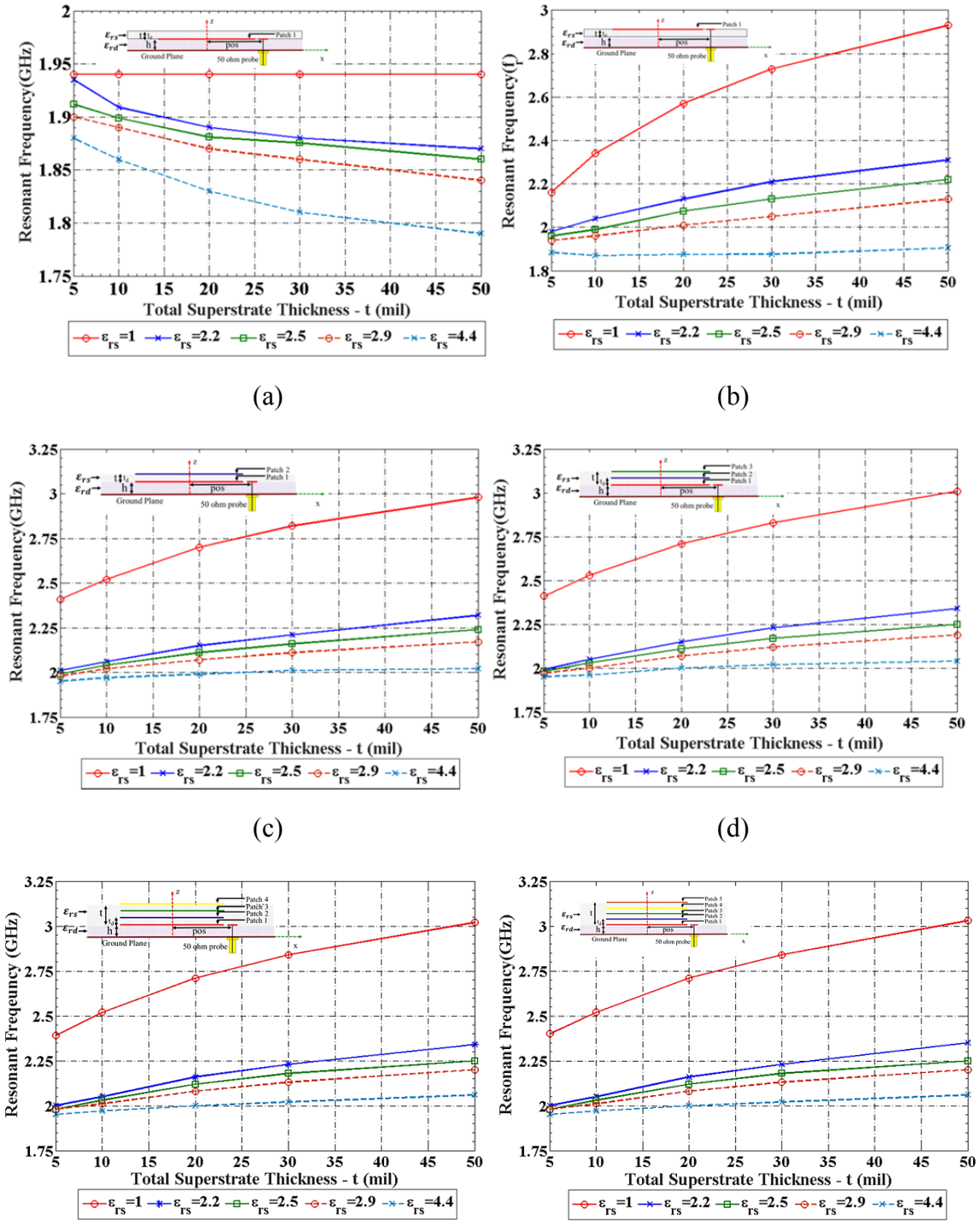

Figure 5.7 HFSS results showing variation of upper resonant frequency of stacked patch antenna for (a) 1 patch with superstrate (b) 1-patch with 2 layered substrate (c) 2-patches (d) 3-patches (e) 4-patches (f) 5- patches for different values of ε_{rs} and t_d

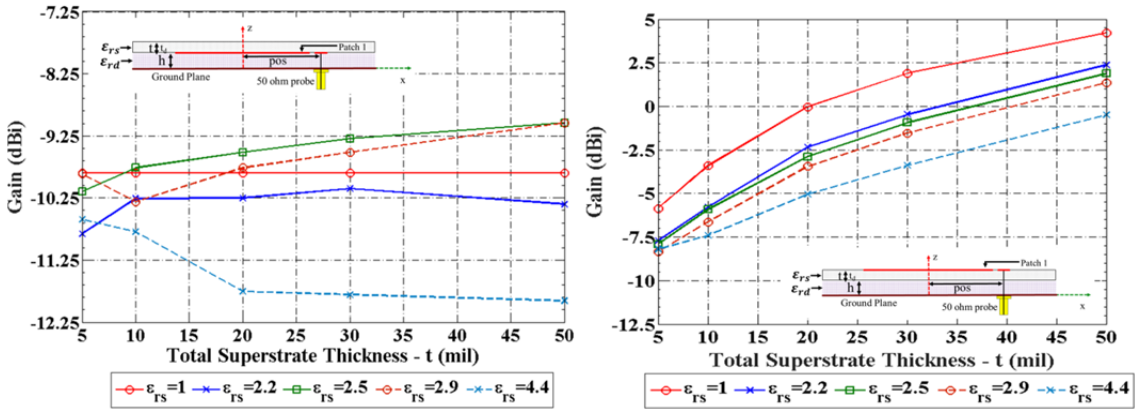

(a) (b)

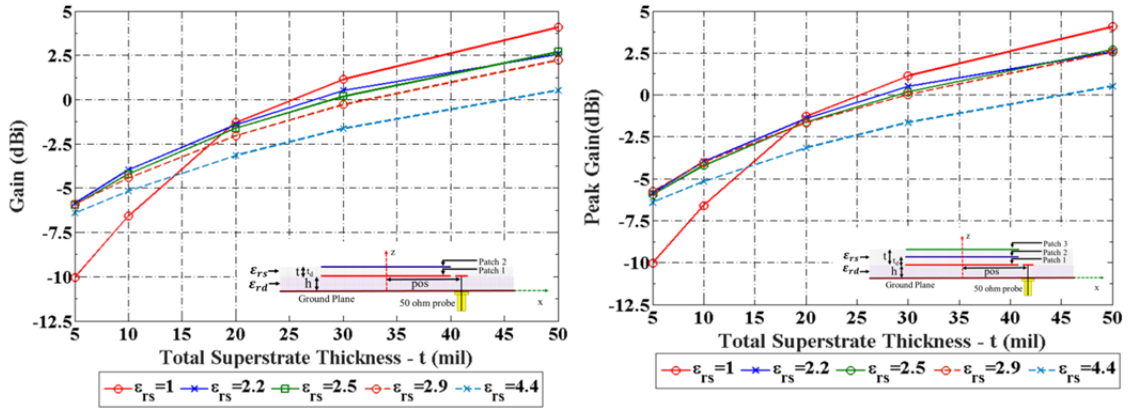

(c) (d)

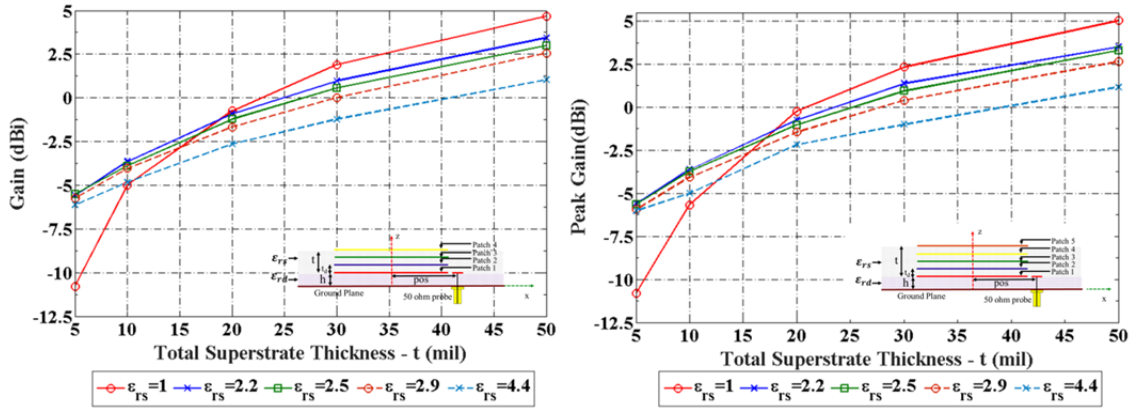

(e) (f)

Figure 5.8 HFSS results showing variation of Peak Gain at the upper resonant frequency of stacked patch antenna shown in Figure 5.5 for (a) 1 patch with superstrate (b) 1-patch with 2 layered substrate (c) 2-patches (d) 3-patches (e) 4-patches (f) 5- patches for different values of ε_{rs} and t_d

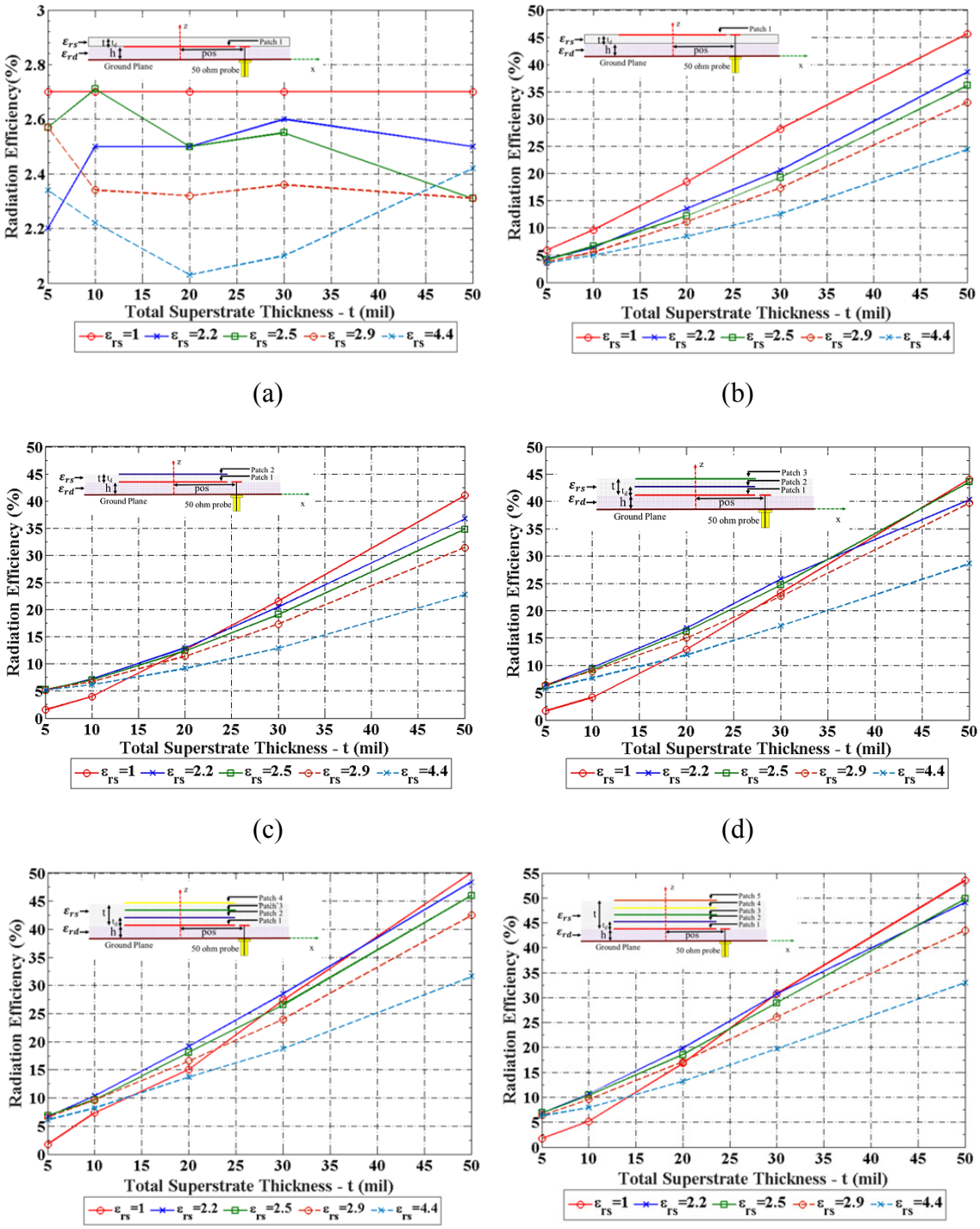

Figure 5.9 HFSS results showing variation of efficiency at the upper resonant frequency of stacked patch antenna shown in Figure 5.5 for (a) 1 patch with superstrate (b) 1-patch with 2 layered substrate (c) 2-patches (d) 3-patches (e) 4-patches (f) 5- patches for different values of ε_{rs} and t_d

Table 5-III (a)
HFSS results showing the effect of number of resonators with different spacing and dielectric constant of the superstrate on antenna efficiency

ε_{rs}	d	No of Patches	Resonant Frequency (GHz)	Directivity (dBi)	Gain (dBi)	Eff (%)
1	5mil	1	1.94	5.7	-9.85	2.7
		2	2.41	6.58	-11.5	1.55
		3	2.41	7.34	-10	1.64
		4	2.39	6.77	-10.8	1.76
		5	2.40	6.72	-10.8	1.75
4.4	5mil	1	1.88	5.73	-10.6	2.34
		2	1.95	5.86	-7.13	5.2
		3	1.95	6.01	-6.41	5.73
		4	1.95	6.04	-6.13	6.1
		5	1.95	5.95	-6.02	6.3

Table 5-III (b)
HFSS results showing the effect of number of resonators with different spacing and dielectric constant of the superstrate on antenna efficiency

ε_{rs}	d	No of Patches	Resonant Frequency (GHz)	Directivity (dBi)	Gain (dBi)	Eff (%)
1	20mil	1	1.94	5.7	-9.85	2.7
		2	2.70	7.49	-1.53	12.53
		3	2.71	7.59	-1.28	12.89
		4	2.71	5.47	-2.63	15.62
		5	2.71	7.51	-0.23	16.8
4.4	20mil	1	1.83	5.17	-11.8	2.03
		2	1.99	6	-4.38	9.157
		3	2.00	6.07	-3.15	11.9
		4	2.00	5.99	-2.64	13.71
		5	2.00	6.08	-2.17	13.2

Table 5-III (c)
HFSS results showing the effect of number of resonators with different spacing and dielectric constant of the superstrate on antenna efficiency

ε_{rs}	d	No of Resonators	Resonant Frequency (GHz)	Directivity (dBi)	Gain (dBi)	Eff (%)
1	50mil	1	1.935	5.7	-9.85	2.7
		2	2.98	7.65	3.78	41
		3	3.01	7.63	4.08	44.07
		4	3.02	5.65	-0.79	22.69
		5	3.03	7.75	5.036	53.5
4.4	50mil	1	1.79	4.26	-11.9	2.42
		2	2.02	5.9	-0.53	22.77
		3	2.04	5.97	0.52	28.6
		4	2.06	6.046	1.04	31.6
		5	2.06	6.01	1.178	33

Figure 5.7 shows the variation of upper resonant frequency for the 6 cases considered here. For *case 1* and *case 2*, the effects of superstrate dielectric constant and the height directly define the resonant frequency of the radiator. The resonant frequency of these cases with single patch antenna may be directly deduced from the effective dielectric permittivity of the antenna. For *case 1*, with the increase in the superstrate dielectric constant and height the resonant frequency shifts lower, while for the *case 2*, where there is a multilayer substrate, the resonant frequency with height of the upper substrate layer for different the values of ε_{rs} are considered here. This shift in resonant the frequency may be directly predicted from the effective dielectric constant of the medium given in [61].

For the *cases 3* to *6,* however, the resonant frequency is also affected by the presence of the parasitic patches. At the upper resonant frequency considered here, the coupling of

energy to the upper patches have the effect of decreasing the effective length (L_{eff}) of the original patch, thereby increasing the resonant frequency. When the dielectric constant is low, the resonant frequency shifts higher much more rapidly with the increase in the superstrate height. For a constant thickness however, for different number of resonant patches, the resonant frequency deviation from the desired one is minimal. With suitable a selection of the dielectric constant ε_{rs} and thickness *t* of the superstrate, the change in the resonant frequency may be controlled. For the current antenna this is obtained at a dielectric constant of $\varepsilon_{rs} = 4.4$ and a total superstrate thickness of 50mils.

Figure 5.8 and Figure 5.9 show the variations of gain and efficiency of the antenna for the six variations considered here. For *case 1*, with the efficiency has very little change with height and dielectric constant of the superstrate. For the *case 2*, the gain and radiation efficiency increases with the increase in the height of the upper layer of the substrate. . For *cases 3* to *6*.the gain and efficiencies increases the most for variations with higher deviation in frequency, in other words, with increase in the antenna size. The increase in resonant frequency has effect on the Directivity, Gain and Efficiency of the antenna. Any increase in the size with respect to the wavelength (W/λ_0, L/λ_0 and h/λ_0) changes the radiation pattern of the antenna. Increase in L/λ_0 and h/λ_0 of the patch increases the E-plane directivity, while increase in W/λ_0 increases the H- plane directivity [8]. As seen in chapter 2, an increase of the resonant frequency increases the effective volume of the antenna and thereby improves the Radiation Efficiency/Gain of the antenna.

The improvement in the efficiency and gain of the antenna for the *case 2* can be attributed to the lower loss in thicker substrate as discussed in chapter 2. With the addition of

multiple resonators however a further improvement in gain and efficiency is achieved. The maximum change in the gain/efficiency occurs for the single resonator case (*case 3*). A summary of the effect of multiple resonators on the gain and efficiency of the antenna is given in Table 5-III. It can be seen that an improvement in the gain by as much as 10dB and efficiency by 30% is achieved for the minimum frequency deviation of 0.1GHz, for the case of ε_{rs} = 4.4 and superstrate height of 50 mils. The radiation patterns for multi-resonators with superstrate dielectric ε_{rs} = 4.4 and different values of thickness *t* are shown in Figure 5.11 to Figure 5.19. For comparison the E-Plane and H-Plane Patterns for the simple single layer case is given in Figure 5.10. From the E plane and H plane directivity plots given in Figure 5.11, Figure 5.12, Figure 5.15, Figure 5.16, Figure 5.19 and Figure 5.20 it can be seen that with addition of a single patch element the maximum change in gain is observed. Furthermore, due to the dielectric loading effect, the pattern broadens and back lobe levels decreases. However, with further addition of resonators there is a minimal change to the radiation pattern shape. For a thinner superstrate (*t=1mil*), the pattern deviation from the single layer case is minimal, a gain improvement of 2.87dBi is observed by addition of one or more parasitic patches. On the other hand, for the thicker superstrate the same gives a much higher improvement in gain (9.47 dB for *t=50mil*) and significant back lobe (~4dB) reduction. Further addition of parasitic resonators increases the gain of the antenna by an additional 1.1 to 2.2 dB, depending on the thickness of the superstrate. The E and H plane gain patterns, for *t=5, 20 & 50* mil and ε_{rs}= 4.4, are given in Figure 5.13 to Figure 5.22.

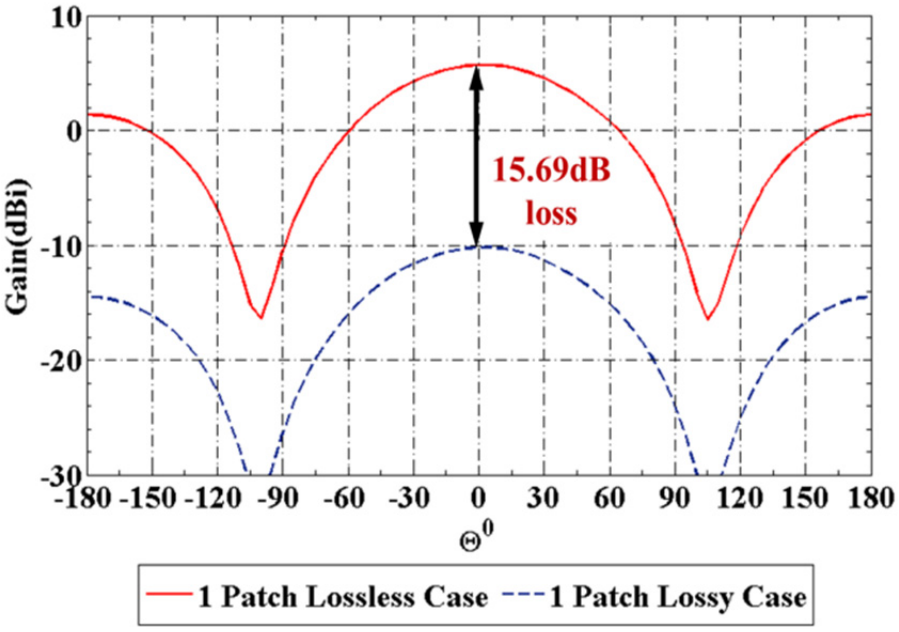

(a)

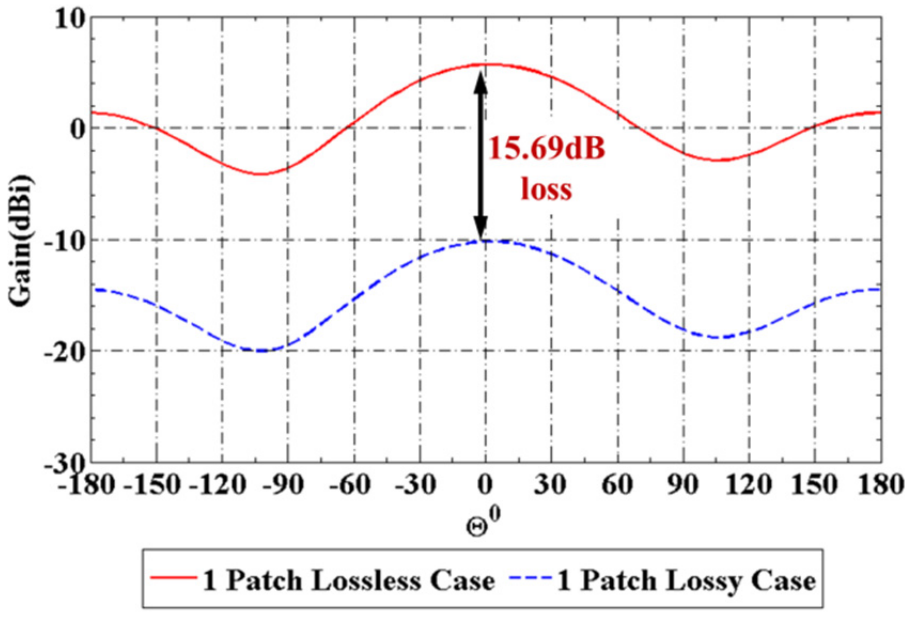

(b)

Figure 5.10 E-Plane (a) and H-Plane (b) Gain patterns for single layer antenna shown of geometry given in Figure 5.5 and dimensions given Table 5-II

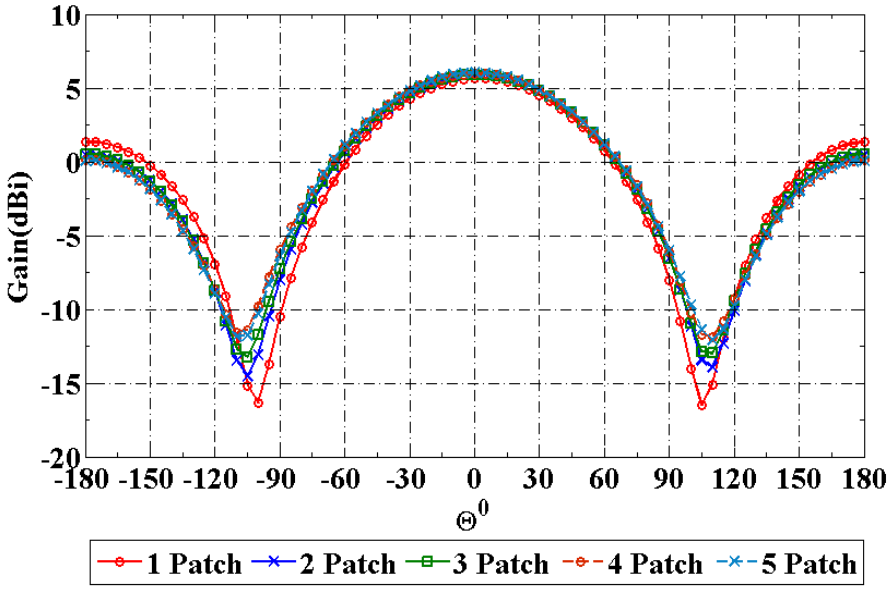

Figure 5.11 E plane Directivity pattern for multi layered antenna shown of geometry given in Figure 5.5 and dimensions given Table 5-II for a superstrate thickness of *t=5 mil*

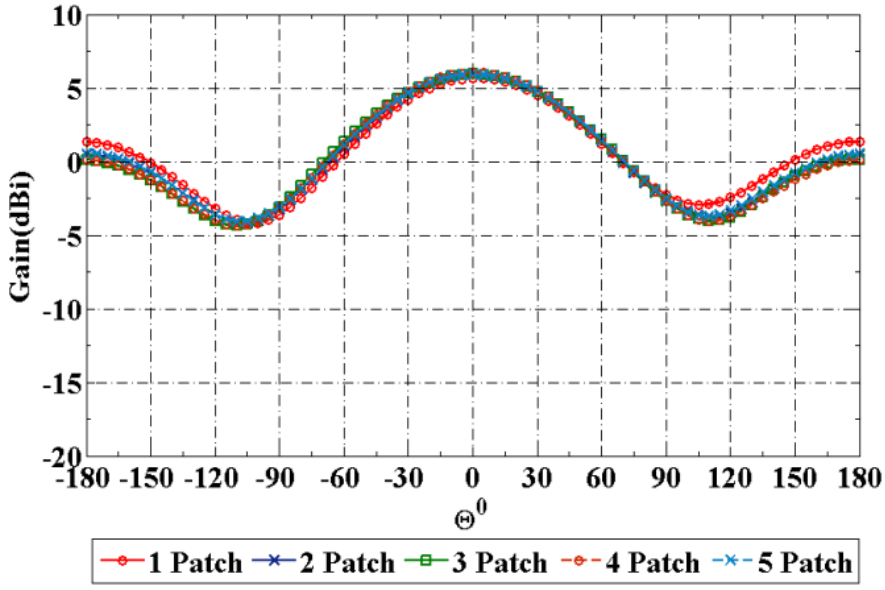

Figure 5.12 H plane Directivity pattern for multi layered antenna shown of geometry given in Figure 5.5 and dimensions given Table 5-II for a superstrate thickness of *t=5 mil*

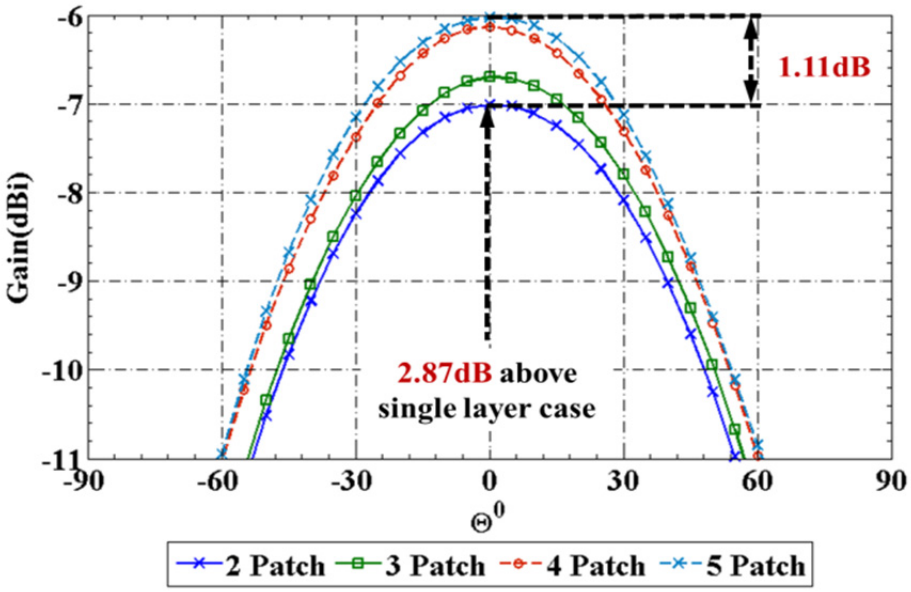

Figure 5.13 E plane Gain pattern for multi layered antenna shown of geometry given in Figure 5.5 and dimensions given Table 5-II for a superstrate thickness of *t=5 mil*

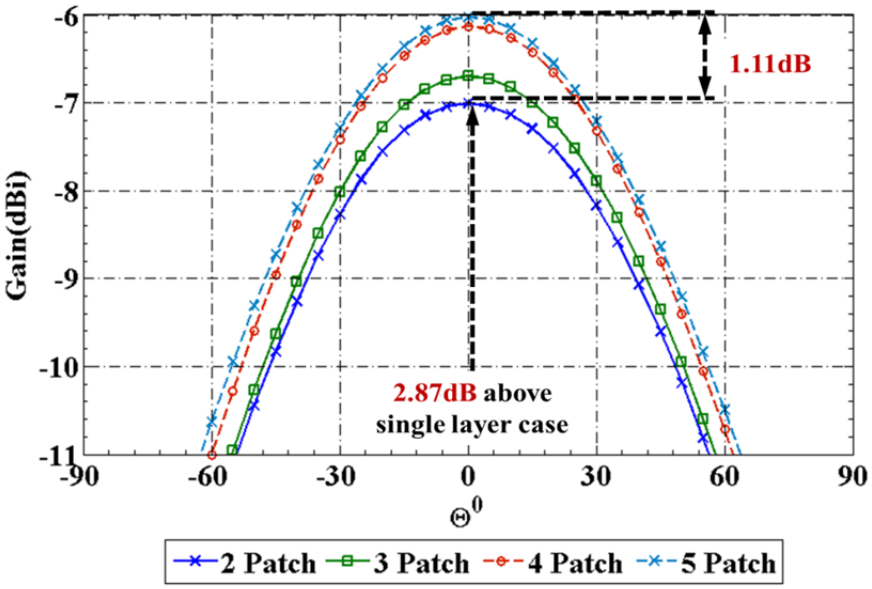

Figure 5.14 H plane Gain pattern for multi layered antenna shown of geometry given in Figure 5.5 and dimensions given Table 5-II for a superstrate thickness of *t=5 mil*

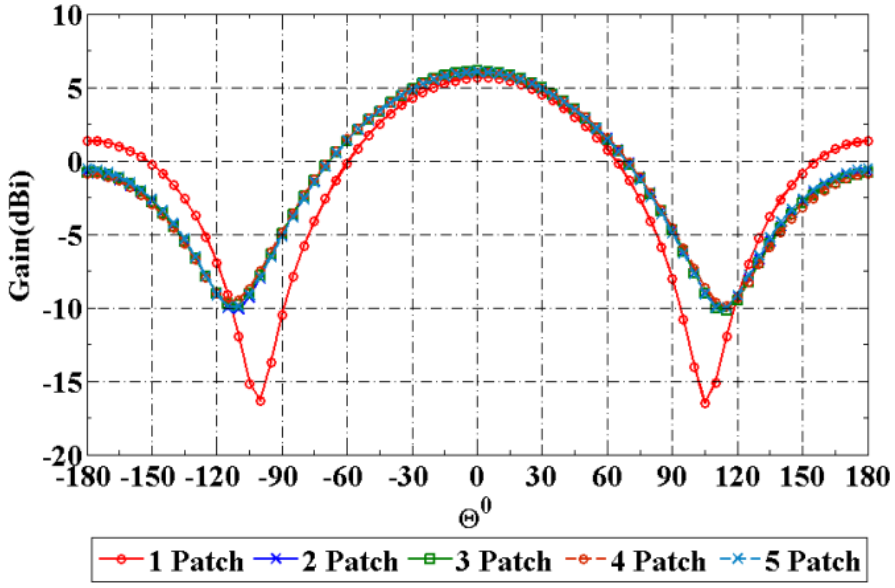

Figure 5.15 E plane Directivity pattern for the multi-layered antenna shown of geometry given in Figure 5.5 and dimensions given Table 5-II for a superstrate thickness of *t=20mil*

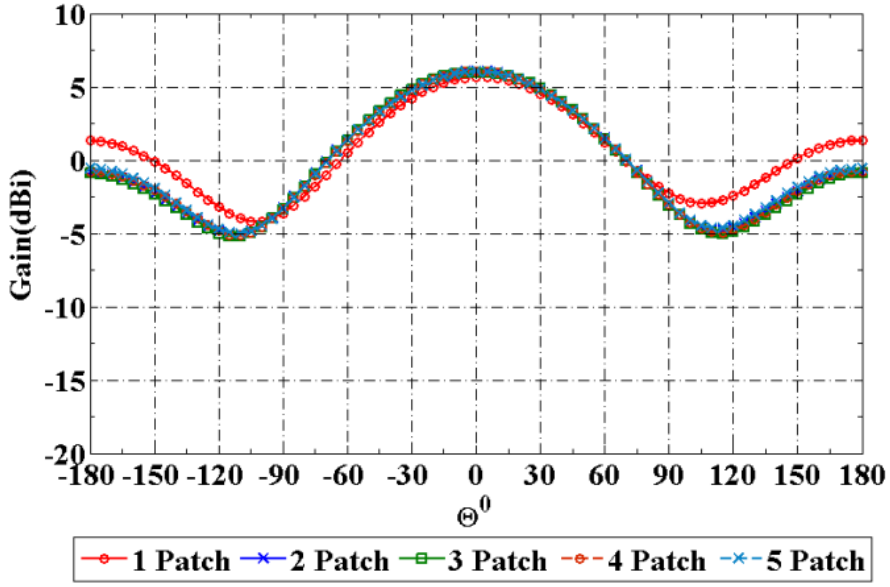

Figure 5.16 H plane Directivity pattern for the multi-layered antenna shown of geometry given in Figure 5.5 and dimensions given Table 5-II for a superstrate thickness of *t=20 mil*

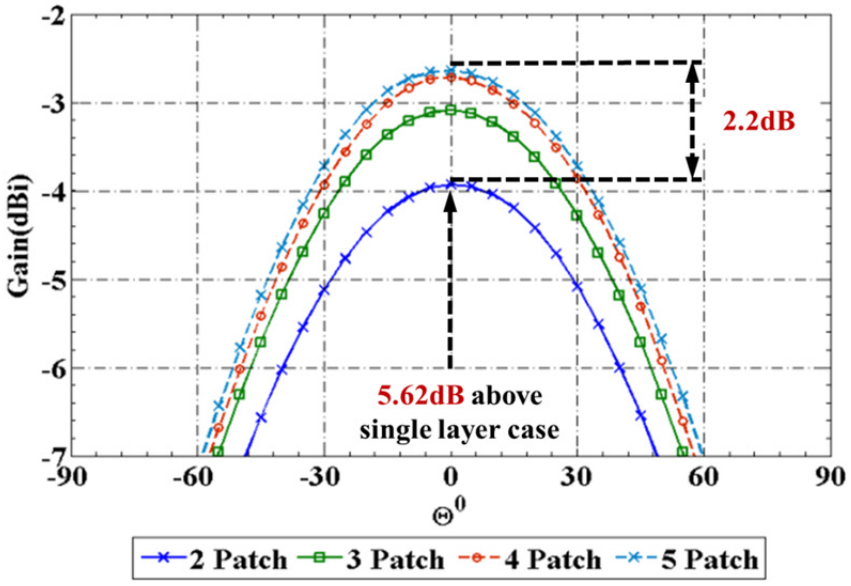

Figure 5.17 E plane Gain pattern for the multi-layered antenna shown of geometry given in Figure 5.5 and dimensions given Table 5-II for a superstrate thickness of *t=20 mil*

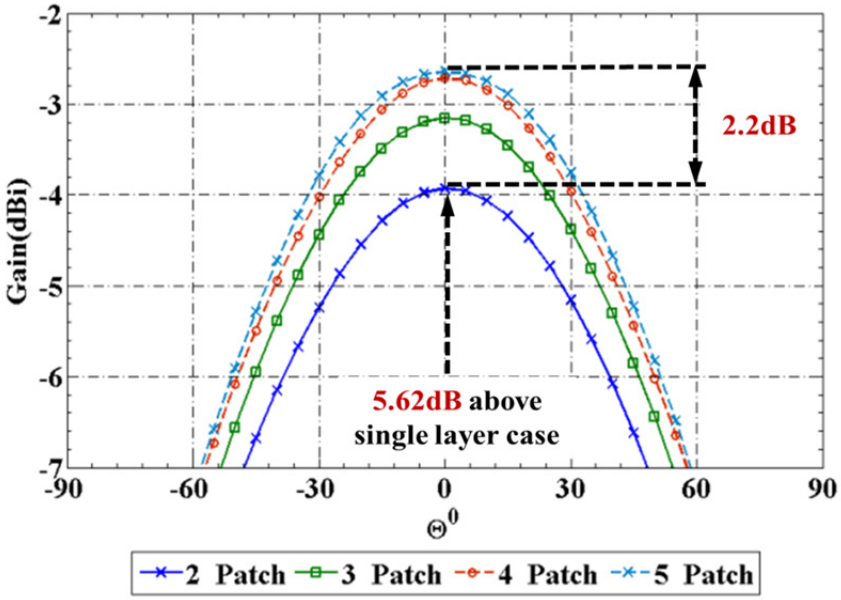

Figure 5.18 H plane Gain pattern for the multi-layered antenna shown of geometry given in Figure 5.5 and dimensions given Table 5-II for a superstrate thickness of *t=20 mil*

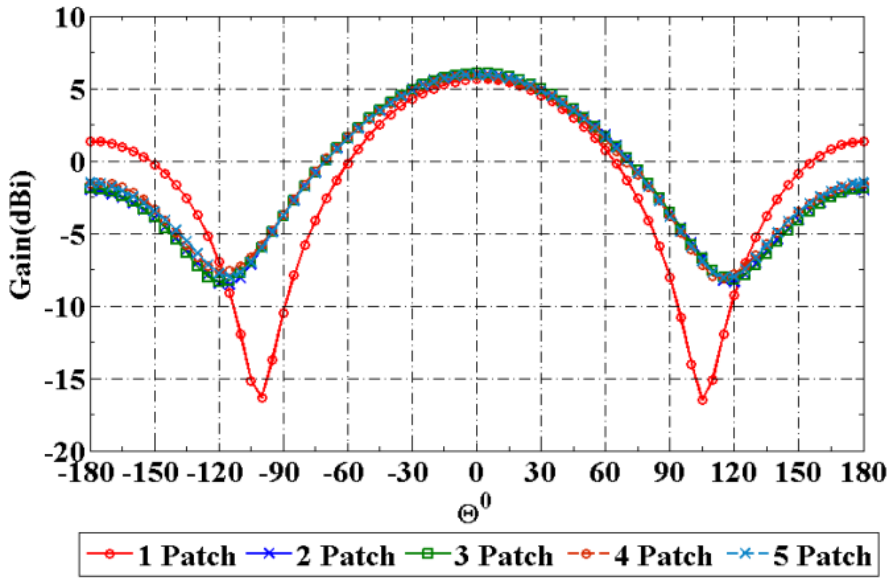

Figure 5.19 E plane Directivity pattern for the multi-layered antenna shown of geometry given in Figure 5.5 and dimensions given Table 5-II for a superstrate thickness of *t=50 mil*

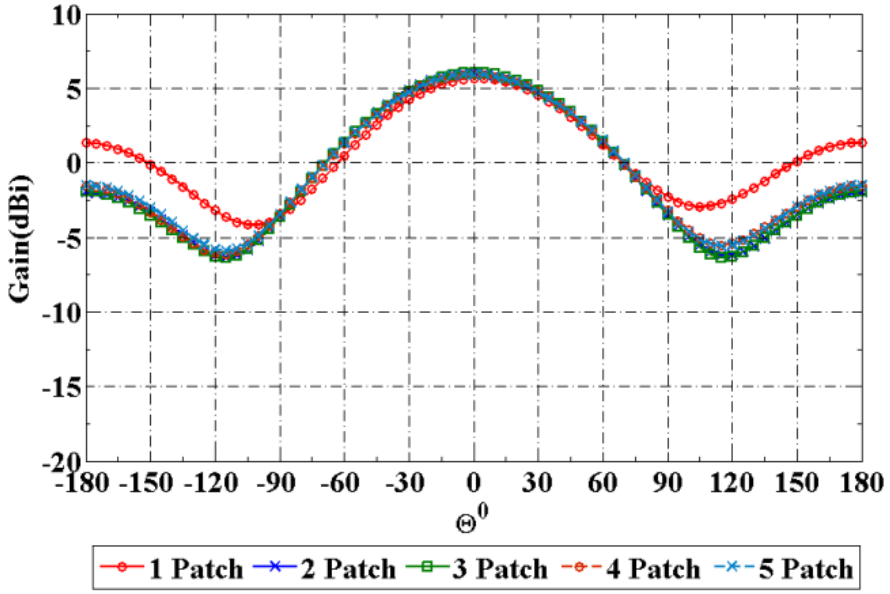

Figure 5.20 H plane Directivity pattern for the multi-layered antenna shown of geometry given in Figure 5.5 and dimensions given Table 5-II for a superstrate thickness of *t=50 mil*

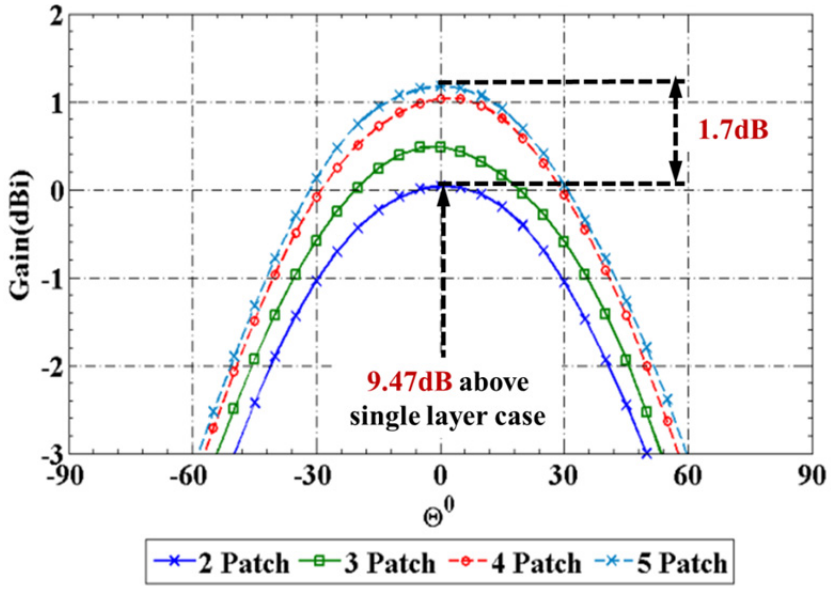

Figure 5.21 E plane Gain pattern for the multi-layered antenna shown of geometry given in Figure 5.5 and dimensions given Table 5-II for a superstrate thickness of *t=50 mil*

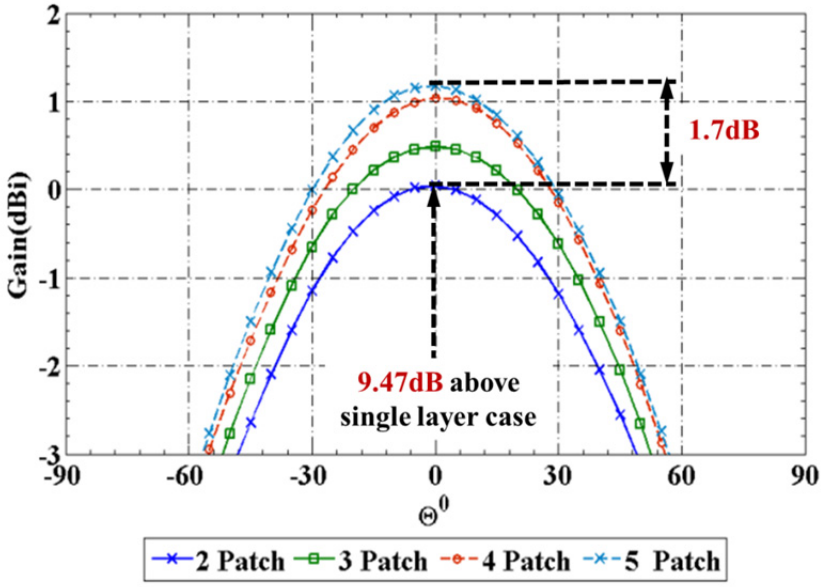

Figure 5.22 H plane Gain pattern for the multi-layered antenna shown of geometry given in Figure 5.5 and dimensions given Table 5-II for a superstrate thickness of *t=50 mil*

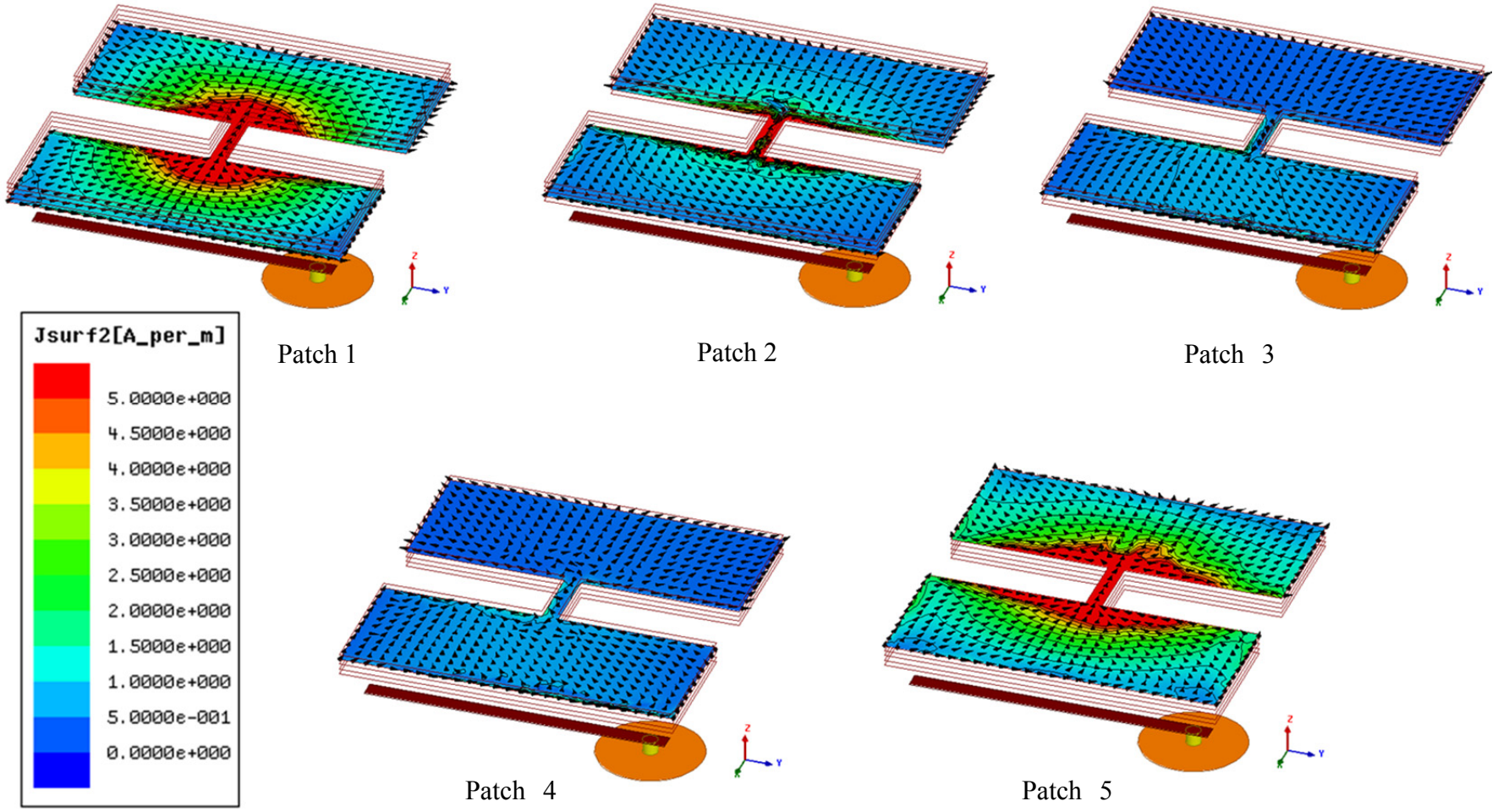

Figure 5.23 Current distribution on the patches at different layers for the multi-layered antenna shown of geometry given in Figure 5.5 and dimensions given Table 5-II for a superstrate thickness of t=50 mil

The gain/efficiency does not however increase indefinitely to the lossless case, for more than 4 resonators the improvement in the gain of the antenna is seen to be minimal. The cross polarization levels in all the cases were found to be ~25dB below the desired patterns and hence are not shown here. Figure 5.23 shows the current distribution on the patches at different layers for a superstrate thickness of t=50 mil. As expected since the frequency under consideration here is the higher resonant frequency and as all patches are identical in size, even/symmetric mode dominates. There by, when compared to that of a single patch case, the multiple layers has higher in-phase current over a larger area, thus improving the gain/radiation efficiency of the antenna by the increase in the radiation conductance of the antenna as discussed in the previous chapter.

5.3 FABRICATION AND MEASUREMENT RESULTS

In the following section the concept discussed previously is experimentally verified. Two different variations of the antenna were fabricated and tested.

Design 1 consists of a patch antenna of geometry and dimensions given in Figure 5.24 and Table 5-IV respectively.

Design 2 consists of a patch antenna of geometry and dimensions given in Figure 5.39 and Table 5-V respectively.

Each of the antennas in *Design 1* and *Design 2* consists of antennas with different levels of miniaturization. *Design 1* corresponds to an electrically larger antenna compared to the parametric study carried out in the previous section, while *Design 2* corresponds to an electrically smaller antenna. This was done in order to effectively evaluate the amount of efficiency improvement that can be achieved for two different levels of miniaturization. The antenna structure was chosen after taking into account various measurement and fabrication

constraints. The feed line length, width and gap were chosen such that the even after addition of multiple layers, reasonable impedance matchings were obtained. In all the cases, the feed line width was also dictated by the diameter of the co-axial probe under use. The ground plane size was chosen to be large enough to avoid reflections from the cables and mount caused by the back radiation of the antenna. The substrate and superstrate were chosen based on their availability and fabrication feasibility.

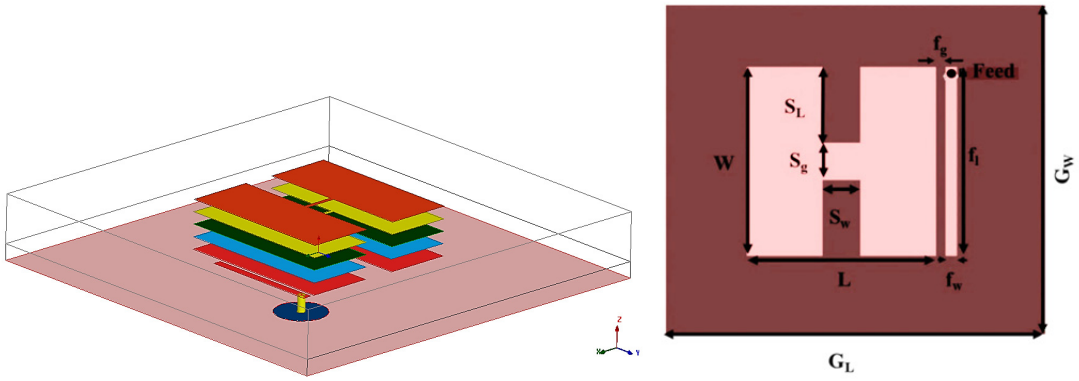

(a)

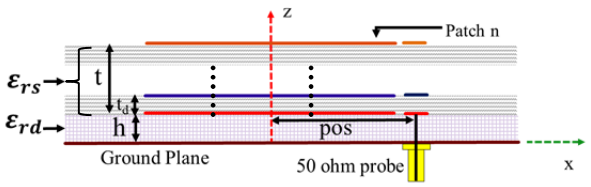

(b)

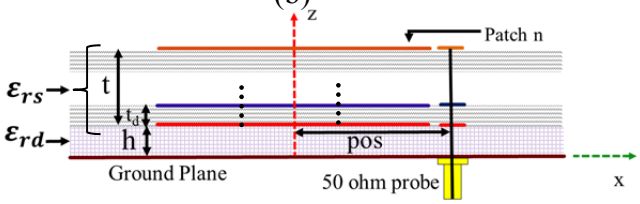

(c)

Figure 5.24 *Design 1* (a) Antenna Geometry (b) side view showing case 1- feed connected only to lower most layer (c) case 2- feed connected all layers layer

Table 5-IV Dimensions of the antenna shown in Figure 5.24 used for fabrication

Parameter	*L* *(mm)*	*W* *(mm)*	S_w *(mm)*	S_L *(mm)*	f_l *(mm)*	f_w *(mm)*	f_g *(mm)*	G_L *(mm)*	G_W *(mm)*	*h* *(mil)*	t_d *(mil)*	S_g *(mm)*
Dimensions	20	20	4	8	20	1.5	0.5	355	355	31	15	4

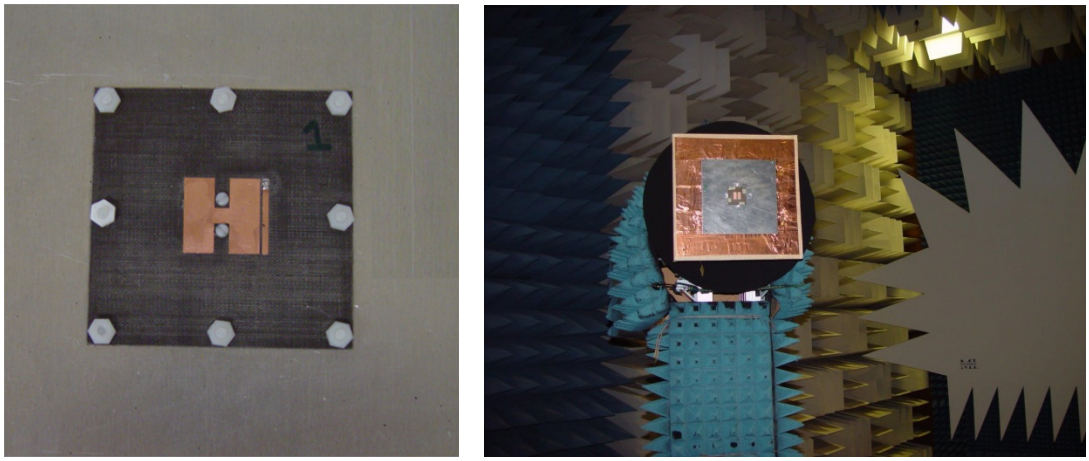

Figure 5.25 *Design 1* - Fabricated antenna (left) and the antenna under test at the University of Manitoba Antenna Measurement chamber (right).

From the mechanical sturdiness and air gap point of view, two antennas with different feed structures were fabricated and measurements were carried out individually. In the first case the coaxial probe was connected only to the bottom most layer feed line, and in the second case. the coaxial probe was connected to the feed lines of all the layers. The Commercially available laminate material - Arlon DiClad 527 with a dielectric constant of ε_{rs} = 2.5 and a loss tangent tan(δ)=0.0018 was used for fabrication of all layers of the antenna. The superstrate layers were each of 15mil thickness, this was limited by the fabrication facility used for building the antenna. Figure 5.25 shows the fabricated antenna and the antenna measurement chamber. For proper alignment of the multi layered structure 2 diametrically alignment holes were used. Nylon screws and silicone glue were used to attach the multiple layers together firmly. The simulation and measurement results thus obtained for the antennas are given in Figure 5.26 to Figure 5.37. A summary of the results are given in Table 5-VI and Table 5-VII . All the measurement results and simulation results are found to be in good agreement.

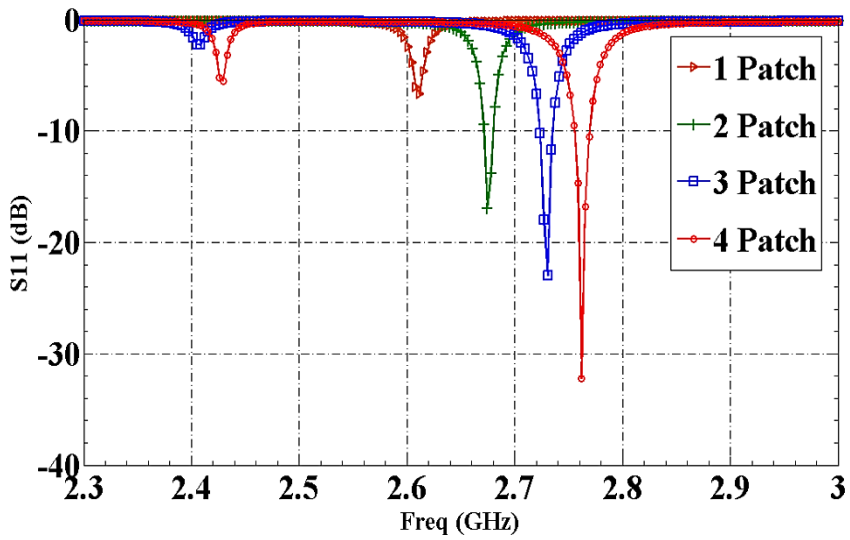

Figure 5.26 *Design 1* - HFSS simulation results showing the return loss for the multi-layered antenna of geometry and dimensions given in Figure 5.24 and Table 5-IV, case 1: feed connected only to the lowest layer

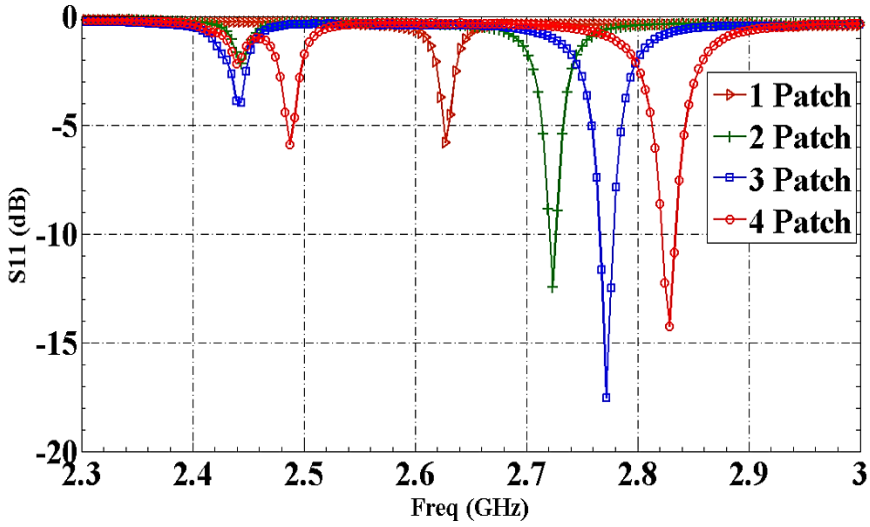

Figure 5.27 *Design 1* - Measurement results showing the return loss for the multi-layered antenna of geometry and dimensions given in Figure 5.24 and Table 5-IV, case 1: feed connected only to the lowest layer

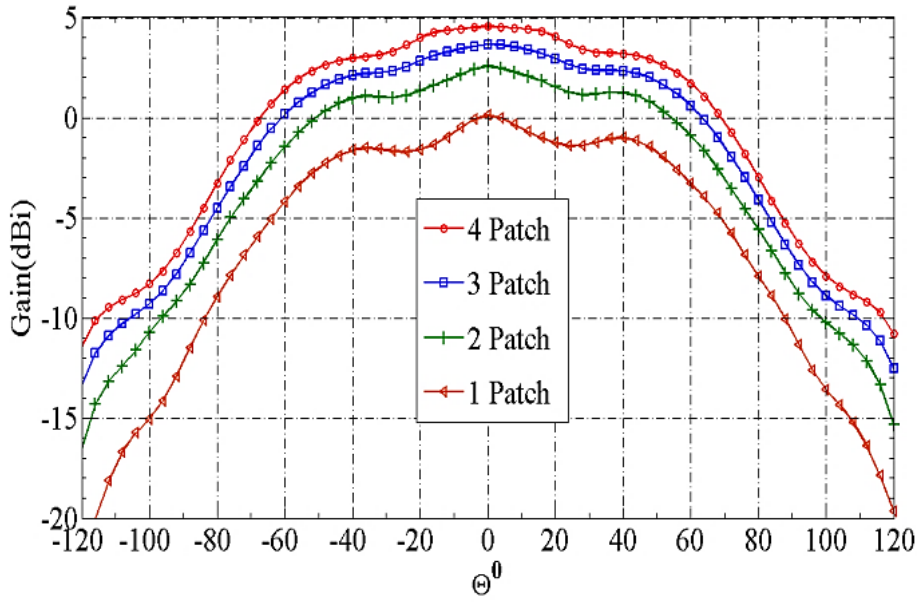

Figure 5.28 *Design 1* - HFSS simulation results showing the E-Plane Pattern for the multi-layered antenna of geometry and dimensions given in Figure 5.24 and Table 5-IV, case 1: feed connected only to the lowest layer

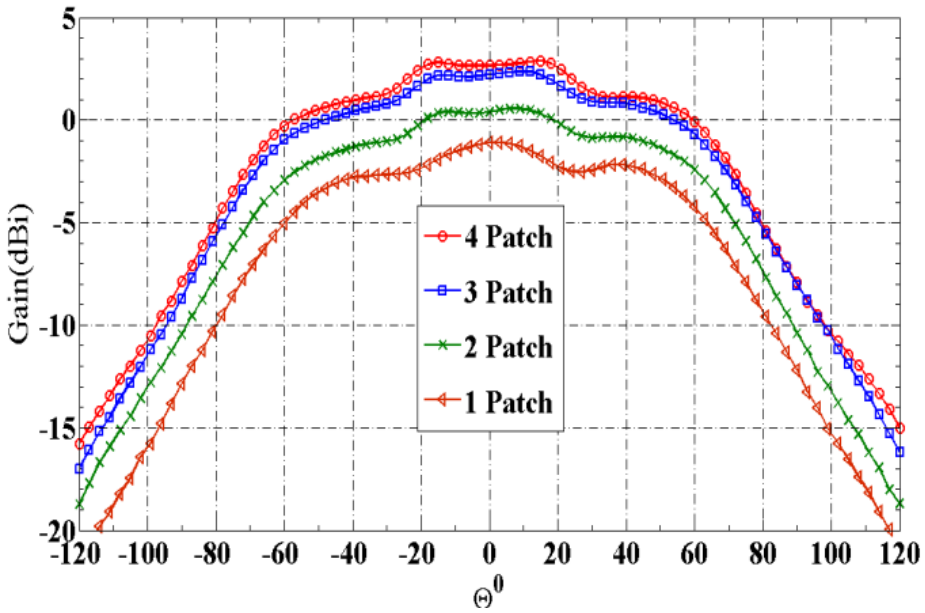

Figure 5.29 *Design 1* - Measurement results showing the E-Plane Pattern for the multi-layered antenna of geometry and dimensions given in Figure 5.24 and Table 5-IV, case 1: feed connected only to the lowest layer

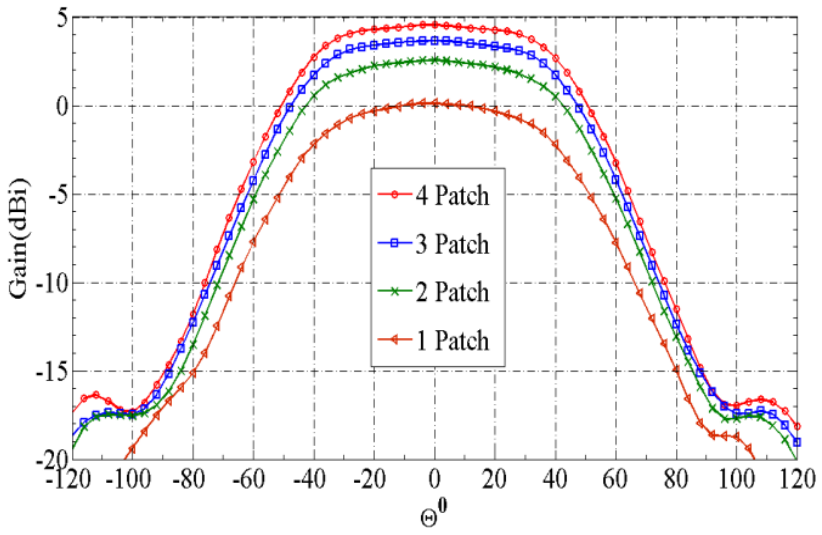

Figure 5.30 *Design 1* - HFSS simulation results showing the H-Plane Pattern for the multi-layered antenna of geometry and dimensions given in Figure 5.24 and Table 5-IV, case 1: feed connected only to the lowest most layer

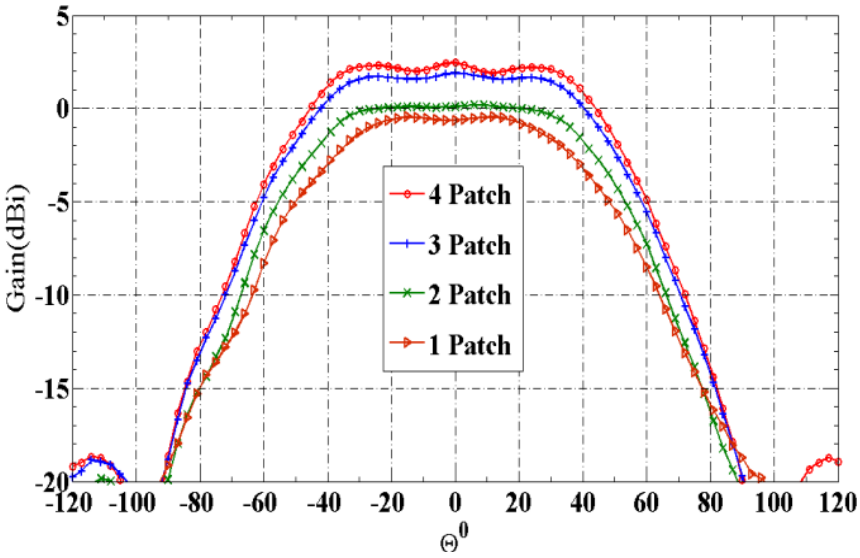

Figure 5.31 *Design 1* - Measurement results showing the H-Plane Pattern for the multi-layered antenna of geometry and dimensions given in Figure 5.24 and Table 5-IV, case 1: feed connected only to the lowest layer

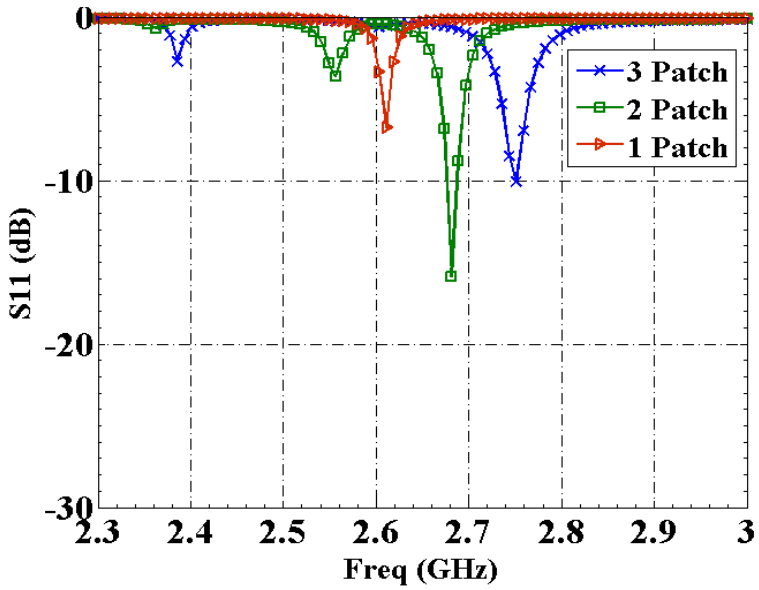

Figure 5.32 *Design 1* - HFSS simulation results showing the return loss for the multi-layered antenna of geometry and dimensions given in Figure 5.24 and Table 5-IV, case 2- feed connected all the layers

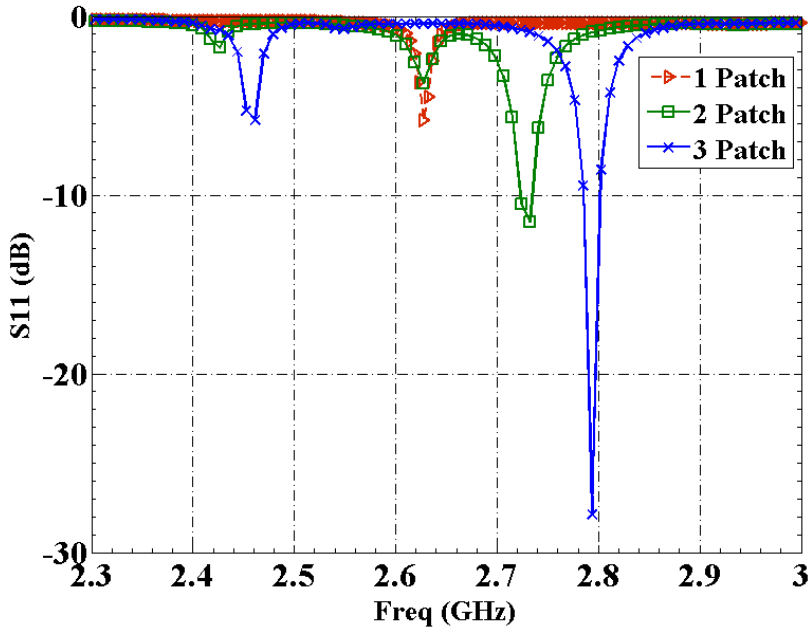

Figure 5.33 *Design 1* - Measurement results showing the return loss for the multi-layered antenna of geometry and dimensions given in Figure 5.24 and Table 5-IV, case 2- feed connected all the layers

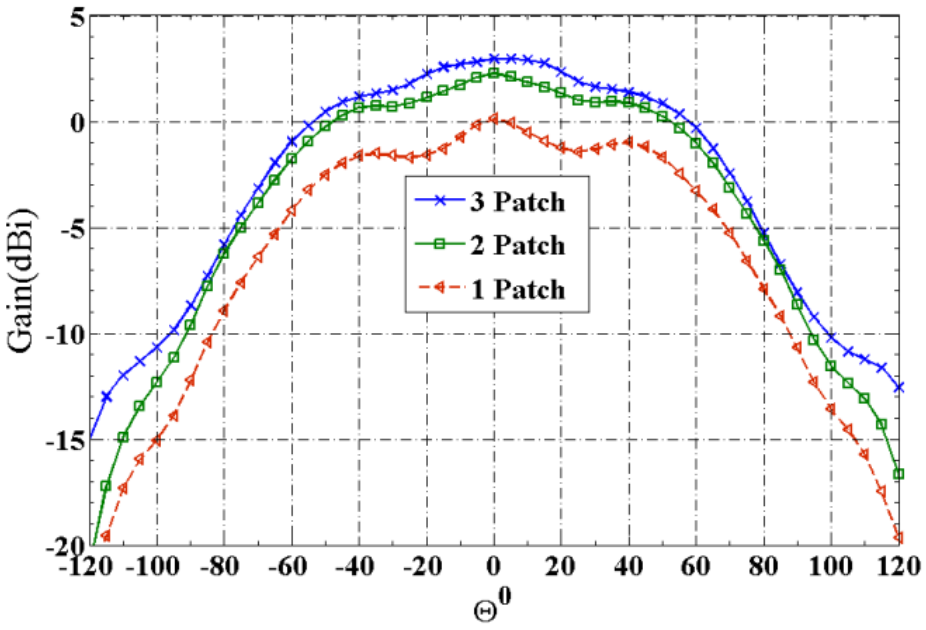

Figure 5.34 *Design 1* - HFSS simulation results showing the E-Plane Pattern for the multi-layered antenna of geometry and dimensions given in Figure 5.24 and Table 5-IV, case 2-feed connected all the layers

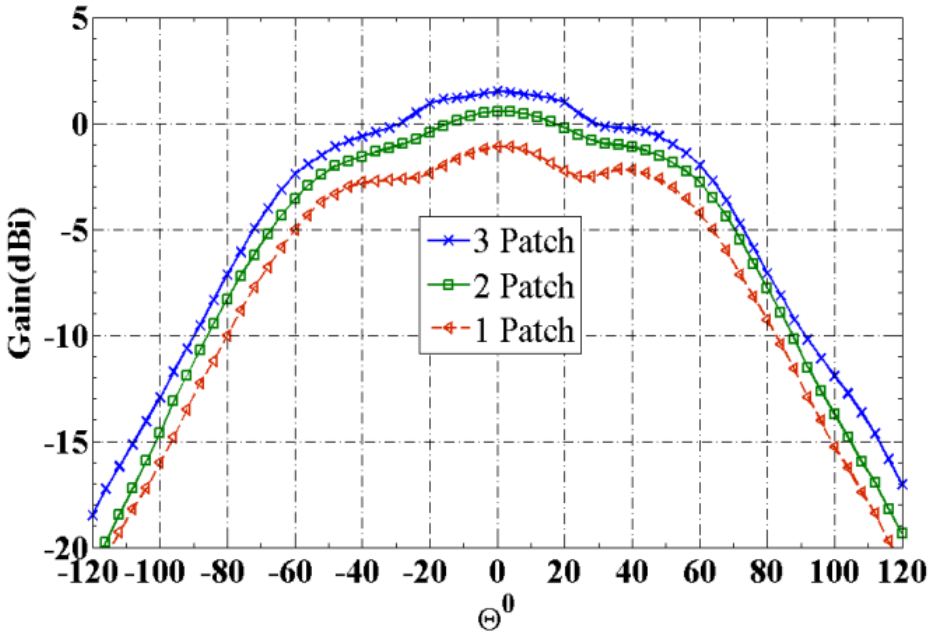

Figure 5.35 *Design 1* - Measurement results showing the E-Plane Pattern for the multi-layered antenna of geometry and dimensions given in Figure 5.24 and Table 5-IV, case 2-feed connected all the layers

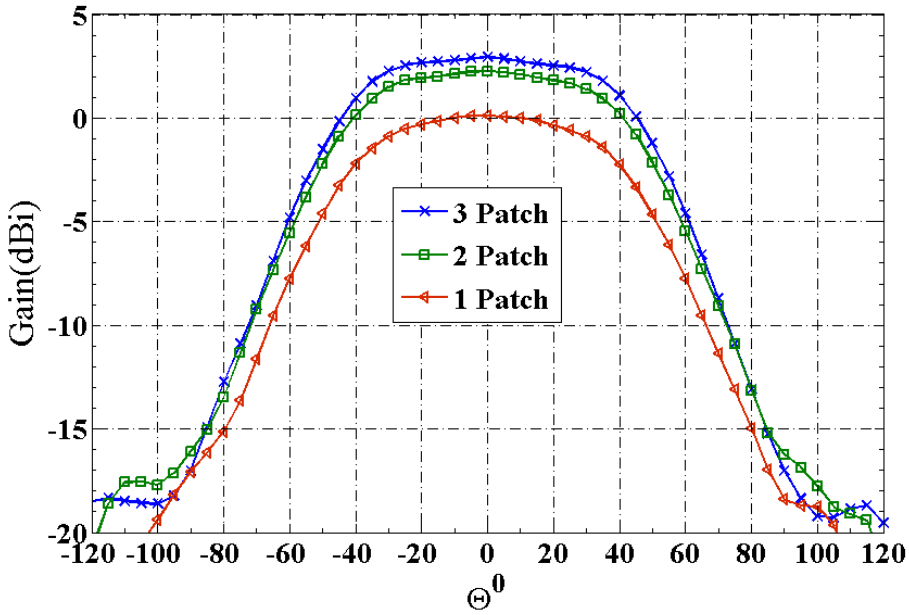

Figure 5.36 *Design 1* - HFSS simulation results showing the H-Plane Pattern for the multi-layered antenna of geometry and dimensions given in Figure 5.24 and Table 5-IV, case 2: feed connected only to all the layers

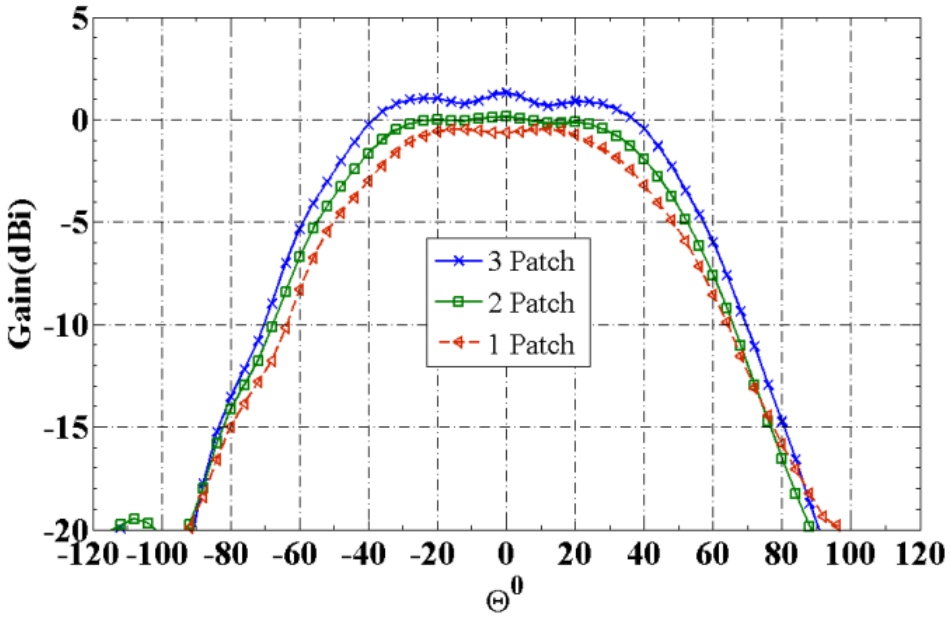

Figure 5.37 *Design 1* - Measurement results showing the H-Plane Pattern for the multi-layered antenna of geometry and dimensions given in Figure 5.24 and Table 5-IV, case 2: feed connected all the layers

It is observed that for the case where the feed lines in all layers were shorted to the coaxial cable did not give as much improvement, as compared to the cases where the feed was connected to the lower patch. This is because of the increase in the cross polarization level when the feeds are shorted. The deviation in the resonant frequency from the simulated value may be attributed to the effect of glue and air gap between the stacked antenna layers. The effect of air gap on the resonant frequency of 2 layered antenna, with only the lower patch connected to coaxial connector, is shown in Figure 5.38.

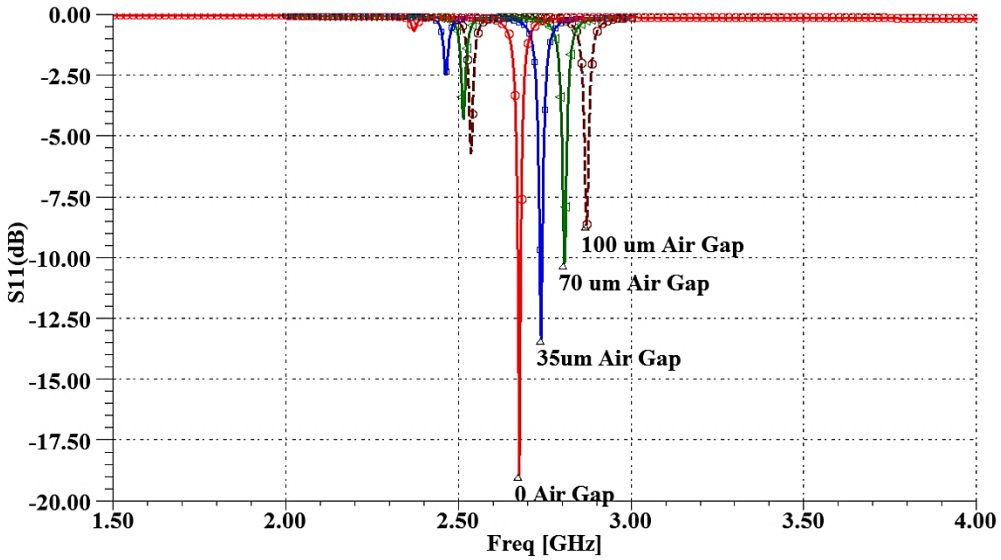

Figure 5.38 *Design 1* - HFSS simulation results showing the effect of air gap on the resonant frequency and matching for the 2-layered antenna of geometry and dimensions given in Figure 5.24 and Table 5-IV, case 1 - feed connected only to lower most layer

Measurements were also carried out for a smaller variation of the H-shaped antenna, which is shown in Figure 5.39. The dimensions of the antenna are given in Table 5-V. The dielectric for the substrate and superstrate were the same as the previous antennas, with ε_{rs} = ε_{rd} = 2.5 and loss tangent tan(δ)=0.0018. Unlike the previous fabricated antennas, in the current structure the feed line is only located at the lowermost layer of the antenna and the other patches do not contain the feed line.

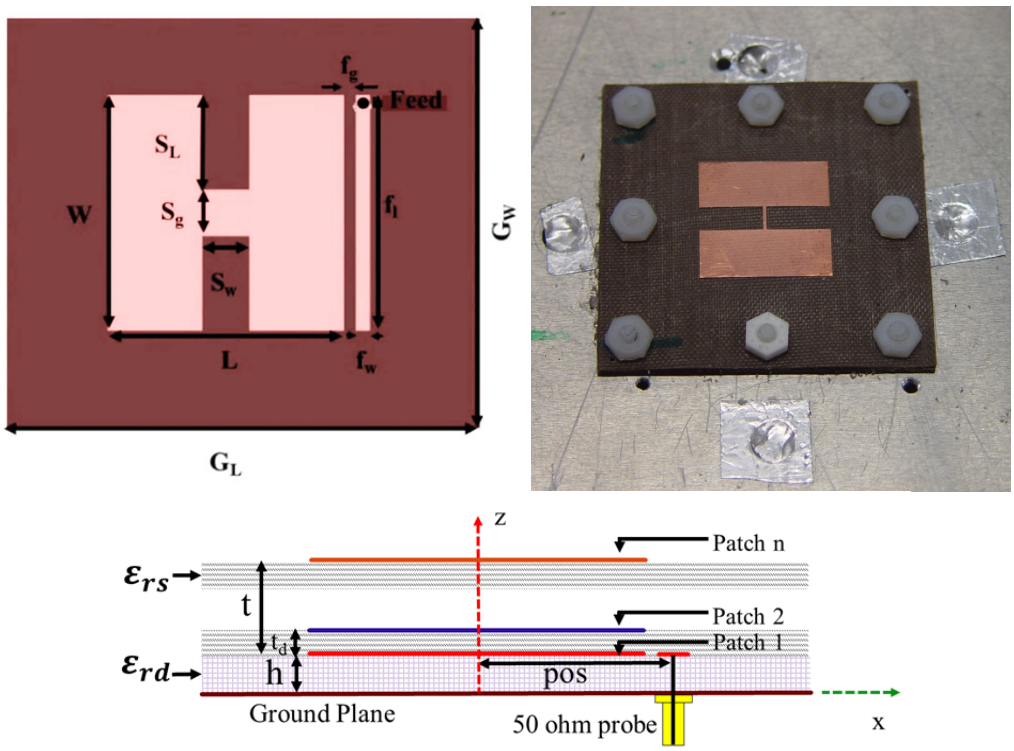

Figure 5.39 *Design 2* - Antenna geometry and the Fabricated antenna with $\varepsilon_{rs} = \varepsilon_{rd} = 2.5$ and loss tangent tan(δ)=0.0018 h=31mil, t_d =15mil

Table 5-V
Design 2 - Dimensions of the patch shown in Figure 5.39

Parameter	*L*	*W*	S_w	S_L	f_l	f_w	f_g	G_L	G_W	S_g
value	*20mm*	*20mm*	*4mm*	*9.75mm*	*15mm*	*1mm*	*0.5mm*	*35cm*	*35cm*	*0.5mm*

Figure 5.40 and shows the simulated and the measured return loss plots of the antenna for different number of resonant upper patches, Figure 5.42 and Figure 5.43 show the corresponding E-plane patterns, and Figure 5.44 and Figure 5.45 show the corresponding H-plane patterns of the antenna. Table 5-VIII shows a summary of the results.

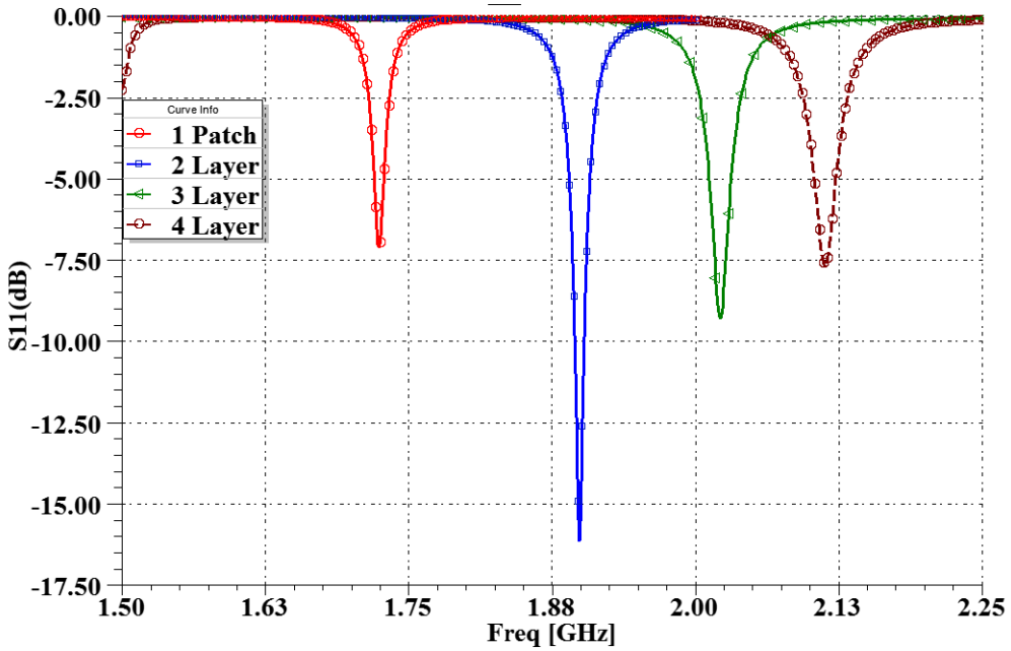

Figure 5.40 *Design 2* - HFSS simulation results showing the return loss for the multi-layered antenna of geometry and dimensions given in Figure 5.39 and Table 5-V

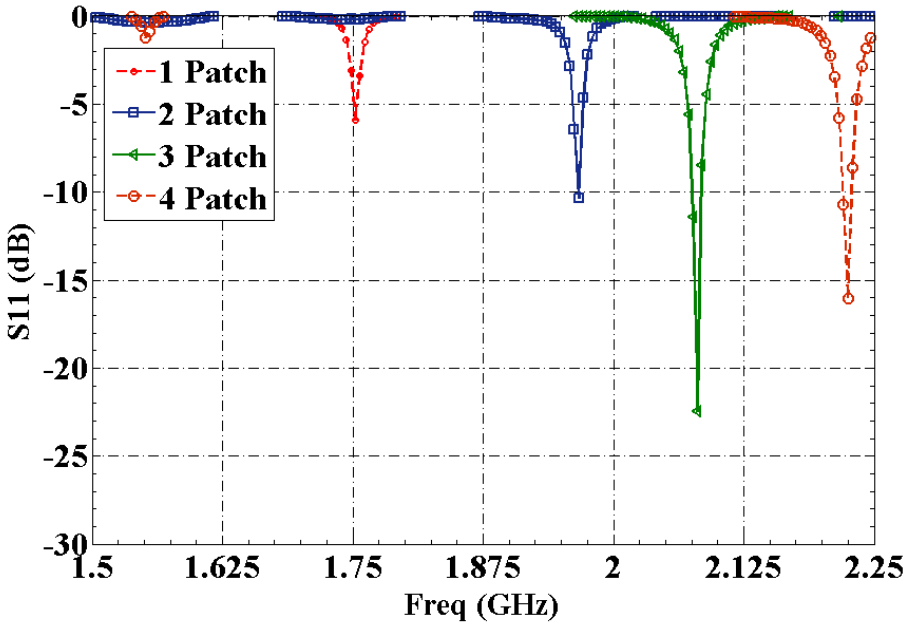

Figure 5.41 *Design 2* - Measurement results showing the return loss for the multi-layered antenna of geometry and dimensions given in Figure 5.39 and Table 5-V

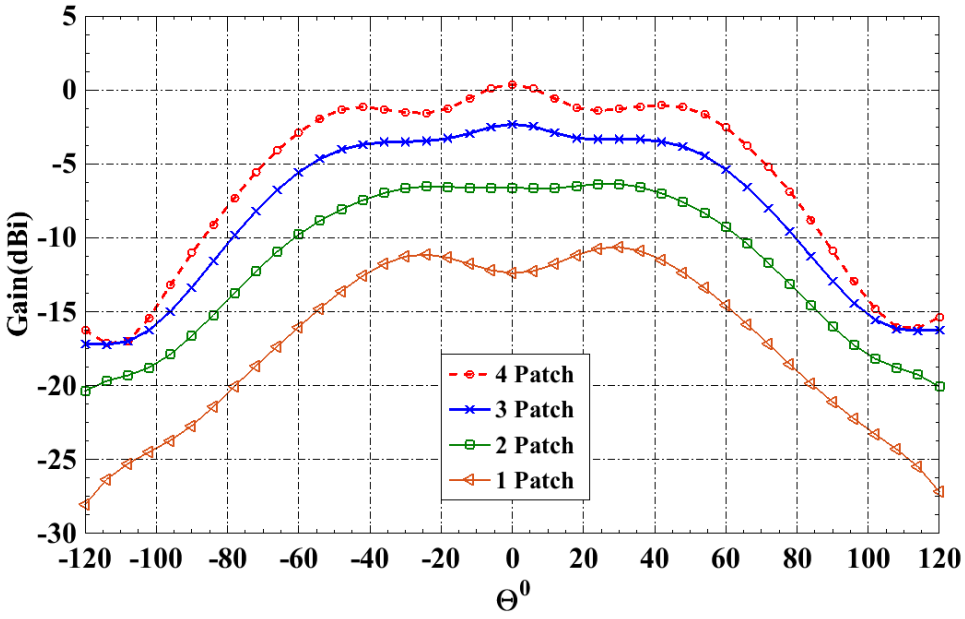

Figure 5.42 *Design 2* - HFSS simulation results showing the E-plane Pattern for the multi-layered antenna of geometry and dimensions given in Figure 5.39 and Table 5-V

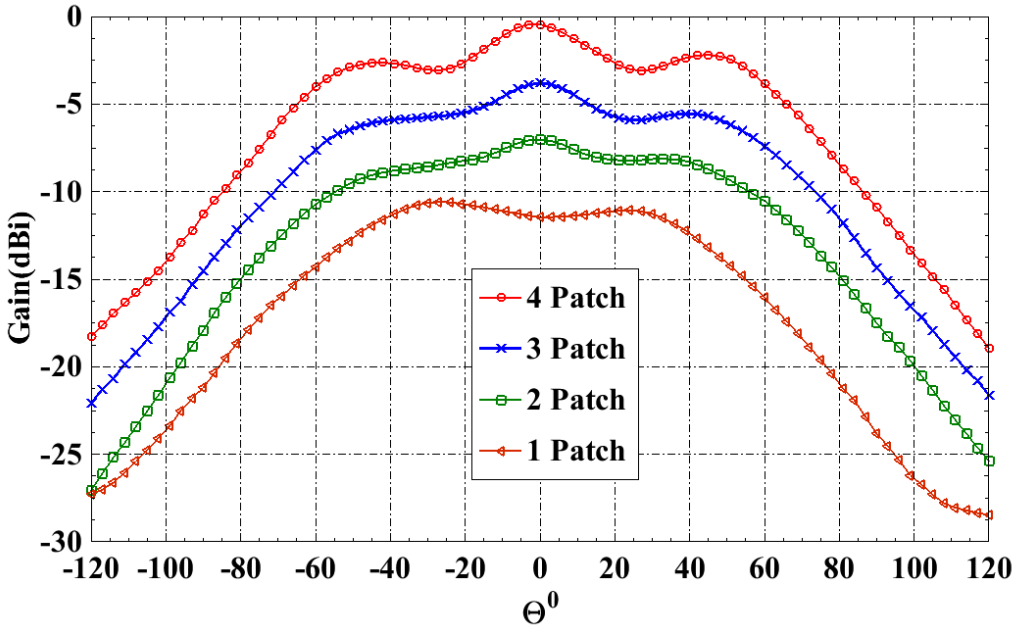

Figure 5.43 *Design 2* - Measurement results showing the E-plane Pattern for the multi-layered antenna of geometry and dimensions given in Figure 5.39 and Table 5-V

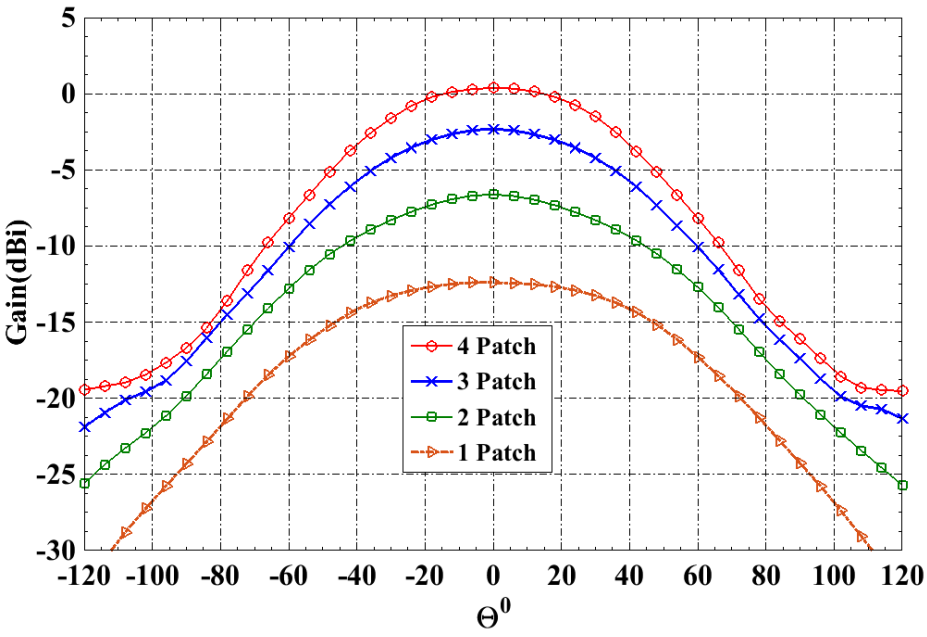

Figure 5.44 *Design 2* - HFSS simulation results showing the H-plane Pattern for the multi-layered antenna of geometry and dimensions given in Figure 5.39 and Table 5-V

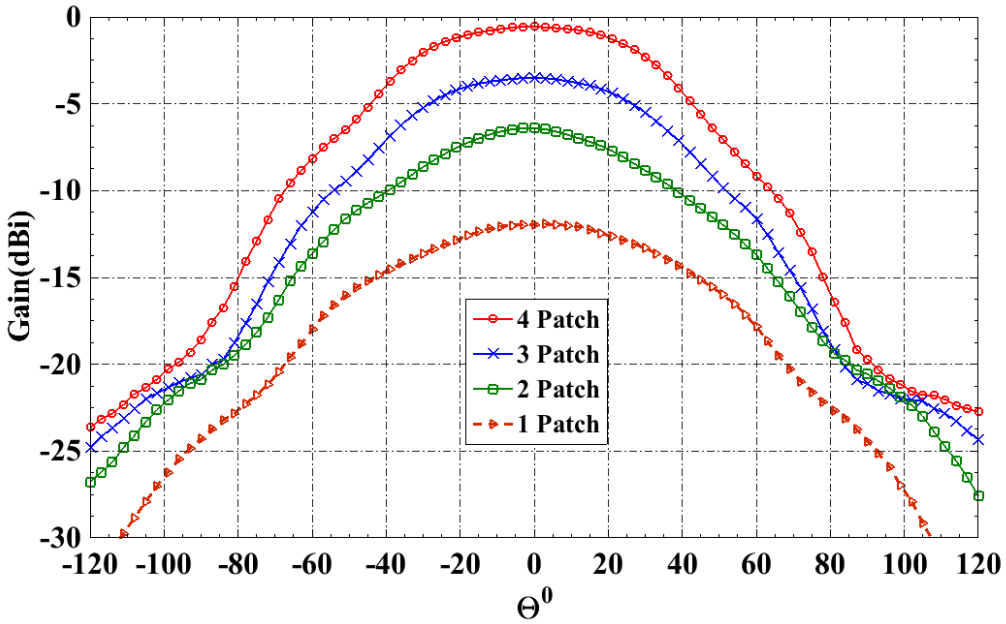

Figure 5.45 *Design 2* - Measurement results showing the H-plane Pattern for the multi-layered antenna of geometry and dimensions given in Figure 5.39 and Table 5-V

In all the cases considered here for the experiments, the gain enhancement was obtained with increase in the number of layers. This increase in the gain however does not

come only from the radiation resistance improvement. As seen from previous sections, the resonant frequency goes higher with the increase in superstrate height. The increase in resonant size of the antenna partly increases its efficiency. This also makes the antenna more directive. It is also seen that the smaller antenna has greater improvement in the gain and drift in the resonant frequency with the increase in the number of layers.

Table 5-VI
Summary of Results showing results showing the *Design 1* - H-Shaped multilayered antenna of geometry and dimensions given in Figure 5.24 and Table 5-IV, case 1 - feed connected only to lower most layer

Number of Elements	Feed Connected to only the lowermost Layer					
	Simulation			Measurement		
	Freq(GHz)	Gain(dBi)	Xpol(dB)	Freq(GHz)	Gain(dBi)	Xpol(dB)
1	2.61	0.12	-21.58	2.617	-1.1	-21.67
2	2.68	2.56	-27.7	2.737	0.4	-24.25
3	2.72	3.66	-27.4	2.786	2.22	-28.33
4	2.76	4.55	-28.53	2.829	2.7	-25.95

Table 5-VII
Summary of Results showing results showing the *Design 1* - H-Shaped multilayered antenna of geometry and dimensions given in Figure 5.24 and Table 5-IV, case 2: feed connected all the layers

Number of Elements	Feed Connected too all the Layers					
	Simulation			Measurement		
	Freq(GHz)	Gain(dBi)	Xpol(dB)	Freq(GHz)	Gain(dBi)	Xpol(dB)
1	2.61	0.12	-21.58	2.617	-1.1	-21.67
2	2.68	2.25	-17.51	2.726	1.24	-15.65
3	2.75	2.95	-13.54	2.803	2.01	-13.85

Table 5-VIII
Summary of Results showing results showing the *Design 2* - H-Shaped multi-layered antenna of geometry and dimensions given in Figure 5.39 and Table 5-V.

Number of Elements	Feed Connected to only the lowermost Layer					
	Simulation			Measurement		
	Freq(GHz)	Gain(dBi)	Xpol(dB)	Freq(GHz)	Gain(dBi)	Xpol(dB)
1	1.74	-12.4	-20.6	1.75	-11.5	-27.12
2	1.9	-6.62	-25.58	1.97	-7.03	-24.08
3	2.02	-2.3	-26.53	2.08	-3.8	-23.53
4	2.11	0.38	-29.92	2.23	-0.44	-26.98

Small changes in the radiation pattern shape are observed in the measured results, which may be due to the misalignment of each layer while manual assembly. The measurement results also show lower values for gain compared to the simulated values. This may be due to several reasons like the loss in the glue used which is dominant for small antennas. The deviation of the simulated designs from actual measurement antenna model also causes deviation in the results. These deviations include factors which inherently come from the laminate manufacturer like surface roughness, adhesive layer between the conductors and the dielectric substrate. Since the measurements are made at different frequencies with different values of return losses, the reflections from the probe and antenna under measurement also affect the measured Gain patterns. Discrete values of Gain for the standard gain horn antenna provided by the manufacturer, which is used for calibration of the measurement chamber, also places a fundamental limit on the achievable accuracy of the measured results.

5.4 CONCLUSION

In this chapter gain and efficiency improvement of miniaturized H-shaped patch antenna using closely coupled multiple resonators were presented. It was seen that by adding multiple layers of parasitic patches and choosing a suitable superstrate dielectric and superstrate height, significant improvement in the gain of the patch antenna was obtained. It was observed that the change in gain is the largest for a single parasitic patch. Addition of further layers by keeping the superstrate height constant also improved the gain and efficiency of the antenna without changes to the radiation pattern. However beyond 4 layers the increase in efficiency and gain becomes relatively small. Two cases of H-shaped antenna were also fabricated and experimentally the gain enhancement by parasitic element loading was studies. The experimental results were found to be in close agreement with the simulations.

Chapter 6

Conclusions and Future Work

In this chapter a summary of the conclusions of this thesis and possible future works are provided.

In chapter 1 an overview of antenna miniaturization techniques and the important challenges in the design of miniaturized antennas were presented. It was seen that the efficiency reduction with reduction in the antenna size is one of the key factors that limits the performance of small antennas. In chapter 2, the effect of miniaturization of a microstrip antenna on its efficiency was studied. The effective dielectric constant and the operating frequency of the patch antenna were shown to be important factors in dictating the efficiency of the antenna. It was shown that the power loss in an antenna made of low loss material comes dominantly from the reduction of the radiation conductance of the antenna, provided the antenna operates at the same frequency. This effect was studied for two widely miniaturization techniques, namely – using high dielectric constant and slot loading.

In chapter 3, for a wave normal incident on a laminated conductor, it was shown using TMM and HFSS that, thin 1-Dimensional Metallo-Dielectric laminated structure can be used to reduce the loss in a thin layer of metal, but a single conductor of thickness greater than the skin depth was found to be more efficient than the laminated conducting media. It was shown that by using 25 or more laminated conductors, each having thicknesses less than the skin depth, the loss in the medium saturated. For the case with a constant overall thickness the loss saturated at 0.05mW (3.125%) and for the case with increasing total

overall thickness the loss saturated at 0.04mW (2.5%). The loss in a single conductor of thickness larger than the skin depth was found to be less than the laminated case. The loss in single conductor saturated at 0.01mW (0.625%) with the increase in its thickness. These results are, however, limited to the structure of infinite extent in two dimensions. Several researchers have successfully shown the application of laminated conductors for loss reduction through skin depth enhancement, in finite sized resonators [38] and transmission lines of infinite extent along its axis [35] [62]. Litz wire is such an example widely used in power transmission lines [63]. These structures have not been analyzed in the current work, the application of which to antennas would be equally interesting and has been proposed as a possible future work.

In chapter 4 the effect of stacking two identical antennas on the radiation characteristics was studied. It was seen that, at the higher resonant frequency of the antenna, the radiation conductance is improved due to increase in the in-phase currents/fields and thus increasing the efficiency of the antenna. With the increase in the distance between the two patches, this effect was seen to further dominate. On the other hand, at the lower resonant frequency the antenna exhibited poor efficiency due to the out of phase currents/fields, but with the increase in the distance between the two patches, the directivity of the antenna was seen to improve and reach the case of upper resonant frequency of the antenna. In addition, it is important to have the parasitic patches to be of identical sizes to obtain even mode dominant field/current distribution at the higher resonant frequency of the patch antenna. It was also shown that any change in the efficiency of the antenna could be easily detected from the relative variation in the Gain levels, provided the antenna pattern remained the same.

In chapter 5, the gain and efficiency improvement of miniaturized H-Shaped patch antenna using closely coupled multiple resonators was presented. It was shown that by adding multiple layers of parasitic patches and choosing a suitable superstrate dielectric and height, significant improvement in the gain of the patch antenna was obtained. It was observed that the change in the gain is the largest for a single parasitic patch. Addition of further layers, by keeping the superstrate height constant, also improved the gain and efficiency of the antenna without any change to the radiation pattern. However, beyond 4 layers the increase in efficiency becomes relatively small. The effect of overall thickness and superstrate dielectric constant on the efficiency improvement was studied parametrically. It was shown that by using 5 radiating resonators and appropriate choice of dielectric constant (ε_{rs} = 4.4), for a small increase in thickness of 0.127mm (5mil), the radiation efficiency increased from 2.34% to 6.3%. Most importantly, an efficiency improvement from 2.4% to 33% can be achieved with an increase in height of 1.27mm (50mil). These translate to a gain improvement of about 4dB and 13dB respectively.

Two designs of H-Shaped patch with different levels of miniaturization operating at two different frequencies were also fabricated and experimentally the gain enhancement by parasitic element loading was studied. The experimental results were found to be in close agreement with the simulations. It was seen that, with the addition of number of layers, the gain improvement and the drift in resonant frequency achieved in the larger level of miniaturization design, was higher than that of the antenna with smaller level of miniaturization. With four resonators the *Design 1* ($L \times W \sim 0.2\lambda_0 \times 0.2\lambda_0$) antenna gain improved by 3.8dB at the expense 0.15GHz frequency drift. For the same considerations, the *Design 2* ($L \times W \sim 0.1\lambda_0 \times 0.1\lambda_0$) *antenna* showed a gain improvement of 11.06 dB at the

expense of 0.37GHz frequency drift. The equivalent change in the electrical size of *Design 2* was 25% more than *Design 1,* due to the increase in height caused by the addition of four multiple resonators.

FUTURE WORK

Based on the study carried out in this thesis the future works that may be carried out are postulated below:

1. It was shown in chapter 3 that the laminated conductors of infinite extent are not suitable for loss reduction due to the skin effect. Thus, future simulation and experimental study may be carried out to investigate the effect of finite sized laminated conductors.
2. In chapter 4 it was shown that the size and shape of the upper and lower resonators of a staked patch antenna affect the symmetry of the modes. In future, further investigation may be carried out on the controllability of the symmetry in the modes for desired radiation characteristics.
3. In chapter 5 it was shown that multiple resonators can be used to improve the efficiency of microstrip antenna. This technique may further be extended to other types of planar antennas, and their effectiveness in efficiency improvement be studied. For further validation, efficiency measurement techniques like the Wheeler Cap method may be employed to directly measure the efficiency improvement of the antennas.

APPENDIX I
Rectangular Microstrip Antenna Design Equations

Some of the commonly used rectangular microstrip antenna design equations are summarized here [11] [8].

Effective dielectric constant of for a grounded substrate, with W/h>1, where *W* is the width of the line/patch and *h* height of the patch, is given by:

$$\epsilon_{reff} = \frac{\varepsilon_r + 1}{2} + \frac{\varepsilon_r - 1}{2}\left[1 + 12\frac{h}{W}\right]^{-1/2}$$

where, ε_r is the dielectric constant of the substrate. The effective length is given by:

$$L_{eff} = L + 2\Delta L$$

Where ΔL is given by

$$\frac{\Delta L}{h} = 0.412\frac{\left(\epsilon_{reff} + 0.3\right)\left(\frac{W}{h} + 0.264\right)}{\left(\epsilon_{reff} - 0.258\right)\left(\frac{W}{h} + 0.8\right)}$$

The resonant frequency of the rectangular patch for the fundamental mode may then be calculated by:

$$f_r = \frac{1}{2L_{eff}\sqrt{\epsilon_{reff}}\sqrt{\mu_0\epsilon_0}}$$

The characteristic impedance of a microstrip line of substrate height h and width W is given by:

$$Z_c = \begin{cases} \frac{60}{\sqrt{\epsilon_{reff}}} ln\left[\frac{8h}{W} + \frac{W}{4h}\right], & \frac{W}{h} \leq 1 \\ \frac{120\pi}{\sqrt{\epsilon_{reff}}\left[\frac{W}{h} + 1.393 + 0.667ln\left(\frac{W}{h} + 1.444\right)\right]}, & \frac{W}{h} > 1 \end{cases}$$

APPENDIX II
MATLAB Code - Plane Wave Incident on a Multilayered Medium

```
%This program calculates the reflection and transmission coefficient for a 1-D multi layered medium, from which for a given input power the total power in the medium is obtained.
clear all;
clc;
clear;
format short
format long e
r = 100;
fmax = 20*10^9;
df = fmax/r;
F=1*10^9;
td=1*10^-6; %Air/Dielectric Thickness
tm=(0.01E-06); %Metal Thickness
cond_layers=1; %Number of Conducting Layers Input
N=(2*cond_layers);
  for k = 1:length(F)
    f = F(k);
    w=2*pi*f;
    %----Vaccum/Air Property------
    ep0(k)= 8.854*10^-12;
    mu0(k)= 4*pi*10^-7;
    sigma_0=0;
    k0(k)=sqrt((1i.*w.*mu0(k)).*(sigma_0+(1i.*w.*ep0(k))));
    alpha0(k)=real(k0(k));
    beta0(k)=imag(k0(k));
    lambda_o(k)=2.*pi./beta0(k);
    Z0(k)=sqrt(mu0(k)./ep0(k));
    Y0(k)=1/Z0(k);
    %----Metal Properties---------
    epr_metal(k)=1;
    ep_m(k)=epr_metal(k)*ep0(k);
    mur_metal(k)=1;
    mu_m(k)=mu0(k)*mur_metal(k);
    sigma_m=100000;
    Ym(k)=sqrt((sigma_m+(1i*w*ep_m(k)))./(1i*w*mu_m(k)));
    Zm(k)=1/Ym(k);
    R(k,1)=(Y0(k)-Ym(k))./(Y0(k)+Ym(k));
    R(k,2)=-R(k,1);
    T(k,1)=1+R(k,1);
```

```
    T(k,2)=T(k,1);
    km(k)=sqrt((1i.*w.*mu_m(k)).*(sigma_m+(1i.*w.*ep_m(k))));
    alpha_m(k)=real(km(k));
    delta(k)=1./alpha_m(k);
    beta_m(k)=imag(km(k));
    lambda_m(k)=2.*pi./beta_m(k);

if N>1
    for n=1:1:N
        %--- if n is odd Assign air-Metal Inerface---
        if (mod(n,2) == 1)    %if m is odd
            T(k,n)=T(k,1);
            R(k,n)=R(k,1);
            A(:,:,k,n)=((1./T(k,n)).*[exp(km(k).*tm),(R(k,n).*exp(-
km(k).*tm));(R(k,n)*exp(km(k).*tm)),exp(-km(k).*tm)];

        end
        if (mod(n,2) == 0)    %if m is even
        %--- if n is even Assign Metal---
            T(k,n)=T(k,2);
            R(k,n)=R(k,2);
            A(:,:,k,n)=(((1./T(k,n)).*[exp(k0(k).*td),(R(k,n).*exp(-
k0(k).*td));(R(k,n)*exp(k0(k).*td)),exp(-k0(k).*td)]));
        end
    end;
    temp=eye(2,2);
    for n=1:1:N
        X(:,:,k)=temp*A(:,:,k,n);
        temp=X(:,:,k);
    end
    C(k)=1./X(1,1,k);
    B1(k)=X(2,1,k).*C(k);
    Pinc(k)=1./(2*Z0(k));
    Ptrans(k)=(abs(C(k)).^2)./(2*Z0(k));
    Prefl(k)=(abs(B1(k)).^2)./(2*Z0(k));
    Ploss(k)=Pinc(k)-(Ptrans(k)+Prefl(k));
 end
  end
    figure(1)
    plot(F,(Ploss./Pinc),'greenx')
    title('Power Loss (W)');
    xlabel('Freq (GHZ)');
    ylabel('Power(W)');
```

APPENDIX III
Return Loss to Mismatch Loss Conversion

Return loss (S_{11} [dB]) is the measure of reflected power due to an impedance mismatch. Lower values of S_{11} indicate better impedance matching. If an antenna is not well matched, this reduces the measured gain of the antenna. This reduction in the gain of the antenna is characterized by the mismatch loss in the antenna. The reflection coefficient (Γ), return loss (S11) and mismatch losses (MS) are related by using the following expressions [59]:

$$\text{Return Loss} = S11\ [\text{dB}] = -20 \log (\Gamma)$$

$$MS = -10 \log (1 - \Gamma^2)$$

The reduction in gain due to mismatch loss may be compensated directly by adding the mismatch loss the measured gain of the antenna to obtain the actual antenna gain under matched condition.

APPENDIX IV
Standard Horn Gain Used for Measurement Chamber Calibration

The following plot shows a typical gain versus frequency plot for a standard horn antenna used for compact range measurement chamber calibration.

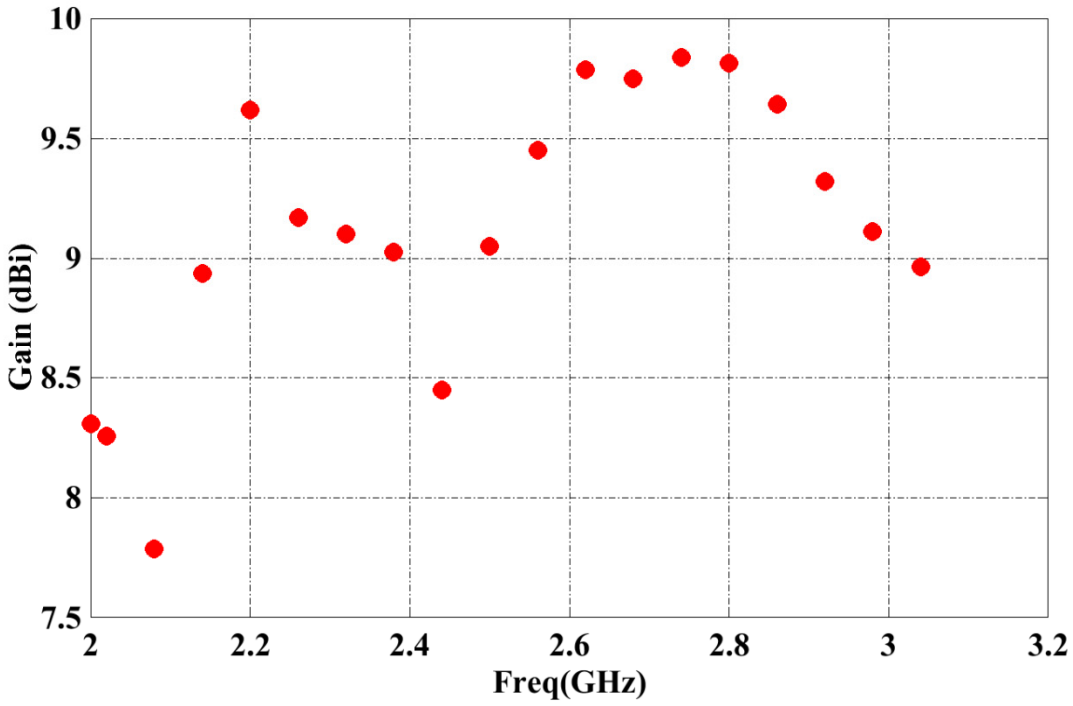

Figure A.6.1 Gain of standard horn antenna used for Measurement

References

[1] R. C. Hansen and M. Burke, "Antennas with magneto-dielectrics," *Microwave and optical technology letters,* vol. 26, no. 2, pp. 75-78, 2000.

[2] G.-M. e. a. Yang, "Tunable miniaturized patch antennas with self-biased multilayer magnetic films," *Antennas and Propagation, IEEE Transactions on,* vol. 57, no. 7, pp. 2190-2193, 2009.

[3] H. Mosallaei and K. Sarabandi, "Magneto-dielectrics in electromagnetics: Concept and applications," *Antennas and Propagation, IEEE Transactions on,* vol. 52, no. 2, pp. 1558-1567, 2004.

[4] L. X. N. Zhanru and Z. Jiangao, "New type organic magnetic materials and their application in the field of microwaves," *Journal of Microwares,* 1999-04.

[5] S. Bae and Y. Mano, "A small meander VHF & UHF antenna by magneto-dielectric materials," in *Asia-Pacific Microwave Conference*, 2005.

[6] T. Tanaka, S. Hayashida, K. Imamura, H. Morishita and Y. Koyanagi, "A study on miniaturization of a handset antenna utilizing magnetic materials," in *International Symposium on Multi-Dimensional Mobile Communications Proceedings*, 2004.

[7] F. He and Z. Wu, "Modelling of a slot loop antenna on magnetic material substrate," in *International Workshop on Antenna Technology: Small and Smart Antennas*, 2007.

[8] R. Garg, Microstrip antenna design handbook, Artech House, 2001.

[9] Shafai L, "Dielectric Loaded Antennas -," in *Wiley encyclopedia of electrical and electronics engineering*, 1999.

[10] J. Volakis, C.-C. Chen and K. Fujimoto, Small Antennas: Miniaturization Techniques and Applications, The McGraw-Hill Companies, 2010.

[11] C. A. Balanis, Antenna theory: Analysis and Ddesign, John Wiley & Sons, 2012.

[12] C.-H. Kang, S.-J. Wu and J.-H. Tarng, "A Novel Folded UWB Antenna for Wireless Body Area Network," *Antennas and Propagation, IEEE Transactions on,* vol. 60, no. 2, pp. 1139-1142, 2012.

[13] A. A. Deshmukh and G. Kumar, "Formulation of resonant frequency for compact rectangular microstrip antennas," *Microwave and Optical Technology Letters,* vol. 49,

no. 2, pp. 498-501, 2007.

[14] H. T. Nguyen, S. Noghanian and L. Shafai, "Microstrip patch miniaturization by slots loading," in *IEEE Antennas and Propagation Society International Symposium*, 2005.

[15] M. Scardelletti, G. Ponchak, S. Merritt, J. Minor and C. Zorman, "Electrically small folded slot antenna utilizing capacitive loaded slot lines," *Radio and Wireless Symposium, 2008 IEEE,* pp. 731-734, 2008.

[16] P.-L. Chi, K. Leong, R. Waterhouse and T. Itoh, "A Miniaturized CPW-Fed Capacitor-Loaded Slot-Loop Antenna," *Signals, Systems and Electronics, 2007. ISSSE '07. International Symposium on,* pp. 595-598, 2007.

[17] D. H. Lee, A. Chauraya, Y. Vardaxoglou and W. S. Park, "A Compact and Low-Profile Tunable Loop Antenna Integrated With Inductors," *Antennas and Wireless Propagation Letters, IEEE,* vol. 7, pp. 621-624, 2008.

[18] D. Sievenpiper, L. Zhang, R. Broas, N. Alexopolous and E. Yablonovitch, "High-impedance electromagnetic surfaces with a forbidden frequency band," *Microwave Theory and Techniques, IEEE Transactions on,* vol. 47, no. 11, pp. 2059-2074, 1999.

[19] F. Yang and Y. Rahmat-Samii, "Reflection phase characterizations of the EBG ground plane for low profile wire antenna applications," *Antennas and Propagation, IEEE Transactions on,* vol. 51, no. 10, pp. 2691-2703, 2003.

[20] P. Maagt, R. Gonzalo, Y. C. Vardaxoglou and J. M. Baracco, "Electromagnetic bandgap antennas and components for microwave and (Sub)millimeter wave applications".

[21] C. Caloz, T. Itoh and A. Rennings, "CRLH metamaterial leaky-wave and resonant antennas".

[22] M. I. Stockman, "Criterion for negative refraction with low optical losses from a fundamental principle of causality," *Physical Review Letters,* vol. 98, no. 17, p. 177404, 2007.

[23] L. J. Chu, "Physical Limitations of Omni-Directional Antennas," *Journal of applied physics ,* vol. 19, no. 12, pp. 1163-1175, 1948.

[24] A. Yaghjian and S. Best, "Impedance, bandwidth, and Q of antennas," *Antennas and Propagation, IEEE Transactions on,* vol. 53, no. 4, pp. 1298-1324, 2005.

[25] M. Gustafsson, C. Sohl and G. Kristensson, "Physical limitations on antennas of arbitrary shape," *Proceedings of the Royal Society of London A: Mathematical, Physical and Engineering Sciences,* vol. 463, no. 2086, pp. 2589-2607, 2007.

[26] M. Gustafsson, C. Sohl and G. Kristensson, "Illustrations of new physical bounds on linearly polarized antennas," *IEEE transactions on antennas and propagation,* vol. 57,

no. 5, pp. 1319-1327, 2009.

[27] R. F. Harrington, "Effect of antenna size on gain, bandwidth, and efficiency," *J. Res. Nat. Bur. Stand,* vol. 64, no. 1, pp. 1-12, 1960.

[28] A. Derneryd and A. Lind, "Extended analysis of rectangular microstrip resonator antennas," *Antennas and Propagation, IEEE Transactions on,* vol. 27, no. 6, pp. 846-849, Nov 1979.

[29] P. Perlmutter, S. Shtrikman and D. Treves, "Electric surface current model for the analysis of microstrip antennas with application to rectangular elements," *Antennas and Propagation, IEEE Transactions on,* vol. 33, no. 3, pp. 301-311, Mar 1985.

[30] A. Bhattacharyya, "Effects of finite ground plane on the radiation characteristics of a circular patch antenna," *Antennas and Propagation, IEEE Transactions on,* vol. 38, no. 2, pp. 152-159, 1990.

[31] S. Noghanian and L. Shafai, "Control of microstrip antenna radiation characteristics by ground plane size and shape," *Microwaves, Antennas and Propagation, IEE Proceedings,* vol. 145, no. 3, pp. 207-212, 1998.

[32] S. Best, "A discussion on the properties of electrically small self-resonant wire antennas," *Antennas and Propagation Magazine, IEEE,* vol. 46, no. 6, pp. 9-22, Dec 2004.

[33] R. F. Harrington, Time-harmonic electromagnetic fields, McGraw-Hill, 1961.

[34] E. C. Jordan and K. G. Balmain, Electromagnetic waves and radiating systems, Englewood Cliffs, NJ: Prentice-Hall, 1968.

[35] A. Clogston, "Reduction of Skin-Effect Losses by the Use of Laminated Conductors," *Proceedings of the IRE,* vol. 39, no. 7, pp. 767-782, 1951.

[36] M. Scalora, M. J. Bloemer, A. S. Pethel, J. P. Dowling, C. M. Bowden and A. S. Manka, "Transparent, metallo-dielectric, one-dimensional, photonic band-gap structures," *Journal of Applied Physics,* vol. 83, no. 5, pp. 2377-2383, 1998.

[37] J. Hattori, S. Hidaka, T. Ise, K. M. N. Kubota and Y. Ishikawa, "Low Profile Dielectric Band Elimination Filter using Thin Film Layered Electrode for 2 GHz Band Cellular Base Station," in *Microwave Symposium Digest*, 1999.

[38] A. Eriksson, A. Deleniv and S. Gevorgian, "Resonant tunneling of microwave energy in thin film multilayer metal/dielectric structures. In Microwave Symposium Digest," in *IEEE MTT-S International*, 2002.

[39] S. I. Latif, L. Shafai and C. Shafai, "An Engineered Conductor for Gain and Efficiency Improvement of Miniaturized Microstrip Antennas," *Antennas and Propagation*

Magazine, vol. 55, no. 2, pp. 77-90, 2013.

[40] S. I. Latif, L. Shafai and C. Shafai, "Gain and Efficiency Enhancement of Compact and Miniaturised Microstrip Antennas using Multi-Layered Laminated Conductors," *IET microwaves, Antennas and Propagation,* vol. 5, no. 4, pp. 402-411, 2011.

[41] R. E. Collin, Field theory of guided waves., Wiley-IEEE Press, 1991.

[42] Ansoft, "HFSS online help version 9.2.," American: Ansoft Inc, 2004.

[43] R. Soltanmoradi, S. A. Dyakov, Q. Wang, M. Qiu and M. Yan, "Multi-resonator structure based on continuous silver thin films for transparent conductor," *Applied Physics Letters,* vol. 105, no. 6, p. 061110, 2014.

[44] H. Y. Yang and N. G. Alexopoulos, "Gain enhancement methods for printed circuit antennas through multiple superstrates," *Antennas and Propagation, IEEE Transactions on,* vol. 35, no. 7, pp. 860-863, 1987.

[45] Gardelli, M. Albani and F. Capolino, "Array thinning by using antennas in a Fabry-Perot cavity for gain enhancement," *Antennas and Propagation, IEEE Transactions on,* vol. 54, no. 7, pp. 1979-1990, July 2006.

[46] A. Ourir, A. de Lustrac and J. M. Lourtioz, "All-metamaterial-based subwavelength cavities ($\lambda/60$) for ultrathin directive antennas," *Applied physics letters,* vol. 88, no. 8, p. 084103, 2006.

[47] A. Foroozesh and L. Shafai, "Investigation into the effects of the patch-type FSS superstrate on the high-gain cavity resonance antenna design.," *Antennas and Propagation, IEEE Transactions on,,* vol. 58, no. 2, pp. 258-270, 2010.

[48] J. Nessel, A. Zaman, R. Q. Lee and K. Lambert, "Demonstration of a X-band multilayer Yagi-like microstrip patch antenna with high directivity and large bandwidth," in *ntennas and Propagation Society International Symposium, 2005 IEEE*, 2005.

[49] G. Kumar and P. Ray K, Broadband microstrip antennas., Artech House, 2002.

[50] J. Anguera, L. Boada, C. Puente, C. Borja and J. Soler, "Stacked H-shaped microstrip patch antenna," *Antennas and Propagation, IEEE Transactions on,* vol. 52, no. 4, pp. 983-993, April 2004.

[51] A. A. Pistolkors, "The Radiation Resistance of Beam Antennas," *Radio Engineers, Proceedings of the Institute of,* vol. 17, no. 3, pp. 562-579, 1929.

[52] A. A. Oliner, D. R. Jackson and J. L. Volakis, Antenna Engineering Handbook, McGraw Hill , 2007.

[53] F. Croq and D. M. Pozar, "Millimeter-wave design of wide-band aperture-coupled stacked microstrip antennas," *Antennas and Propagation, IEEE Transactions on,* vol. 39, no. 12, pp. 1770-1776, 1991.

[54] Ansari, S. P. J. A., S. K. Dubey, R. U. Khan and B. R. Vishvakarma, "H-shaped stacked patch antenna for dual band operation," *Progress In Electromagnetics Research B,* pp. 291-302, 2008.

[55] D. M. Pozar and B. Kaufman, " (1988). Comparison of three methods for the measurement of printed antenna efficiency 36(1), 136-139.," *IEEE transactions on antennas and propagation,* vol. 39, no. 1, pp. 136-139, 1988.

[56] H. Wheeler, "The Radiansphere around a Small Antenna," *Proceedings of the IRE,* vol. 47, no. 8, pp. 1325-1331, 1959.

[57] R. Johnston and J. McRory, "An improved small antenna radiation-efficiency measurement method," *Antennas and Propagation Magazine, IEEE,* vol. 40, no. 5, pp. 40-48, 1998.

[58] J. Gomez-Tagle and C. G. Christodoulou, "Extended cavity model analysis of stacked microstrip ring antennas," *Antennas and Propagation, IEEE Transactions on,* pp. 1626-1635, 1997.

[59] D. M. Pozar, Microwave engineering, John Wiley & Sons, 2009.

[60] R. W. P. King and W. H. J. Charles, ANTENNAS AND WAVES: A MODERN APPROACH, The MIT Press, 1969.

[61] S.-S. Zhong, G. Liu and G. Qasim, "Closed form expressions for resonant frequency of rectangular patch antennas with multidielectric layers," *Antennas and Propagation, IEEE Transactions on,* vol. 42, no. 9, pp. 1360-1363, Sep 1994.

[62] F. E. Terman, Radio Engineers' Handbook, McGraw-Hill, 1943, pp. 37,74,80.

[63] C. R. Sullivan, "Optimal choice for number of strands in a litz-wire transformer winding," *IEEE Transactions on Power Electronics,* vol. 2, no. 14, pp. 283-291, 1999.